ACTIVE SPERM SEPARATION TECHNIQUE USING AN INERTIAL MICROFLUIDIC DEVICE

by

Jiyoung Son

A dissertation submitted to the faculty of
The University of Utah
in partial fulfillment of the requirements for the degree of

Doctor of Philosophy

Department of Electrical and Computer Engineering

The University of Utah

August 2017

:

The University of Utah Graduate School

STATEMENT OF DISSERTATION APPROVAL

The dissertation of **Jiyoung Son**

has been approved by the following supervisory committee members:

Bruce K. Gale	, Chair	**April 27 2017** Date Approved
Douglas T. Carrell	, Member	**April 27 2017** Date Approved
Carlos Mastrangelo	, Member	**April 29 2017** Date Approved
Florian Solzbacher	, Member	**April 27 2017** Date Approved
Prashant Tathireddy	, Member	**April 27 2017** Date Approved

and by **Gianluca Lazzi** , Chair/Dean of

the Department/College/School of **Electrical and Computer Engineering**

and by David B. Kieda, Dean of The Graduate School.

ABSTRACT

Microfluidic technology has the unique potential to separate sperm from unwanted debris while improving the effectiveness of assisted reproductive technologies (ART). Limitations of current clinical protocols regarding separation of sperm from other cells and cellular debris can lead to low sperm recovery when the sample contains low concentrations of mostly low motility sperm and a high concentration of unwanted cells or cellular debris, such as occurs with surgical testis dissection samples from nonobstructive azoospermia (NOA) patients who have undergone microsurgical testicular sperm extraction (mTESE), and semen samples from leukospermia patients (high white blood cell (WBC) semen).

Over the years, most microfluidic sperm separation approaches have relied on sperm motility for separation with added features through which only highly motile sperm can pass. Thus, these techniques can separate only progressive motile sperm from semen samples, but they lose a significant number of sperm cells including viable nonprogressive motile and nonmotile sperm. This dissertation demonstrates label-free separation of sperm from challenging sperm samples using inertial microfluidics. The approach does not require any externally applied forces except the movement of the fluid sample through the instrument. In this way, it is possible to recover not only any motile sperm, but also viable less-motile and nonmotile sperm with high recovery rates. The results show the usefulness of inertial microfluidics to significantly reduce the concentrations of unwanted

cells/cellular debris (Red blood cells/White blood cells) significantly by flow focusing of debris within a spiral channel flow. The majority (~80%) of sperm cells collect to the designated outlet and ~98% of debris goes to the waste outlet. The estimated sample process time is more rapid (~5minutes) and autonomous than conventional methods which may take between ~1 hour (semen purification) and 10 ~18 hours (manual mTESE sample search process).

The flow focusing results of sperm and blood cells included that sharp flow focusing of RBC and WBC, but not of sperm cell where sharp flow focusing didn't appear. The successful flow focusing of RBC and WBC imply that the spherical model did accurately predict the behavior of RBCs and WBCs, but the lack of definitive focusing of sperm cells imply that the modeling of sperm cells wasn't accurate. This partial success of sperm modeling was caused by a lack of understanding of sperm behavior in the curved channel. This dissertation presents an improved model of sperm cell behavior in curved channels based on both 2D COMSOL ® simulations and experimental studies. The results show promising evidence that the proposed method should able to generate more precise sperm separation for mTESE samples. Lastly this dissertation also performed viability, toxicity, and recovery tests on the proposed sperm separation method for biocompatibility verification. These tests should provide initial validation of clinical usefulness.

I dedicate this dissertation to God, Jesus Christ, my parents (Seung-Ju Son, Nam-Soon Park), my parents in law (Chang-Gyu Park, Gum-Rang Lee), my sister (Hyo-Jin Son), my brothers in law (Woo-Pill Shim, Jin-Ha Park), My nephews (Hyun-Jae Shim, Hyun-Soo Shim, Hyun-Seung Shim), my children (Mina A. Son, Gina V. Son), uncles, aunts, cousins, my many dear friends and most importantly the eternal love of my life, Mi-Jin Park.

“The important thing is not to stop questioning. Curiosity has its own reason for existing. One cannot help but be in awe when he contemplates the mysteries of eternity, of life, of the marvelous structure of reality. It is enough if one tries merely to comprehend a little of this mystery every day. Never lose a holy curiosity.”
-Albert Einstein

“And if a person gains more knowledge and intelligence in this life through his diligence and obedience than another, he will have so much the advantage in the world to come”
-Doctrine and Covenants 130:19

TABLE OF CONTENTS

LIST OF TABLES

ACKNOWLEDGEMENTS

This dissertation is based upon work supported by the National Science Foundation under Grant IIP-1549659. The author would also like to thank Dr. Bruce K. Gale from the University of Utah Mechanical Engineering Department, and Dr. Douglas T. Carrell and Dr. James M. Hotaling from the University of Utah Andrology program for their support.

CHAPTER 1

INTRODUCTION

Over several decades, the fields of biochemistry and molecular biology have improved basic scientific understanding through newly developed supporting technologies. The demand for high throughput experimentation and highly sensitive analytical methods has emerged along with scientific progress. However, the capability of conventional tools has became inadequate to meet the demands of the latest research projects and field applications [1]. Microfluidic technology, one of the modern tools, that has been utilized to satisfy the new demands, promises massively parallel sample processing, rapid process times, small work volumes with minimal losses, and high-throughput biological processes [2]. Microfluidic approaches and devices have been growing rapidly over the past 20 years, and started in earnest with the introduction of soft-lithography using polymer molding and poly-di-methyl-siloxane(PDMS) enabled rapid fabrication of cheap microfluidic devices [3] at the end of the 1990s.

The influence of microfluidic technology has reached highly demanding fields such as genetic analysis[4]. As an effective tool for genetic analysis, microfluidics provides high throughput sequencing and DNA amplification tools, which have been popular the past few years. As an example, numerous microfluidic polymerse chain reaction (PCR) devices have been demonstrated successfully with measurable real-time amplification incorporated in the microfluidic PCR chip. The chips even demonstrate amplification completed in a few minutes with a single cell input [2], [4], [5]. Dozens of other similar examples are also available.

1.1 Separation/Manipulation With Microfluidics

In recent biological studies, the focus has shifted from genetic analysis to cell biology as individual cells are considered the basic component of biological understanding. In molecular analysis, there have been challenges to making measurements at the single cell level, because cell samples are highly complex, and contain many different species at widely different abundance levels [6]–[13]. In addition, rare cells are often the primary target for molecular diagnostics. For example, analysis of whole blood to identify specific cells is a well-known protocol in medical diagnostics when searching for parasite-infected red blood cells (RBC) for malaria diagnosis [14], and separation of nucleated RBCs (NRBCs) for screening fetal aneuploidies and pregnancy complications [15]. Recently, separating circulation tumor cells (CTCs) has been spotlighted for rapid and simpler cancer diagnostics [16]. For these reasons and others, manipulating (sorting or separating) single cells using microfluidics technology has created highly valuable tools with high degrees of automation and high throughput sample processing capabilities. Nevertheless, with all the advantages above, there is still a possibility of generating misleading data because a small sample volume cannot represent an entire target population, especially when analyzing rare cell types that statistically may not be represented in the small sample. Thus large numbers of test cycles with a series of statistical analyses may be required to prevent this problem.

Conventional cell separation systems have mostly utilized membrane-based filtering techniques or centrifuge-based technology to separate target cells [11], [17]. However, membrane based technologies are susceptible to plugging due to limited membrane pore sizes [11]. Centrifuge based technologies can lead to possible target sample loss when there is only a small concentration of target particles in the initial sample, which can also limit

the sensitivity of the target cell detection. To overcome the limitations of conventional methods, microfluidic technologies have been used to provide the following advantages: small work volume, rapid process time, high sensitivity and detection accuracy, high automation, high portability, and low cost [7], [8], [10], [12], [14]–[21].

Microscale cell separation techniques takes advantage of the distinctive intrinsic properties of different cell populations to achieve separation. Among the intrinsic properties, surface biomarkers labeled by an antibody are widely used to separate target cells with the assistance of fluorescent molecules. This technique is called fluorescent activated cell sorting (FACS)[6], [7], [10]–[12], [19], [22]. Another popular surface biomarker separation technique utilizes biochemical and electromagnetic properties of antibody tagged magnetic microbeads[6], [19].

Unlike active separation techniques utilizing different properties of surface biomarkers of cells, there are passive techniques that utilize the mechanical and physical properties of cells such as size, shape, density, adhesion, deformability, and motility[6], [12], [23]. This differentiation doesn't require external markers, which makes it even simpler to operate the technique than active techniques (such as FACS and electromagnetic methods). The tools for passive separation can be structures inside of channels (e.g., deterministic lateral displacement; DLD), flow control (pinched flow fractionation, hydrodynamic filtration), channel design (inertial flow focusing), and biomimetic design (chemotaxis, Fahraeus effect)[12]. Passive methods are preferred, when possible, due to this simplicity and especially since there is no requirement for labeling the cells.

1.2 Inertial Particle Migration and Focusing

Among passive particle separation techniques, inertial microfluidic particle separation techniques have been attracting noticeable interest in last few years due to their unique advantages. Passive particle separation is appealing to the clinical and single cell research communities who are concerned about the negative effects of utilizing additional external separation factors on live cells.

1.2.1 Inertial Lift Force

In inertial microfluidics, for flows within the lower Reynolds number (~1< *Re* <~100s) range, particles migrate across the flow due to the presence of some unique force, and particles can be focused to equilibrium positions. This orderly arrangement of particles was reported by Segre and Silberberg where they observed that randomly dispersed 1mm diameter particles migrated laterally to focus on an annulus with a radius ~0.6 times the radius from the middle of a 1 cm diameter pipe[24].

Segre and Silberberg's study triggered further theoretical analysis on the cause of particle lateral motion in these conditions by some form of lift force. Later theoretical analysis suggested that there are two dominant forces in straight channels: first, the wall induced lift force, due to the interaction between the particle and the surrounding walls, which pushes the particle away from the wall, and second, the shear gradient induced lift force, due to the curvature of the parabolic velocity profile, which pushes the particle away from the channel center (the highest velocity). In short, inertial particle migration is mostly caused by a balance of two lift forces [25]–[27].

Theoretical investigations also have estimated the lateral migration of particles under

Poiseuille flow. The currently established lift force theory is described in terms of physical variables within the channel which are: particle diameter(a_p), hydraulic diameter(D_h) of channel, maximum flow velocity(U_m), and fluid density(ρ). Additionally, Asmolov[28] introduced the nondimensional lift coefficient(C_L) to relate the net lift force(F_L) to the dependent variable,

$$F_L = \frac{C_L \rho U_m^2 a_p^4}{D_h^2} \tag{1.1}$$

where the hydraulic diameter of the rectangular channel is defined as

$$D_h = \frac{2 \times H \times W}{H+W}, \tag{1.2}$$

where H is the channel height and W is the channel width. Recent studies have shown that the lift force scaling (nondimensional lift coefficient, C_L) depends on the particle position in the channel[29], [30], suggesting that different fluidic dynamic effects act to create the inertial lift equilibrium positions. Note that Di Carlo et al. showed C_L is less than 0.05[29].

The motion pattern of particles near the channel center is dominated by the shear induced lift force due to the velocity around the particle surface. The direction of this force is toward channel walls (Figure 1.1.A). Studies have shown that vorticity near walls is in the direction opposite to the shear induce lift force (Figure 1.1.A), which cause the wall-induced lift force to push particles away from walls[30].

With the balance of the two lift forces, particle focusing in square channel, and rectangular channels can be explained (Figure 1.1.B, C). A balance of the two major lift

forces causes particles to migrate away from channel center (shear induced) and channel walls (wall induced) resulting in particles reaching a stable equilibrium position[30]. Experimental studies identified that there are four stable focusing positions as illustrated in Figure 1.1.B. These four positions are different from those reported by Segre and Silberberg where circular channels have annulus shaped focusing points in the channel, which suggests that there are additional lateral migration forces that cause particles to focus toward wall centers[25], [30]–[31].

Additional minor lift forces are generated when the particle leads, lags, or rotates in the flow, and these forces are weaker or negligible most of time[27]. When a particle leads or lags the fluid in Poiseuille flow, the effect is called slip-shear lift. This effect was reported by Saffman showing that a particle lagging or leading the fluid in the flow causes a lift force towards the channel center or wall[32].

Particle rotation may cause a rotation induced lift force which originates from differences in velocity between the particle and the underlying flow (Slip-spin) [33], [34]. There have been claims about its usefulness as an additional particle migration factor. A study reported by Zhou et al. suggested the slip-spin effect can help to explain the different number of equilibrium positions in square and rectangular microchannels[30]. Nevertheless the slip-spin effects are generally considered minimal compared to wall-effects and shear-gradient lift forces in Poiseuille flow [27], [34].

1.2.2 Secondary Flow in Curved Channel

The secondary flow induced by a curved channel is a widely utilized inertial effect, which is known as Dean flow. The Dean flow was first reported by W. R. Dean [35] and a

more clear description of the phenomenon was presented by Berger et al. [36]. According to the description by Berger et al., the secondary flow pattern arises because the centrifugally-induced pressure gradient, approximately uniform over the cross section, drives the slower-moving fluid near the wall inward, while faster-moving fluid in the core is swept outward. As a result of this effect, vortices are almost symmetrically arranged perpendicular to the primary flow direction (Figure 1.2). There are two major physical roles of Dean flow in microfluidic platforms. First, it allows particles to reach equilibrium positions faster. At sufficiently higher Dean number, the distance required for particle focusing is nearly 5 times shorter when compared to the case of a straight channel with the same cross-sectional channel dimensions [37]. Second, it allows for unique equilibrium positions for particles with different particle dimensions at locations across the channel[31], [38].

In order to describe the magnitude of this flow, a dimensionless number called the Dean number (De) has been utilized

$$De = \frac{\rho U_f D_h}{\mu}\sqrt{\frac{D_h}{2R}} = Re\sqrt{\frac{D_h}{2R}}, \tag{1.3}$$

where μ is the fluid viscosity, U_f is the average fluid velocity, R is the radius of curvature of the path of the channel, and Re is the flow Reynolds number. As shown in equation 1.3, the magnitude of De is directly related to the curvature of the channel (R), hydraulic diameter(D_h), and average flow velocity (U_f).

Particles flowing in a curved channel experience a drag force due to vortices like Dean flows. The Dean drag force causes particles to move along the Dean flows, which means

particles may move towards either the inner or outer channel wall[39]. Note that the Dean force induced particle movement is heavily dependent on particle size. The magnitude of the Dean force is formulated in terms of Dean velocity with a given *De.* The Dean force equation is described as following:

$$F_D = 3\pi\mu U_{Dean} a_p \tag{1.4}$$

where U_{Dean} is formulated as following by OoKawara et. al[40].

$$U_{Dean} = 1.8 \times 10^{-2} De^{1.63} \tag{1.5}$$

1.2.3 General Curved Microfluidic Channel Design Guidelines

Even with the number of works that have reported on the many different effects of inertial microfluidics on particle focusing, there is no simple explanation for its physical origins. In order to organize all the reported aspects for design purposes, there have been a number of experimental and theoretical attempts to construct standardized guidelines. Dean flow effects have been presented as the ratio between the net lift force and the Dean drag force(R_f) with dependence on channel aspect ratio, the ratio between particle and channel dimensions (λ), the required channel length for focusing(L_I, L_D), particle concentration effects, and the relationship between *Re* and focusing positions.

The force ratio (R_f) is the ratio between net left force(F_L) and Dean drag force(F_D) and it is one of the key characteristics that determines if flow focusing occurs in a curved channel. If this ratio is too small, Dean drag can lead to mixing and disrupt particle

focusing. As a result, the following guideline is generally accepted when designing curved microchannels to exhibit flow focusing [27], [30]:

$$R_f = \frac{F_L}{F_D} > \sim 0.08 \, . \tag{1.6}$$

Note that as an exception to this guideline, there have been reports about losing the benefit of Dean flow effects if the inertial lift is dominant ($R_f \gg 1$) [27].

Experimental work to show the effects of channel aspect ratio was presented by Martel and Toner, which determined that the aspect ratio of the channel should be between 1:2 ~ 1:4 (height : width) for the desired equilibrium position behavior[26]. The ratio of particle diameter and hydraulic diameter is also one of the critical considerations for effective particle focusing (for near the side wall focusing) in high aspect ratio channels[38], [41]. From the experimental data and theoretical calculations, a large region for successful particle focusing can be defined where the ($\lambda = a_p/D_h > 0.07$).

The channel length required for particles to reach their lateral equilibrium positions (L_I) in straight, rectangular channels can be given by [39]:

$$L_I = \frac{U_f}{U_L} \times L_M \tag{1.7}$$

where L_M is the migration length and U_L is the particle lateral migration velocity, which is described as:

$$U_L = \frac{\rho U_m^2 a_p^3 C_L}{3\pi\mu D_h^2} \quad (1.8)$$

For curved, rectangular channels, Dean flows in the spiral channel will aid the migration of particles toward their equilibrium positions, so the length is expected to be shorter than for a straight channel. Amini et al. reported that this expectation can be true depending on the *Re* and *De* values. When *Re* and *De* are low, the focusing length of straight and curved channels are about the same. However, for increased *Re* and *De* (about four times higher than the lower case), the focusing length of a curved channel is nearly 5 times shorter than the focusing length using a straight channel[27].

High particle concentrations lead to interactions between particles that cause particles to disperse and can lead to reduced particle focusing (focusing length). This phenomenon can be defined by the number of particles per channel length [27], [42] using the following relation:

$$\beta = \frac{3WHV_f}{4\pi a_p^2} \quad (1.9)$$

where V_f is volume fraction. According to previous reports, for the case of $\beta > 1$, particles cannot be expected to focus due to collision interactions between particles. Based on this relationship and observations, it has been noted that the length fraction significantly increases as particle diameter decreases. In other words, concentration should be reduced, as particle diameter is increased.

Altering *Re* can also be a useful tool to control the location of the equilibrium position of particles. At higher *Re* (~150) the equilibrium positions in square and rectangular

channels tend to shift slightly toward the wall. This can be explained by relative change in the nature of the two opposing lift forces (wall induced lift force and shear gradient lift force). When the flow velocity or *Re* is increased, both forces will be increased. However, the increase in the shear gradient lift is relatively larger than the wall induced lift for certain high *Re* cases[28]. Therefore, increasing *Re* or flow velocity can cause the shear gradient to be dominant, which can induce the particle equilibrium positions to shift closer to the channel wall [27].

1.2.4 Understanding Particle Behavior in Inertial Microfluidics Channels

In most inertial microfluidics case studies, the target particles are mostly spherical and the foundation of inertial theory was built upon the spherical particle assumption. However, in the real world, live cell samples are not always spherical, as in this case where sperm cells are used. Therefore, there have been numerous attempts to understand the behavior of nonspherical particles[43]–[52]. For example, there has been a study comparing the equilibrium position of spherical particles with a certain diameter and nonspherical particles with the same rotational diameter[50]. The study found that the rotational diameter of a particle, regardless of its cross-sectional shape, determined the final focused position in most of the cases. Particles have also been found to self-align when traveling within the channel[44]. Uspal reported the possibility of tailoring self-steering particles by specifically designing the particle shape and geometric confinement of a rigid micro-particle. These particle behavior studies can help to estimate the equilibrium position of naturally asymmetrical or nonspherical particles.

1.2.5 Applications of Inertial Particle Focusing

Particle separation approaches utilizing inertial effects can separate bioparticles without external forces or additional substances added to the media. Recently the separation of rare cells from blood, such as circulating tumor cells (CTC) and stem cells, has become a major research focus due to the various biomedical applications for these cells, such as disease detection, diagnosis, therapeutic treatment monitoring, and conducting fundamental scientific studies. However, these separations have proven very challenging due to the extreme rareness of the cells, leading to the application of inertial microfluidic cell separation techniques [53]–[64] in hopes of finding success with these methods. Currently, the most popular rare targets separated using inertial microfluidics are CTCs and bacteria. There have been numerous applications of inertial microfluidic technology to improve CTC and bacteria separation processes [53]–[56], [58], [60]–[63].

A number of curved channel designs can induce inertial lift forces and the Dean drag force, and have been utilized for target cell separation. Bhagat et al. demonstrated inertial effects through a combination of high-aspect-ratio rectangular microchannel patterns with a contraction-expansion array (Figure 1.3). Two continuous square patterns of contraction-expansion channels were utilized for rare cell focusing and pinching purposes and lead to enhanced target cell separation[62]. The continuous square-pattern microfluidic device was also utilized (Figure 1.3) by Lee et al. and Shen et al. with a prefiltering structure [58], [63] to demonstrate a successful separation. In a device with a similar square pattern design from Di Carlo et al., a serpentine pattern curved channel array (Figure 1.3) was used to generate a combination of lift forces and the Dean drag force [64] to enable separations.

Another popular Dean flow inducing design is a spiral channel. Recently, rare cell

separations utilizing a spiral channel have shown great potential due to the simplicity of the design and rapidity of the process [53], [54], [56]–[61]. The spiral channel design can be a very effective design that takes significant advantage of inertial effects, and so can provide much quicker particle focusing than straight channels [26]. Another physical advantage of spiral channels is the reduced footprint of the channel device, as Sun et al. reported a double spiral channel where the second spiral is interposed into the gap of the first spiral channel (Figure 1.3) [53].

1.3 Particle Separation in Reproductive Medicine

In recent years infertility has become a serious threat. According to a report by Boivin et al., approximately 15-20% of couples in industrialized countries fail to conceive after one year[65], and male factor infertility, characterized by semen parameters that fall below the World Health Organization (WHO) cut-offs for normozoospermia, is responsible for nearly half of infertility cases[66]. There are several forms of male infertility that require assisted reproductive technology (ART) procedures and the major forms are obstructive azoospermia (OA), nonobstructive azoospermia (NOA), and leukospermia[67].

1.3.1 Overview of Male Factor Infertility

OA refers to lacking all sperm in an ejaculated semen sample and results from various problems with sperm delivery. The common causes of OA include previous vasectomy, congenital bilateral absence of vas deferens (CABVD), postinfective epididymitis (commonly Young's syndrome), testicular trauma, and retrograde ejaculation[68]. With the development of in vitro fertilization (IVF) and intracytoplasmic sperm injection (ICSI),

the importance of testicular-derived sperm in OA has become obvious[69]. To obtain testicular sperm, the use of a surgical testicular sperm extraction (TESE) method and nonsurgical methods such as testicular sperm aspiration (TESA) are employed to harvest tissue from the testis. From the harvested tissue, sperm have to be manually separated from unwanted debris such as blood cells and tissue cells. This process may be time consuming and tedious, but it is relatively easier to spot sperm cells in a mechanically minced sample than in a direct surgical sample from NOA patients[70]. While techniques like TESE and TESA have proven to be effective methods for retrieving sperm from patients with OA, these techniques have been less successful in obtaining sperm from patients with NOA. Because spermatogenesis is often sporadic and isolated to rare seminiferous tubules in NOA patients, a nonselective tissue abstraction approach usually misses sites of sperm production, leading to poor sperm recovery [67], [71].

NOA is known as the most severe form of male infertility and it is defined by the lack of sperm in the ejaculate and very little to no sperm production within the seminiferous tubules[72]. There are many potential causes for NOA, including genetic and congenital abnormalities, postinfection issues, exposure to gonadotoxins, medicatons, varicocele, trauma, endocrine disorders, and idiopathic causes[73]. NOA appears in about 10% of male infertility cases and in about 1% of the general male population[74].

Due to the extremely low number of sperm in NOA patients, finding and collecting sperm cells from these patients requires specially designed procedures. In order to collect sperm from NOA patients, a procedure called microdissection testicular sperm extraction (MicroTESE or mTESE) has been developed. MicroTESE (mTESE) is a modified version of TESE that includes the assistance of a high-powered operative microscope. This

modification made it possible to distinguish between seminiferous tubules with any germ cells and seminiferous tubules with focal spermatogenesis. This procedure has become significantly more successful in retrieving sperm from NOA patients than TESE.

Tissue obtained by mTESE requires careful processing in the laboratory in order to identify sperm among other unwanted debris such as blood cells. First, the collected seminiferous tubules are mechanically minced with syringe needles and glass slides, then resuspended in sperm media. Next, the tissue processing step requires manually searching through the testicular tissue specimens for sperm. However, testicular sperm are generally nonmotile and lie among a combination of red blood cells, white blood cells, Sertoli cells, sperm precursor cells, and cell tissue debris, which makes the search process extremely difficult and time consuming [76]. Each microscope field must be examined under 200-400× magnification to look for sperm in a sample that contains debris that must distinguished from the spermatocytes. Depending on the level of spermatogenesis and the number of sperm cells present, this procedure may take as little as one hour to find a sufficient number of sperm, or as long as 12-14 hours with multiple personnel examining tissue specimens to find just a few sperm cells[76]. In many cases, no sperm cells are found. The manual microscopic testicular specimen examination is extremely time-consuming and tedious, and is also greatly dependent on a person's skill level[67], [76]. Therefore, there is a need for a sample processing method with rapid and autonomous sample processing capability.

Leukospermia is a condition characterized by abnormally high white blood cell (WBC) concentrations in semen (>1 million WBCs/milliliter of semen), which may lead to infertility and render ineffective ART procedures such as Intrauterine Insemination (IUI).

As highlighted by Gambera [77], high concentrations of WBCs in the semen can cause disruption during fertilization. To deal with leukospermia, a density gradient centrifugation preparation method is widely utilized in fertility clinics as a WBC separation method. It consists of filtering sperm by centrifugal forces through either one or multiple layers of increasingly concentrated silane-coated silica particles. The process is able to generate a pellet at the bottom of the tube which contains a higher percentage of clean, motile sperm for IUI [78]. Unfortunately, this method can lead to low sperm recovery when the starting sample has a low concentration of sperm [79]. Additionally, it also requires significant time (~1 hr) to prepare the sample, which creates a potentially problematic time gap between sample preparation and insemination. Therefore, there is demand for a simple, rapid method that separates sperm from semen samples highly contaminated with unwanted debris. Additionally, a time reduction in sample preparation can provide a great deal of relief to IUI patients who are under stress from the IUI procedure itself.

1.3.2 Examples of Sperm Separation Approaches Utilizing Microfluidic Technology

Recently, a number of microfluidic approaches have been tried to separate sperm from unwanted debris and to improve the efficiency and the effectiveness of assisted reproductive technologies (ART) (Table 1.1). In one of the earliest approaches, a glass microfluidic chip containing multiple microchannels connecting an input reservoir to a collecting reservoir enabled motile sperm to swim to specific reservoirs where they could be collected while removing nonmotile sperm and debris [80], [81]. This technology first demonstrated the value of microfluidic platforms for sperm separation.

More recently, a common microfluidics approach for sperm separation has been

developed involving parallel laminar fluid streams of media through straight microchannels: one stream constituting a dilute semen sample, and the other stream constituting of sperm media [82], [83]. At the micro scale, the two fluid streams do not mix readily, so only motile sperm can travel across the interface between the two parallel streams. The two streams are separated again after a length sufficient to allow motile sperm to cross the boundary in high numbers, generating separation of motile sperm from nonmotile sperm and debris. Following a series of device optimizations, the utility of this technology for ART has been verified using sperm collected from the outlet for IVF [23], [84]–[88].

Another novel microfluidic approach to sperm separation utilizes chemotaxis in addition to motility. This approach induces sperm to travel through microchannels toward chemo-attractants which were applied to the bottom surface of the collection reservoirs at the periphery of the device [89]–[91].

Most of the sperm separation approaches utilizing microfluidics rely on sperm motility for separation with added features through which only highly motile sperm can pass: chemo-attractants, physical obstacles, and microdiffusers [80], [81], [90]–[99]. Thus, these techniques can separate only progressive motile sperm from semen samples, but they lose a significant number of sperm cells including viable nonprogressive motile and nonmotile sperm, and are not feasible for use with immature and nonmotile sperm that may be the only sperm produced by some patients (OA and NOA).

1.4 Dissertation Summary

This work will present methods to overcome the problems associated with OA and NOA by using a microfluidic system to separate sperm from a variety of contaminants. Chapter 2 describes the separation of sperm from red blood cells (RBCs) using a spiral channel. Chapter 3 describes a similar device for the separation of white blood cells from sperm samples. Chapter 4 describes a series of biocompatibility tests done to verify that the proposed devices would be usable in the clinic. Chapter 5 develops a mathematical model and simulations of sperm traveling through the channel to provide design insights related to an optimized spiral channel design. Chapter 6 provides the conclusions from this work.

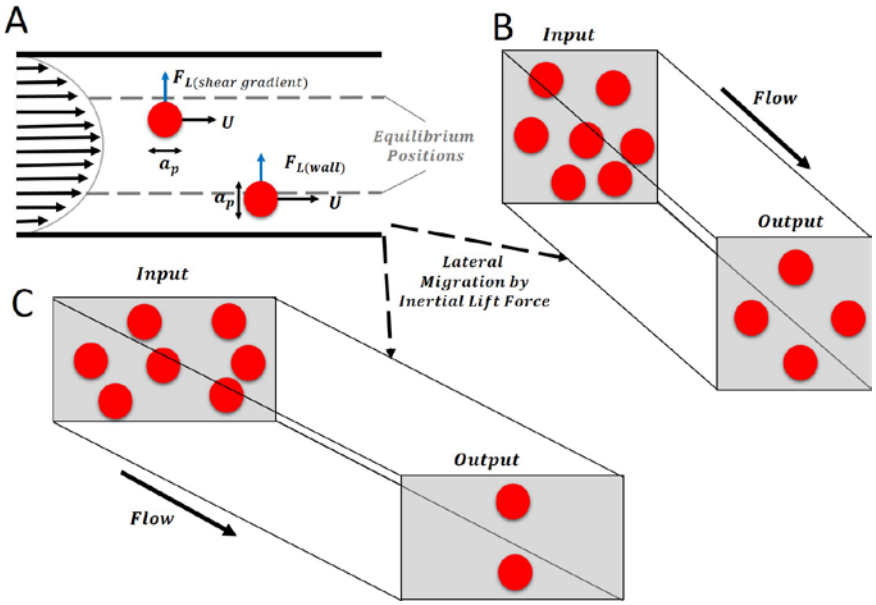

Figure 1.1 Inertial lift force in straight channels. (A) Two lift forces act on a particle between containg walls (a channel). Shear gradient lift force pushes a particle away from the center of channel while wall induced lift force push a particle away from the wall. The balance between the two forces defines the equilibrium position for the particle. (B) A channel with s square cross-section has four equilibrium positions due to lateral migration of particles with inertial lift force. (C) If the channel cross-section is rectangular, there are two equilibrium positions.

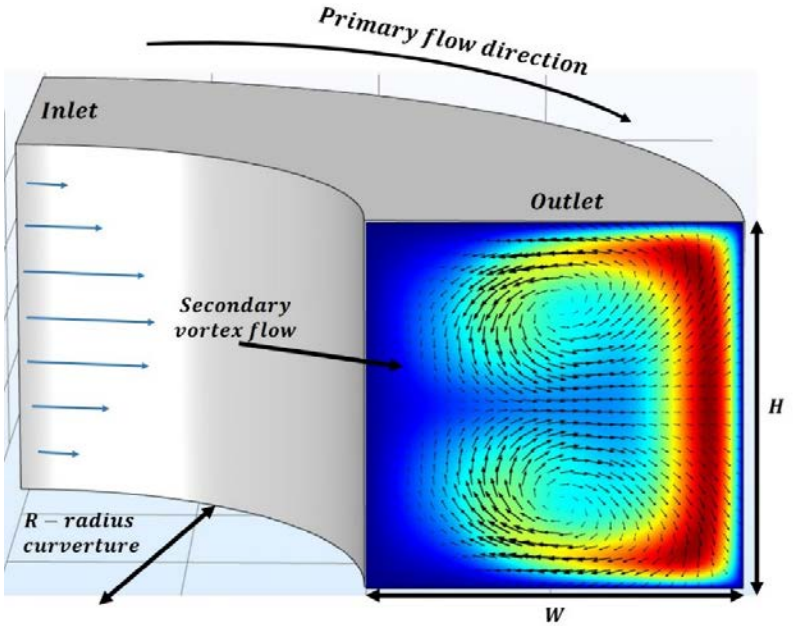

Figure 1.2 Dean flow in a curved channel. Symmetrically placed flow vortices are generated due to the velocity mismatch in the flow direction between fluid in the center and fluid near the wall area of a curved channel.

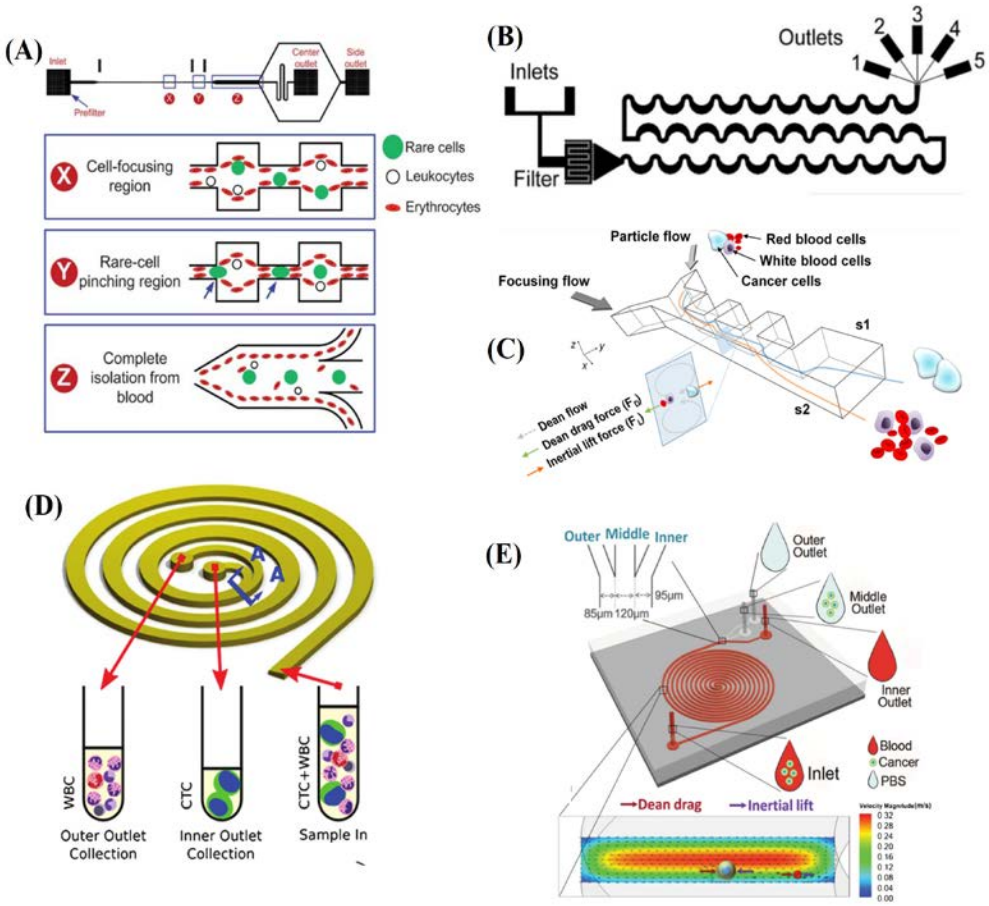

Figure 1.3 Examples of applying inertial particle focusing: (A) a high aspect ratio rectangular microchannel pattern with a contraction-expansion array[62], (B) a serpentine pattern curved channel array[64], (C) continuous square pattern channel[58], (D) a spiral channel[60], and (E) a sequential double spiral channel[53].

Table 1.1 Summary of conventional sperm separation techniques

Method	Mode of Separation/ Sorting	Separation/ Sorting Criteria	Collected Sample	Application	Reference
Microstructures	Micro channels + well + sperm motility	Sperm motility	Motile sperm (human / mouse)	Semen Testing	[80], [81]
Microstructures	Linear velocity distribution + Sperm motility	Sperm motility	Motile sperm (human, mouse, boar)	Motile sperm separation	[82], [86], [87], [93]
Microstructures	Sperm chemotaxis + Micro channels	Sperm motility	Motile sperm (mouse)	Motile sperm separation	[89]–[91]
Microstructures	Micro obstacle integrated micro fluidic channel + sperm motility	Sperm motility	Motile sperm (bull, mouse)	Sperm separation / screening	[96], [98]
Microstructures	Diffusing + sperm motility	Sperm motility	Motile sperm	Motile sperm sorting	[97]
Optical	Lens-less charge coupled device + sperm motility	Sperm motility	Motile sperm (mouse)	Motile sperm sorting / monitoring	[116]
Microstructures	Electrode integrated micro channels + sperm motility + electrode	Sperm motility	Motile sperm (boar)	Sperm concentration measurement	[117]

1.5 References

[1] G. Velve-Casquillas, M. Le Berre, M. Piel, and P. T. Tran, "Microfluidic tools for cell biological research," *Nano Today*, vol. 5, no. 1, pp. 28–47, Feb. 2010.

[2] S. Cho, D. K. Kang, J. Choo, A. J. deMello, and S. I. Chang, "Recent advances in microfluidic technologies for biochemistry and molecular biology," *BMB Rep.*, vol. 44, no. 11, pp. 705–712, Nov. 2011.

[3] D. C. Duffy, J. C. McDonald, O. J. A. Schueller, and G. M. Whitesides, "Rapid prototyping of microfluidic systems in poly(dimethylsiloxane)," *Anal. Chem.*, vol. 70, no. 23, pp. 4974–4984, Oct. 1998.

[4] K. Ohno, K. Tachikawa, and A. Manz, "Microfluidics: Applicatons analytical purposes in chemistry and biochemistry," *Electrophoresis*, vol. 29, pp. 4443–4453, Nov. 2008.

[5] Y. Zhang *et al.*, "DNA methylation analysis on a droplet-in-oil PCR array.," *Lab Chip*, vol. 9, no. 8, pp. 1059–1064, Apr. 2009.

[6] C. Wyatt Shields IV, C. D. Reyes, and G. P. López, "Microfluidic cell sorting: A review of the advances in the separation of cells from debulking to rare cell isolation," *Lab Chip*, vol. 15, no. 5, pp. 1230–1249, Jan. 2015.

[7] H. Andersson and A. Van den Berg, "Microfluidic devices for cellomics: A review," *Sensors Actuators, B Chem.*, vol. 92, no. 3, pp. 315–325, Jul. 2003.

[8] S. M. Kim, S. H. Lee, and K. Y. Suh, "Cell research with physically modified microfluidic channels: A review," *Lab a Chip - Miniaturisation Chem. Biol.*, vol. 8, no. 7, pp. 1015–1023, Jul. 2008.

[9] R. N. Zare and S. Kim, "Microfluidic platforms for single-cell analysis," *Annu. Rev. Biomed. Eng.*, vol. 12, no. 1, pp. 187–201, Apr. 2010.

[10] A. Lenshof and T. Laurell, "Continuous separation of cells and particles in microfluidic systems," *Chem. Soc. Rev.*, vol. 39, no. 3, pp. 1203–1217, Feb. 2010.

[11] D. R. Gossett *et al.*, "Label-free cell separation and sorting in microfluidic systems," *Anal. Bioanal. Chem.*, vol. 397, no. 8, pp. 3249–67, Aug. 2010.

[12] A. A. S. Bhagat, H. Bow, H. W. Hou, S. J. Tan, J. Han, and C. T. Lim, "Microfluidics for cell separation," *Med. Biol. Eng. Comput.*, vol. 48, no. 10, pp. 999–1014, Oct. 2010.

[13] S. Choi and J.-K. Park, "Microfluidic system for dielectrophoretic separation based on a trapezoidal electrode array," *Lab Chip*, vol. 5, no. 10, pp. 1161–1167, Oct.

2005.

[14] A. F. Cowman and B. S. Crabb, “Review invasion of red blood cells by malaria parasites,” *Cell,* pp. 755–766, Feb. 2006.

[15] W. J. Kleijer, M. L. T. van der Sterre, V. H. Garritsen, A. Raams, and N. G. J. Jaspers, “Prenatal diagnosis of the Cockayne syndrome: Survey of 15 years experience,” *Prenat. Diagn.*, vol. 26, no. 10, pp. 980–984, Oct. 2006.

[16] S. Nagrath *et al.*, “Isolation of rare circulating tumour cells in cancer patients by microchip technology,” *Nature*, vol. 450, pp. 1235-1239, December, 2007.

[17] F. Petersson, L. Åberg, A. M. Swärd-Nilsson, and T. Laurell, “Free flow acoustophoresis: Microfluidic-based mode of particle and cell separation,” *Anal. Chem.*, vol. 79, no. 14, pp. 5117–5123, Jun. 2007.

[18] E. L. Tóth, E. Holczer, P. Földesy, K. Iván, and P. Fürjes, “Microfluidic particle sorting system for environmental pollution monitoring applications,” *Procedia Eng.*, vol. 168, pp. 1462–1465, Sep. 2016.

[19] N. Xia *et al.*, “Combined microfluidic-micromagnetic separation of living cells in continuous flow,” *Biomed. Microdevices*, vol. 8, no. 4, pp. 299–308, Dec. 2006.

[20] B. H. Weigl and P. Yager, “Microfluidic diffusion-based separation and detection,” *Science*, vol. 283, no. 5400, p. 346 LP-347, Jan. 1999.

[21] D. W. Inglis, “Efficient microfluidic particle separation arrays,” *Appl. Phys. Lett.*, vol. 94, no. 1, Jan. 2009.

[22] J. Nam, H. Lim, D. Kim, H. Jung, and S. Shin, “Continuous separation of microparticles in a microfluidic channel via the elasto-inertial effect of non-Newtonian fluid,” *Lab Chip*, vol. 12, no. FEBRUARY, p. 1347, Jan. 2012.

[23] J. E. Swain, D. Lai, S. Takayama, and G. D. Smith, “Thinking big by thinking small: Application of microfluidic technology to improve ART,” *Lab Chip*, vol. 13, no. 7, pp. 1213–24, Apr. 2013.

[24] G. Segré and A. Silberberg, “Radial particle displacements in poiseuille flow of suspensions,” *Comput. Geotech.*, vol. 189, no. 4760, pp. 209–210, Jan. 1961.

[25] D. Di Carlo, “Inertial microfluidics,” *Lab Chip*, vol. 9, no. 21, pp. 3038–3046, Nov. 2009.

[26] J. M. Martel and M. Toner, “Inertial focusing dynamics in spiral microchannels,” *Phys. Fluids*, vol. 24, no. 3, p. 32001, Mar. 2012.

[27] H. Amini, W. Lee, and D. Di Carlo, "Inertial microfluidic physics," *Lab Chip*, vol. 14, no. 15, pp. 2739–61, May. 2014.

[28] E. S. Asmolov, "The inertial lift on a spherical particle in a plane Poiseuille flow at large channel Reynolds number," *J. Fluid Mech.*, vol. 381, pp. 63–87, Jan. 1999.

[29] D. Di Carlo, J. F. Edd, K. J. Humphry, H. A. Stone, and M. Toner, "Particle segregation and dynamics in confined flows," *Phys. Rev. Lett.*, vol. 102, no. 9, pp. 1–4, Mar. 2009.

[30] J. Zhou and I. Papautsky, "Fundamentals of inertial focusing in microchannels," *Lab Chip*, vol. 13, no. 6, pp. 1121–32, Mar. 2013.

[31] J. M. Martel and M. Toner, "Particle focusing in curved microfluidic channels," *Sci. Rep.*, vol. 3, pp. 1–8, Nov. 2013.

[32] P. G. Saffman, "The lift on a small sphere in a slow shear flow," *J. Fluid Mech.*, vol. 22, no. 2, pp. 385–400, Fe. 1965.

[33] S. I. Rubinow and J. B. Keller, "The transverse force on a spinning sphere moving in a viscous fluid," *J. Fluid Mech.*, vol. 11, no. 3, pp. 447–459, Nov. 1961.

[34] B. P. Ho and L. G. Leal, "Migration of rigid spheres in a two-dimensional unidirectional shear flow of a second-order fluid," *J. Fluid Mech.*, vol. 65, no. 2, pp. 365–400, Aug. 1974.

[35] W. R. Dean, "LXXII. The stream-line motion of fluid in a curved pipe (Second paper)," *London, Edinburgh, Dublin Philos. Mag. J. Sci.*, vol. 5, no. 30, pp. 673–695, Apr. 1928.

[36] S. A. Berger, L. Talbot, and L. S. Yao, "Flow in curved pipes," *Annu. Rev. Fluid Mech.*, vol. 15, pp. 461–512, Jan. 1983.

[37] D. R. Gossett and D. Di Carlo, "Particle focusing mechanisms in curving confined flows," *Anal. Chem.*, vol. 81, no. 20, pp. 8459–8465, Sep. 2009.

[38] D. Di Carlo, D. Irimia, R. G. Tompkins, and M. Toner, "Continuous inertial focusing, ordering, and separation of particles in microchannels," *Proc. Natl. Acad. Sci. U. S. A.*, vol. 104, no. 48, pp. 18892–18897, Nov. 2007.

[39] A. A. S. Bhagat, S. S. Kuntaegowdanahalli, and I. Papautsky, "Continuous particle separation in spiral microchannels using Dean flows and differential migration," *Lab Chip*, vol. 8, no. 11, pp. 1906–1914, Nov. 2008.

[40] S. Ookawara, R. Higashi, D. Street, and K. Ogawa, "Feasibility study on concentration of slurry and classification of contained particles by microchannel,"

Chem. Eng. J., vol. 101, no. 1–3, pp. 171–178, Aug. 2004.

[41] A. A. S. Bhagat, S. S. Kuntaegowdanahalli, and I. Papautsky, "Enhanced particle filtration in straight microchannels using shear-modulated inertial migration," *Phys. Fluids*, vol. 20, no. 10, 2008.

[42] D. Di Carlo, "Inertial microfluidics," *Lab Chip*, vol. 9, no. 21, pp. 3038–46, Nov. 2009.

[43] F. P. Bretherton, "The motion of rigid particles in a shear flow at low Reynolds number," *J. Fluid Mech.*, vol. 14, no. 2, pp. 284–304, Oct. 1962.

[44] W. E. Uspal, H. Burak Eral, and P. S. Doyle, "Engineering particle trajectories in microfluidic flows using particle shape," *Nat. Commun.*, vol. 4, p. 2666, Apr. 2013.

[45] T. Kaya and H. Koser, "Characterization of hydrodynamic surface interactions of escherichia coli cell bodies in shear flow," *Phys. Rev. Lett.*, vol. 103, no. 13, pp. 1–4, Sep. 2009.

[46] G. B. Jeffery, "The motion of ellipsoidal particles immersed in a viscous fluid," *Math. Phys. Eng. Sci.*, pp. 161–179, Nov. 1922.

[47] C. Y. Wu, K. Owsley, and D. Di Carlo, "Rapid software-based design and optical transient liquid molding of microparticles," *Adv. Mater.*, vol. 27, no. 48, pp. 7970–7978, Oct. 2015.

[48] M. L. Ekiel-Jeżewska and E. Wajnryb, "Hydrodynamic orienting of asymmetric microobjects under gravity," *J. Phys. Condens. Matter*, vol. 21, no. 20, p. 204102, May. 2009.

[49] P. J. A. Janssen, M. D. Baron, P. D. Anderson, J. Blawzdziewicz, M. Loewenberg, and E. Wajnryb, "Collective dynamics of confined rigid spheres and deformable drops," *Soft Matter*, vol. 8, no. 28, pp. 7495–7506, Aug. 2012.

[50] S. C. Hur, S. E. Choi, S. Kwon, and D. Di Carlo, "Inertial focusing of non-spherical microparticles," *Appl. Phys. Lett.*, vol. 99, no. 4, pp. 1–4, Jul. 2011.

[51] J. Elgeti, U. B. Kaupp, and G. Gompper, "Hydrodynamics of sperm cells near surfaces," *Biophysj*, vol. 99, no. 4, pp. 1018–1026, Aug. 2010.

[52] W. Lee, H. Amini, H. A Stone, and D. Di Carlo, "Dynamic self-assembly and control of microfluidic particle crystals," *Proc. Natl. Acad. Sci. U. S. A.*, vol. 107, no. 52, pp. 22413–22418, Dec. 2010.

[53] J. Sun *et al.*, "Double spiral microchannel for label-free tumor cell separation and

enrichment," *Lab Chip*, vol. 12, no. 20, p. 3952, Jul. 2012.

[54] M. Jimenez, B. Miller, and H. L. Bridle, "Efficient separation of small microparticles at high flowrates using spiral channels: Application to waterborne pathogens," *Chem. Eng. Sci.*, vol. 157, pp. 247–254, Jan. 2017.

[55] Z. Wu, B. Willing, J. Bjerketorp, J. K. Jansson, and K. Hjort, "Soft inertial microfluidics for high throughput separation of bacteria from human blood cells," *Lab Chip*, vol. 9, no. 9, pp. 1193–9, May. 2009.

[56] A. J. Mach and D. di Carlo, "Continuous scalable blood filtration device using inertial microfluidics," *Biotechnol. Bioeng.*, vol. 107, no. 2, pp. 302–311, Oct. 2010.

[57] X. Wang, C. Liedert, R. Liedert, and I. Papautsky, "A disposable, roll-to-roll hot-embossed inertial microfluidic device for size-based sorting of microbeads and cells," *Lab Chip*, vol. 16, pp. 1821–1830, May. 2016.

[58] M. G. Lee, J. H. Shin, C. Y. Bae, S. Choi, and J. K. Park, "Label-free cancer cell separation from human whole blood using inertial microfluidics at low shear stress," *Anal. Chem.*, vol. 85, no. 13, pp. 6213–6218, Jun. 2013.

[59] N. Nivedita and I. Papautsky, "Continuous separation of blood cells in spiral microfluidic devices," *Biomicrofluidics*, vol. 7, no. 5, Sep. 2013.

[60] M. E. Warkiani *et al.*, "Slanted spiral microfluidics for the ultra-fast, label-free isolation of circulating tumor cells," *Lab Chip*, vol. 14, no. 1, pp. 128–37, Jan. 2014.

[61] T. H. Kim, H. J. Yoon, P. Stella, and S. Nagrath, "Cascaded spiral microfluidic device for deterministic and high purity continuous separation of circulating tumor cells," *Biomicrofluidics*, vol. 8, no. 6, p. 64117, Dec. 2014.

[62] A. A. S. Bhagat, H. W. Hou, L. D. Li, C. T. Lim, and J. Han, "Pinched flow coupled shear-modulated inertial microfluidics for high-throughput rare blood cell separation," *Lab Chip*, vol. 11, no. 11, pp. 1870–1878, Apr. 2011.

[63] S. Shen *et al.*, "High-throughput rare cell separation from blood samples using steric hindrance and inertial microfluidics," *Lab Chip*, vol. 14, no. 14, pp. 2525–38, Jul. 2014.

[64] D. Di Carlo, J. F. Edd, D. Irimia, R. G. Tompkins, and M. Toner, "Equilibrium separation and filtration of particles using differential inertial focusing," *Anal. Chem.*, vol. 80, no. 6, pp. 2204–2211, Feb. 2008.

[65] J. Boivin, L. Bunting, J. A. Collins, and K. G. Nygren, "International estimates of

infertility prevalence and treatment-seeking: Potential need and demand for infertility medical care," *Hum. Reprod.*, vol. 22, no. 6, pp. 1506–1512, Jun. 2007.

[66] T. G. Cooper *et al.*, "World Health Organization reference values for human semen characteristics," *Hum. Reprod. Update*, vol. 16, no. 3, pp. 231–245, May-Jun. 2009.

[67] R. Samuel *et al.*, "Microfluidics: The future of microdissection TESE?," *Syst. Biol. Reprod. Med.*, vol. 62, no. 3, pp. 161–70, Jun. 2016.

[68] K. Baker and E. Sabanegh, "Obstructive azoospermia: Reconstructive techniques and results," *Clinics*, vol. 68, no. S1, pp. 61–73, Feb. 2013.

[69] I. Craft *et al.*, "Percutaneous epididymal sperm aspiration and intracytoplasmic sperm injection in the management of infertility due to obstructive azoospermia," *Fertil. Steril.*, vol. 63, no. 5, pp. 1038–42, May. 1995.

[70] P. N. Schlegel, "Testicular sperm extraction: Microdissection improves sperm yield with minimal tissue excision," *Hum. Reprod.*, vol. 14, no. 1, pp. 131–135, Jan. 1999.

[71] P. N. Schlegel and L. M. Su, "Physiological consequences of testicular sperm extraction," *Hum. Reprod.*, vol. 12, no. 8, pp. 1688–1692, Aug. 1997.

[72] R. Kumar, "Medical management of non-obstructive azoospermia," *Clinics.* vol. 2013, pp. 75–79, Feb. 2013.

[73] P. Donoso, H. Tournaye, and P. Devroey, "Which is the best sperm retrieval technique for non-obstructive azoospermia? A systematic review," *Hum. Reprod. Update*, vol. 13, no. 6, pp. 539–549, Nov-Dec. 2007.

[74] C. Krausz, "Male infertility: Pathogenesis and clinical diagnosis," *Best Pract. Res. Clin. Endocrinol. Metab.*, vol. 25, no. 2, pp. 271–85, Apr. 2011.

[75] A. Bettegowda and M. F. Wilkinson, "Transcription and post-transcriptional regulation of spermatogenesis," *Philos. Trans. R. Soc. Lond. B. Biol. Sci.*, vol. 365, no. 1546, pp. 1637–1651, May. 2010.

[76] M. Ostad, D. Liotta, Z. Ye, P. N. Schlegel, "Teticular sperm extraction for nonobstructive azoospermia: Results of a multibiopsy approach with optimized tissue dispersion," *Urology*, vol. 4295, no. 98, pp. 692–696, Oct. 1998.

[77] L. Gambera, F. Serafini, G. Morgante, R. Focarelli, V. De Leo, and P. Piomboni, "Sperm quality and pregnancy rate after COX-2 inhibitor therapy of infertile males with abacterial leukocytospermia," *Hum. Reprod.*, vol. 22, no. 4, pp. 1047–1051, Apr. 2007.

[78] C. M. Peterson, A. O. Hammoud, E. Lindley, D. T. Carrell, and K. Wilson, "Assisted Reproductive Technology Practice Management", *Reproductive Endocrinology and Infertility*, D. T. Carrell, C. M. Peterson, Ed. New York: Springer, 2010, pp. 7-37.

[79] M. J. Chen and A. Bongso, "Comparative evaluation of two density gradient preparations for sperm separation for medically assisted conception," *Hum. Reprod.*, vol. 14, no. 3, pp. 759–764, Mar. 1999.

[80] L. J. Kricka *et al.*, "Micromachined analytical devices: Microchips for semen testing," *J. Pharm. Biomed. Anal.*, vol. 15, no. 9–10, pp. 1443–7, Jun. 1997.

[81] S. Tasoglu *et al.*, "Exhaustion of racing sperm in nature-mimicking microfluidic channels during sorting," *Small*, vol. 9, no. 20, pp. 3374–3384, Oct. 2013.

[82] B. S. Cho, T. G. Schuster, X. Zhu, D. Chang, G. D. Smith, and S. Takayama, "Passively driven integrated microfluidic system for separation of motile sperm," *Anal. Chem.*, vol. 75, no. 7, pp. 1671–1675, Feb. 2003.

[83] T. G. Schuster, B. Cho, L. M. Keller, S. Takayama, and G. D. Smith, "Isolation of motile spermatozoa from semen samples using microfluidics," *Reprod. Biomed. Online*, vol. 7, no. 1, pp. 75–81, Jan. 2003.

[84] H. Huang, "Motile human sperm sorting by an integrated microfluidic system," *J. Nanomed. Nanotechnol.*, vol. 5, no. 3, pp. 193-199, May. 2014.

[85] H.-Y. Huang *et al.*, "Isolation of motile spermatozoa with a microfluidic chip having a surface-modified microchannel," *J. Lab. Autom.*, vol. 19, no. 1, pp. 91–9, Feb. 2013.

[86] K. Matsuura, M. Takenami, Y. Kuroda, T. Hyakutake, S. Yanase, and K. Naruse, "Screening of sperm velocity by fluid mechanical characteristics of a cyclo-olefin polymer microfluidic sperm-sorting device," *Reprod. Biomed. Online*, vol. 24, no. 1, pp. 109–15, Jan. 2012.

[87] H. Sano, K. Matsuura, K. Naruse, and H. Funahashi, "Application of a microfluidic sperm sorter to the in-vitro fertilization of porcine oocytes reduced the incidence of polyspermic penetration," *Theriogenology*, vol. 74, no. 5, pp. 863–70, Sep. 2010.

[88] J. M. Wu, Y. Chung, K. J. Belford, G. D. Smith, S. Takayama, and J. Lahann, "A surface-modified sperm sorting device with long-term stability," *Biomed. Microdevices*, vol. 8, no. 2, pp. 99–107, Jun. 2006.

[89] S. Koyama, D. Amarie, H. Soini, M. Novotny, and S. Jacobson, "Chemotaxis assays of mouse sperm on microfluidic devices," *Anal. chem.*, vol. 78, no. 10, pp.

3354–3359, Apr. 2006.

[90] L. Xie *et al.*, "Integration of sperm motility and chemotaxis screening with a microchannel-based device," *Clin. Chem.*, vol. 56, no. 8, pp. 1270–8, Aug. 2010.

[91] Y.-J. Ko, J.-H. Maeng, B.-C. Lee, S. Lee, S. Y. Hwang, and Y. Ahn, "Separation of progressive motile sperm from mouse semen using on-chip chemotaxis," *Anal. Sci.*, vol. 28, no. 1, pp. 27–32, Jan. 2012.

[92] S. S. Suarez and M. Wu, "Microfluidic devices for the study of sperm migration," *Mol. Hum. Reprod.*, pp. 1–8, Apr. 2017.

[93] C.-Y. Chen *et al.*, "Sperm quality assessment via separation and sedimentation in a microfluidic device," *Analyst*, vol. 138, no. 17, pp. 4967–74, Sep. 2013.

[94] S. M. Knowlton, M. Sadasivam, and S. Tasoglu, "Microfluidics for sperm research," *Trends Biotechnol.*, vol. 33, no. 4, pp. 221–229, Apr. 2015.

[95] R. Ma *et al.*, "In vitro fertilization on a single-oocyte positioning system integrated with motile sperm selection and early embryo development," *Anal. Chem.*, vol. 83, no. 8, pp. 2964–2970, Mar. 2011.

[96] Y. Lin, P. Chen, R. Wu, L. Pan, and F. Tseng, "Micro diffuser-type movement inversion sorter for high-efficient sperm sorting," *Int. Conf Nano/Micro Eng. Mol. Syst.*, pp. 7–10, Apr. 2013.

[97] M. D. C. Lopez-Garcia, R. L. Monson, K. Haubert, M. B. Wheeler, and D. J. Beebe, "Sperm motion in a microfluidic fertilization device," *Biomed. Microdevices*, vol. 10, no. 5, pp. 709–718, Oct. 2008.

[98] M. Wheeler and M. Rubessa, "Integration of Microfluidics and Mammalian IVF," *Mol. Hum Regrod,* vol. 23, iss. 4, pp. 248–256, Apr. 2017.

[99] R. S. Suh, X. Zhu, N. Phadke, D. A. Ohl, S. Takayama, and G. D. Smith, "IVF within microfluidic channels requires lower total numbers and lower concentrations of sperm," *Hum. Reprod.*, vol. 21, no. 2, pp. 477–483, Feb. 2006.

[100] J. Son, K. Murphy, R. Samuel, B. Gale, D. Carrell, and J. Hotaling, "Non-motile sperm cell separation using a spiral channel," *Anal. Methods*, iss. 7, pp. 8041-8047, May. 2015.

[101] S. S. Kuntaegowdanahalli, A. A. S. Bhagat, G. Kumar, and I. Papautsky, "Inertial microfluidics for continuous particle separation in spiral microchannels," *Lab Chip*, vol. 9, no. 20, pp. 2973–80, Oct. 2009.

[102] P. R. Wheater, H. G. Burkitt, and V. G. Daniels, *Functional Histology. A Text and*

Colour Atlas. Edinburgh: Churchill, 1979.

[103] M. Diez-Silva, M. Dao, J. Han, C.-T. Lim, and S. Suresh, "Shape and biomechanical characteristics of human red blood cells in health and disease," *MRS Bull.*, vol. 35, no. 5, pp. 382–388, May. 2010.

[104] J. A. Mossman, J. T. Pearson, H. D. Moore, and A. A. Pacey, "Variation in mean human sperm length is linked with semen characteristics," *Hum. Reprod.*, vol. 28, no. 1, pp. 22–32, Jan. 2013.

[105] L. Maree, S. S. Du Plessis, R. Menkveld, and G. Van Der Horst, "Morphometric dimensions of the human sperm head depend on the staining method used," *Hum. Reprod.*, vol. 25, no. 6, pp. 1369–1382, Jun. 2010.

[106] J. E. Lackner, I. Märk, K. Sator, J. Huber, and M. Sator, "Effect of leukocytospermia on fertilization and pregnancy rates of artificial reproductive technologies," *Fertil. Steril.*, vol. 90, no. 3, pp. 869–871, Sep. 2008.

[107] N. Nivedita and I. Papautsky, "Continuous separation of blood cells in spiral microfluidic devices," *Biomicrofluidics*, vol. 7, no. 5, pp. 1–14, Sep. 2013.

[108] J.-P. Frimat *et al.*, "Make it spin: Individual trapping of sperm for analysis and recovery using micro-contact printing," *Lab Chip*, vol. 14, no. 15, pp. 2635–41, Aug. 2014.

[109] C. Ainsworth, B. Nixon, R. P. S. Jansen, and R. J. Aitken, "First recorded pregnancy and normal birth after ICSI using electrophoretically isolated spermatozoa," *Hum. Reprod.*, vol. 22, no. 1, pp. 197–200, Sep. 2007.

[110] R. Zeggari, B. Wacogne, C. Pieralli, C. Roux, and T. Gharbi, "A full micro-fluidic system for single oocyte manipulation including an optical sensor for cell maturity estimation and fertilisation indication," *Sensors Actuators, B Chem.*, vol. 125, no. 2, pp. 664–671, Aug. 2007.

[111] A. A. El-Ghobashy and C. R. West, "The human sperm head: A key for successful fertilization," *J. Androl.*, vol. 24, no. 2, pp. 232–8, Mar-Apr. 2003.

[112] WHO, *Examination and processing of human semen*, 5th ed, WHO, Geneva: Swiss. 2010.

[113] M. Ionescu *et al.*, "Enhanced biocompatibility of PDMS (polydimethylsiloxane) polymer films by ion irradiation," *Nucl. Inst. Methods Phys. Res. B*, vol. 273, pp. 161–163, Feb. 2012.

[114] C. Garrett, D. Y. Liu, R. I. McLachlan, and H. W. G. Baker, "Time course of changes in sperm morphometry and semen variables during testosterone-induced

suppression of human spermatogenesis," *Hum. Reprod.*, vol. 20, no. 11, pp. 3091–3100, Nov. 2005.

[115] N. Guz, M. Dokukin, V. Kalaparthi, and I. Sokolov, "If cell mechanics can be described by elastic modulus: Study of different models and probes used in indentation experiments," *Biophys. J.*, vol. 107, no. 3, pp. 564–575, Aug. 2014.

[116] X. Zhang *et al.*, "Lensless imaging for simultaneous microfluidic sperm monitoring and sorting," *Lab Chip*, vol. 11, no. 15, pp. 2535–2540, Aug. 2011.

[117] L. I. Segerink, A. J. Sprenkels, P. M. ter Braak, I. Vermes, and A. van den Berg, "On-chip determination of spermatozoa concentration using electrical impedance measurements," *Lab Chip*, vol. 10, no. 8, pp. 1018–24, Apr. 2010.

CHAPTER 2

NONMOTILE SPERM CELL SEPARATION USING A SPIRAL CHANNEL

Analytical Methods

PAPER

View Article Online
View Journal | View Issue

CrossMark click for updates

Cite this: *Anal. Methods*, 2015, 7, 8041

Non-motile sperm cell separation using a spiral channel

Jiyoung Son,[a] Kristin Murphy,[b] Raheel Samuel,[c] Bruce K. Gale,[c] Douglas T. Carrell[b] and James M. Hotaling[b]

Microfluidic sperm sorting has historically relied on sperm motility. However, a motility-based sperm separation technology will not work when viable, non-motile sperm need to be separated from other tissues as occurs when performing testicular sperm extraction (TESE) and microdissection testicular sperm extraction (mTESE) techniques. This work demonstrates the use of inertial microfluidics technology using spiral channels to separate sperm from blood cells. The separation method, which is label-free, does not rely on sperm motility for sorting. Basic principles of spiral channel separations were used to design a specific channel and flow parameters for separating non-motile sperm from blood. The spiral channels dimensions were: initial radius, 0.7 cm; final radius, 0.899 cm; channel width, 150 μm; channel height, 50 μm; turns of spiral, 4 turns; and space between channels, 310 μm. If sperm are modeled as a 5 μm sphere, inertial microfluidics theory suggests that the sperm could be focused and separated from red blood cells (RBCs). Channels to implement these features were validated in a series of experiments. Mixed samples of RBCs and sperm were used to test the sperm separation capability of the device with the sample injection flow rate ranging from 0.1–0.52 ml min^{-1}. After running the sample through the spiral channel, the samples were collected from four outlets and were inspected using microscopy. The best results were obtained at a 0.52 ml min^{-1} flow rate and generated a concentration ratio of 81%, representing the percent of sperm collected from the two outer outlets. For the same conditions, 99% of RBCs were collected from the two inner wall outlets. Using a high speed scanner, we were able to observe the focusing of the RBCs and general focusing of the sperm. As the sperm are not a uniform shape, they did not focus in a tight band, but were collected in a general region of the channel. Nevertheless, the purification ratio for these sperm was sufficient to greatly enhance the likelihood of finding rare sperm in TESE/mTESE samples containing millions of blood cells. Sequentially processing of the samples in the system proved to further improve the ratio of sperm to blood cells.

Received 21st August 2015
Accepted 24th August 2015

DOI: 10.1039/c5ay02205c

www.rsc.org/methods

Introduction

Microfluidic techniques for cell manipulation and analysis have proven to be valuable tools for understanding molecular and cell biology. In addition, microfluidic technologies enable the development of diagnostics and treatments for human disease.[1] In the field of *assisted reproductive technology* (ART), microfluidics has become beneficial for gamete (sperm or egg) sorting and selection. In recent years, a number of microfluidic devices have been developed for sperm manipulation, allowing the sorting of healthy sperm to use for *in vitro* fertilization (IVF).[1] These technologies enable automation to replace tedious, manual approaches to viable sperm cell sorting from semen specimens, which requires hours of work by highly trained personnel.

One of the earliest microfluidic approaches for sperm manipulation contained multiple, straight microchannels connecting an input reservoir to a collection reservoir, enabling motile sperm to swim to the specific reservoir where they could be collected, while non-motile sperm and debris stayed behind in the inlet reservoir.[2] Today, the most popular microfluidics approach for sperm separation utilizes the introduction of parallel laminar streams of media through a straight microchannel. The parallel laminar streams are generated by introducing a dilute semen sample as well as media though two inlets. According to hydrodynamic principles,[3] these two streams do not readily mix together, creating a boundary between the streams. Because motile sperm can swim across the boundary, they are able to enter the collection stream, while the non-motile sperm and debris are washed away to a waste collection area. Another notable sperm separation technique utilizes chemotaxis of sperm in addition to sperm mobility by inducing sperm to swim through microchannels toward chemoattractants applied to the surface of outlet reservoirs.[4]

[a]*Department of Electrical and Computer Engineering, University of Utah, USA*
[b]*Urology Division, Department of Surgery, University of Utah School of Medicine, USA. E-mail: Jim.Hotaling@hsc.utah.edu*
[c]*Department of Mechanical Engineering, University of Utah, USA*

Techniques have also been utilized in which a sample is inserted into an induced slow flow through a horizontal obstacle within a microchannel. This method screens out non-motile sperm and debris, which settle behind the inlet area, while motile sperm swim under/over the obstacle toward the outlet reservoir.[5] There have also been efforts to improve sperm quality with electrophoretic isolation methods, which require porous membrane filters to isolate the desired sperm cells.[6,7]

Most existing conventional sperm separation approaches, such as those described above, utilize the motility of sperm to generate a separation. However, these motility based techniques cannot be applied to sperm samples containing only non-motile sperm, such as those obtained from non-obstructive azoospermia (NOA) patients from which no sperm is found within the ejaculate. For these patients immature testicular sperm may be obtained by surgical procedures called testicular sperm extraction (TESE) and microdissection testicular sperm extraction (mTESE). TESE/mTESE specimens contain a combination of red blood cells (RBCs), white blood cells, Sertoli cells, and debris that must be distinguished from a limited number of non-motile spermatocytes (0–4000 ea ml^{-1}), making the search for and separation of sperm extremely difficult using current manual approaches (Fig. 1).[8] Even active sperm isolation techniques, such as electrophoretic sperm isolation,[6,7] will cause a loss of sperm and possible DNA damage.

Recently cell separations using inertial microfluidics have been demonstrated for collecting rare cells from blood such as circulating tumor cells. Without the use of any cell labelling, these studies show great potential for pure mechanical separation of other rare cells using inertial microfluidics. These studies suggest that a precisely designed spiral channel could generate flow focusing of sperm and be a suitable solution for precision sperm separations.[9–12]

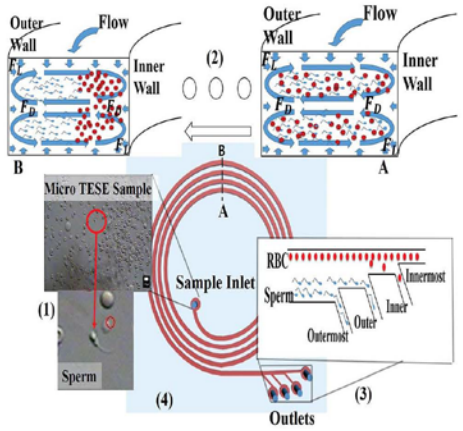

Fig. 1 Overview of the device, (1) a sample (mTESE/TESE or simulated) injecting in the inlet of the channel, (2) flow focusing caused by lift forces (F_L) and Dean drag (F_D) from inertial microfluidics effect, (3) separated sperm and RBC by flow-focusing.

In this work we demonstrate the use of inertial microfluidic technology to separate sperm from the major contaminant of TESE/mTESE samples, RBCs, by focusing the sperm and RBCs to different areas of the flow. Unlike other work on microfluidic sperm isolation, this separation method is not based on sperm motility and is label-free, which is required if the separated sperm are to be used clinically in a later step. The results show moderate non-motile sperm focusing and clear RBC focusing, which could be used for sperm separation from surgical samples derived using TESE/mTESE.

Design principle/theory

Substantial theory on the physics of flow focusing in spiral channels exists and was used to design a spiral channel for flow-focusing of non-motile sperm cells. The optimal dimensions of the spiral channel can be precisely calculated based on previously studied inertial microfluidics principles such as: the ratio of the inertial lift forces to the Dean drag force (R_f), the ratio between particle and channel dimension (λ), and the aspect ratio of the channel cross-section.[13–17] Flow focusing in spiral channels requires a balance between inertial lift forces (F_L), which push particles away from a wall, and Dean drag (F_D), a force generated by a lateral, secondary-vortex flow along a spiral channel. The balance can be established for a given particle type when certain physical parameters of the flow are in specified ranges. The inertial lift forces (F_L) and Dean drag (F_D) can be calculated by

$$F_D = 3\pi\mu U_{Dean} a_p \quad (1)$$

$$F_L = 0.05\frac{a_p^4 \rho U_m^2}{D_h^2} \quad (2)$$

where μ is fluid viscosity, U_{Dean} is average Dean velocity, a_p is particle diameter, U_m maximum fluid velocity, and D_h is hydrodynamic diameter for a rectangular channel. For focusing, the ratio (R_f) between inertial lift forces, and Dean drag, is given by[16]

$$R_f = \frac{F_L}{F_D} \geq \sim 0.08. \quad (3)$$

R_f should be greater than 0.08, which makes the Dean drag dominant (eqn (3)). For strong focusing, the particle/channel dimension ratio (λ), given by

$$\lambda = \frac{a_p}{D_h} \geq 0.07, \quad (4)$$

should be greater than 0.07.[17] Based on previous experimental studies, the aspect ratio of the channel should be between ~1 : 2 and 1 : 4 (height : width).[18,19] Using these theoretical principles, calculations were performed to determine possible spiral channel designs that might effectively separate sperm. One challenge of this analysis was due to the irregular shape of sperm cells (approx. sperm head length: 4.79 ± 0.26 μm, width: 2.82 ± 0.23),[20] and the theory assumes spherical particles. As an initial estimate, the sperm were considered to be 5 μm diameter spheres. For resolution estimates, RBCs were approximated as 9

μm diameter spheres (measured RBC dimensions – diameters: 7.5–8.7 μm, thickness: 1.7–2.2 μm).[21] In our search for appropriate channel geometries, the sample injection flow rate was limited to be 0.1 to 7 ml min^{-1} in 0.1 ml min^{-1} increments.

Based on these calculations, a set of spiral channels with dimensions: initial radius, 0.7 cm; final radius, 0.899 cm; channel width, 150 μm; channel height, 50 μm; turns of spiral, 4 turns; and space between channels, 310 μm; were manufactured and tested. These channels should generate the following metrics for a 0.55 ml min^{-1} flow: R_f of 5 μm diameter particle, 0.0806, and R_f of 9 μm diameter particle, 0.4702; λ for 9 μm diameter particle, 0.2, and λ for 5 μm diameter particle, 0.0667. Four gradual-splitter-type outlets were designed to allow separate collection of the particles and to allow investigation of the location of the various particles in the flow (Fig. 1).

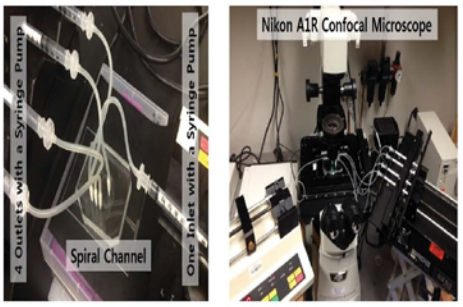

Fig. 2 Experimental setup, (left) two syringe pump with a spiral channel device, (right) stained sample run observation setup with Nikon A1R microscope and high speed scanner.

Methodology/experimental

To demonstrate the capability of the designed spiral channel to focus and separate sperm cells from RBCs and other unwanted debris (such as white blood cells), multiple channels were built and tested.

Fabrication of the actual device was carried out using SU-8 (SU-8 3000, Microchem, MA, USA) as a mold for polydimethylsiloxane (PDMS, Sylgard 184, Dow Corning, MI, USA). The SU-8 mold was fabricated on a 100 mm (4 inch) wafer according to the manufacturer's instructions in a clean room environment. 40 ml of uncured PDMS at a 10 : 1 (polymer : curing agent) ratio was poured on the mold, and it was placed in an oven at 60 °C for at least 6 hours. The molded PDMS was peeled off from the mold and any excess PDMS removed. Inlets and outlets were cored with a 1.5 mm diameter coring tool. After cleaning the surface of the PDMS, a glass slide (70 × 50 mm) was plasma bonded with the PDMS to form closed channels.

The experimental system utilized two syringe pumps (one dual syringe capable and one four syringe capable), five 1 ml syringes and one spiral channel device. The dual syringe pump was used to inject sample through inlets of the channel, and the four channel syringe pump was arranged to pull sample from the four outlets. The removal flow rate was kept steady and slightly lower than the injection flow rate to obtain equal amounts of sample from each outlet.

All sperm and blood samples were acquired under an Institutional Review Board approved study, IRB00072239. Written informed consent was obtained from all participants for their tissues to be utilized for this study. Sperm samples were prepared from previously frozen semen specimens which were resuspended in water for 30 s to immobilize the sperm. The sperm samples were then resuspended in either PBS or sperm media (Quinn's Advantage media with HEPES (Sage, CT, USA) and 3% of serum protein substitute (Sage, CT, USA)). RBC samples were obtained from whole blood specimens within one week of collection. Collected blood samples were also resuspended in either PBS or sperm media. As required, the sperm and RBC samples were diluted or concentrated using PBS or sperm media. Samples were placed within two 1 ml BD plastic syringes and connected to the spiral channel inputs using platinum-cured silicone tubing and 1/16 inch barbs. 1 ml syringes were connected to the outlets of the spiral channel and placed in the 4 channel syringe pump in withdrawal mode (Fig. 2).

For the sperm-alone experiments, the base concentration of sperm samples was 25 million per ml and sperm samples were injected into the spiral channel under flow rates from 0.1 to 0.22 ml min^{-1}. For mixed samples (sperm and RBC) characterization, the concentration of sperm was 1∼2 million per ml and the RBC concentration was 7–9 million per ml, which approximated a TESE/mTESE sample. The sperm concentration was selected because 1∼2 million per ml is the minimum concentration for use with a cell counting chamber. Mixed samples were injected into the spiral channel at flow rates from 0.1 to 0.52 ml min^{-1}. The sperm and RBC concentrations in the collected samples from each of the four outlets were measured using a Mackler cell counting chamber under 20× magnification. 1 ml of sperm sample was injected into the spiral channel and about 0.2 ml of sample was collected in each of the outlet syringes, which means 0.2 ml of sample might remain within the spiral channel and connecting tubing. To visualize focusing of the RBC and sperm cells, samples containing mixtures of sperm and whole blood were injected into the spiral channel, and observed with a Nikon AR1 confocal microscope under 4× magnification. Mixtures of sperm and whole blood samples were injected at flowrates from 0.1 to 0.52 ml min^{-1}. The sperm samples were stained with DAPI and the RBCs stained with PKH26 (Sigma, MO, USA) to enhance their visual signal. Outlet channel concentrations were measured as described above. To achieve optimal flow-focusing of each cell type, the input sample total cell concentration was experimentally investigated to minimize inter-particle interaction effects.[13] Based on the results of these experiments, the input samples were diluted down to a total cell concentration of <∼10 million per ml.

A projection image of a section of the obtained high-speed (230 fps) video was analysed to determine cell focusing patterns within a section of the spiral channel close to the outlets on the 4th ring (Fig. 4 and 6). For initial sample runs, 10 s videos were recorded after the initial 30 second sample injection. Additional videos were recorded in several lengths (10, 30, 50 s, 1 min,

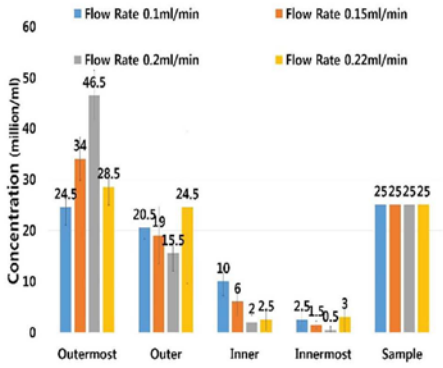

Fig. 3 Sperm characterization in various flowrate (0.1–0.22 ml min^{-1}). The starting material of this experiment is human semen. Each bar represents concentration ratio among outlets, actual concentration are located on top of each bar.

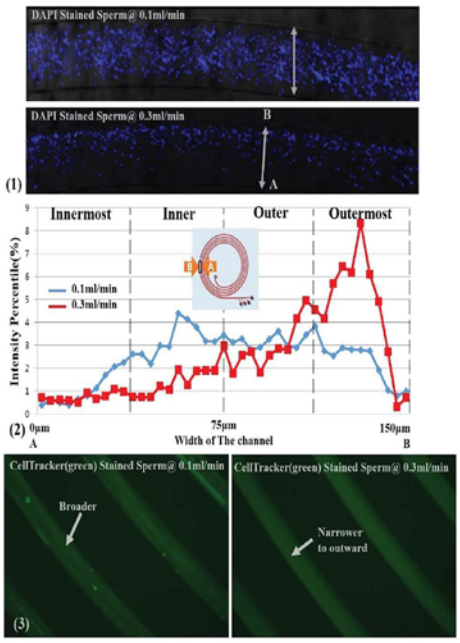

Fig. 4 (1) High speed projection images of only stained sperm sample run with flow rate of 0.1 ml min^{-1} and 0.3 ml min^{-1}, (2) DAPI (blue) stained sperm population intensity analysis throughout width of the channel between two flow rates (0.1, 0.3 ml min^{-1}), (3) CellTracker (green) stained sperm flow-focusing observation within a section of all four rings of channel (up 0.1 ml min^{-1}, down 0.3 ml min^{-1}).

10 min) after the initial 30 second sample injection. Videos were analysed using NIS-element's analysis feature. A projection image from a selected section of the video file, was analysed to obtain intensity data for each wavelength for the different cell stains (DAPI and PKH26).

For cell streak visualization experiments, a second image recording technique was employed with CellTracker green (Invitrogen, USA) stained sperm samples, using an inverted microscope with a digital camera. The camera shutter exposure time was increased to 10 s per image, which generates a streak image and shows a section of all four rings of the channel.

In order to both validate the separation mechanism and to investigate the possibility of serial purification using the spiral channel to increase the purification ratios, we performed a set of sequential sample runs (three steps) and analysed cell concentrations following each step. For these experiments, 1 ml of sample from the previous step's collected outlet sample was used as the next step's input sample. After each step, collected samples were evaluated for cell concentration. To eliminate sample remaining within the device and tubing from previous runs, a flushing run (1 ml of sperm media) was executed after each run.

Results and discussion

The collected samples from the outlets showed enrichment of sperm and blood cells at different outlets, suggesting that at least some focusing of these cells was occurring in the microchannel. Sperm cells, at the conditions tested, tended to accumulate near the outer walls, both when tested alone and when mixed with RBCs. Specifically, sperm concentrations were higher in samples collected from the outermost and outer outlets, which represent the outer wall of the channel, while sperm concentrations were lower in samples collected from inner and innermost outlets, which represent the inner wall of the channel (Fig. 3). In general, there was a trend of high sperm concentrations at the outer wall with the concentration decreasing towards the inner walls. The reverse occurred for the

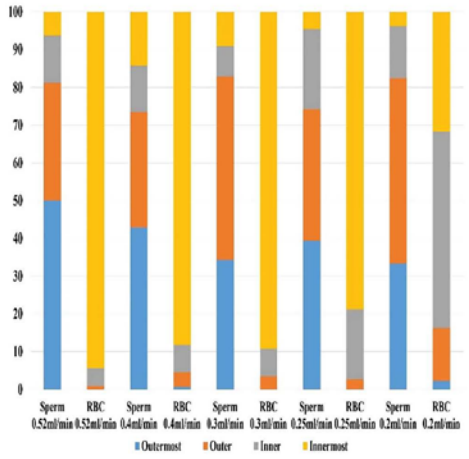

Fig. 5 Mixed sample (sperm/RBC) characterization under various flowrate (0.2–0.52 ml min^{-1}), each bar represents outlet collected ratio (in percentile) for each cell types (sperm or RBC).

RBCs, and for the fastest flow rates there were almost no RBCs in the outermost exits (Fig. 5).

The flow-focusing trend became more distinct as flow rates increased up to 0.2 ml min^{-1}, in which concentrations of the outer wall channel exits (outermost and outer) were 46.5 and 15.5 million per ml. As a ratio, 71% of sperm eluted from the outer wall outlets (outermost and outer) (Fig. 3). High speed projection images of a sample of stained sperm (Fig. 4), supported the earlier sperm characterization results and indicated a improving flow-focusing trend for higher flow rates (0.3 ml min^{-1}). The plot in Fig. 4(2) shows a comparison of the light intensity as a function of channel location generated by DAPI-labelled sperm for flow rates of 0.1 and 0.3 ml min^{-1}. The concentration readings from Fig. 3, clearly indicate that sperm are move towards the outer wall for all flow rates; however, a sharp focus near the outer wall was not obtained for the sperm in contrast to previous work using micro beads,[13,15–19] most likely due to the fact that sperm are not spherical and their geometry as presented to the flow field may be somewhat random. Even though a sharp focus for the sperm was not obtained, the overall trend suggests that this method may be valuable for enriching sperm in complex samples.

In order to ascertain whether the spiral channels could facilitate sperm separation from other cell types beyond RBCs, outlet samples obtained after processing mixtures of whole blood and human sperm were analysed to determine sperm and RBC concentrations. RBCs (stained red) clearly focused toward the inner wall of the channel, while sperm (stained blue) focused more broadly toward the outer wall of the channel (Fig. 6). At a flow rate of 0.52 ml min^{-1}, the sperm concentration is higher in outermost and outer outlets than in innermost and inner outlets, with measurements of 1.0, 0.6, 0.3 and 0.1 million per ml respectively. The relative ratios of overall collected sperm at outlet outermost to innermost were 50%, 31.3%, 12.5%, and 6.3%, respectively. In contrast, the concentration of RBCs at a flow rate of 0.52 ml min^{-1} was markedly higher at the innermost outlet than in outlets outermost, outer and inner with measurements (outlets outermost to innermost) of 0, 0.23, 1.1, and 22.6 million per ml respectively. The concentration ratios of overall collected RBCs in outermost to innermost outlets were 0, 0.9, 4.6, and 94.4% respectively. As expected, based on previous inertial microfluidic studies, relatively small particles exited the outer outlets (sperm cells, 81.2%) while larger cells mostly collected within the inner outlets (RBC, 99.0%) (Fig. 5).

Fig. 6 shows a compilation of stained-cell intensity measurements of the stained sperm and RBCs acquired using high speed video for flow rates of 0.1 ml min^{-1} and 0.52 ml min^{-1}. Four minutes of video images were overlaid to obtain the images in Fig. 6(1–3) is a "projection" of the images with the light intensity plotted as a function of channel position. For these experiments, the sperm and RBCs were flowed separately. At the lowest flow rates (*i.e.* 0.1 ml min^{-1}), there is essentially no difference between the positions of the sperm and RBCs (Fig. 6(2 and 3)). At 0.52 mi min^{-1}, there is a clear shift between the two cell populations, but they never quite separate, which is consistent with our earlier data showing enrichment, but not separation (Fig. 6(1 and 3)). The lack of tight focusing is thought

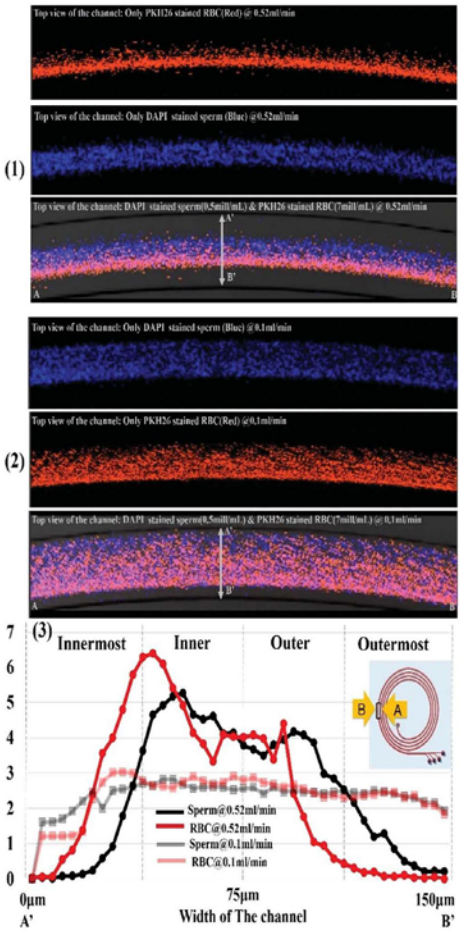

Fig. 6 (1) High speed projection images of mixed stained sample (sperm/RBC) with flow rate of 0.52 ml min^{-1}, (2) high speed projection images of mixed stained sample (sperm/RBC) with flow rate of 0.1 ml min^{-1}, (3) stained cell population intensity analysis throughout width of the channel.

to be due to the asymmetrical shape of sperm. On the other hand, better flow-focusing of RBCs occurred, likely because of the RBC's somewhat more symmetric geometry.

As noted previously, the shape of the sperm likely limits their ability to be tightly focused. Modeling may be helpful in determining a flow rate or condition that would help the sperm cells to align with some aspect of the flow, and then possibly be focused. Current inertial microfluidics models only work with symmetrical particles (spheres), so development of a more extensive model involving sperm would be valuable.

Since there was clear evidence that faster flow rates generate some separation and sperm enrichment, an effort was made to drive the flow faster. Unfortunately, it was generally difficult to go above 0.52 ml min^{-1}, lower than calculated flow rate 0.55 ml min^{-1}, as the pressures in the channel tended to cause leaks

and ultimately ruin the devices. Even with the modest focusing, the substantial enrichment of sperm should make it much easier to find sperm in samples processed through the channel when compared to a raw TESE/mTESE sample.

Sequential step runs were performed in order to determine whether the spiral channel can be used to improve purification of the samples through repeatedly treating the same sample (Fig. 7). Reprocessing the cells of outlet 1 and outlet 2 from step 1, which were at a concentration of: RBC, 0.3 million per ml and sperm, 1.97 million per ml, and outlet 2 of: RBC, 0.74 million per ml and sperm, 1.6 million per ml. Step 2 results with outlet sample 1 from step 1, were: RBC, 0 million per ml and sperm, 1.55 million per ml from outlet 1, and RBC, 0.05 million per ml and sperm, 1.3 million per ml from outlet 2 (Fig. 7(a)). These results show that the RBC concentration of a reprocessed sample exiting outlet 1 is much less than for the original sample and that essentially all of the RBCs have been removed. The same trend is observed when the sample is reprocessed again (step 3) results, which were: RBC, 0 million per ml at outlet 1 and 2 of step 3 and sperm: 1.3 million per ml (outlet 1) and 1.15 million per ml (outlet 2) (Fig. 7(a)). Based on the cell concentration results from step 1 to step 3, the sample is clearly collecting more sperm cells from outlet 1 while rejecting all of the RBCs, suggesting that this method could be used to eliminate RBCs from the sample. In this case, it is 100% filtering the RBCs from the original sample which went from 9.95 million RBCs per ml to 0 RBCs per ml (Fig. 7(a)). Similar results were obtained for the later levels of processing, where all RBCs could be eliminated from nearly all of the outlets. In addition, the sperm cells that were lost through outlet 3 in step 1 could be recovered by further processing, as shown in Fig. 7(b) and (c). Thus, sequential processing has significant promise for allowing the collection of all sperm in a sample, which is critical in these mTESE samples that may have only 10 s or 100 s of sperm.

The overall result of step runs suggest that even though the spiral channel was only able to generate a weak focus with sperm cells towards the outer walls, the sharply focused RBC flow can purify the RBCs away from the sperm. In each step run, the concentration of sperm in outlets 1 and 2 was increased compared to the previous step. Despite the sequential step purification results achieved, there is still a possibility of sperm loss, measured to be about 19% with the current spiral design, which occurs with every stepwise run, so it is unlikely that these steps can be repeated indefinitely, though reprocessing of samples can be used to recover some portion of the lost cells.

A close observation of the data also indicates that cells that were focused to outlet 1 originally do not always return to outlet 1 in the next separation step, suggesting that there is either some randomness to the focusing, which would be expected due to the non-spherical sperm and RBCs used here, or some interactions at high concentration that limit focusing. The

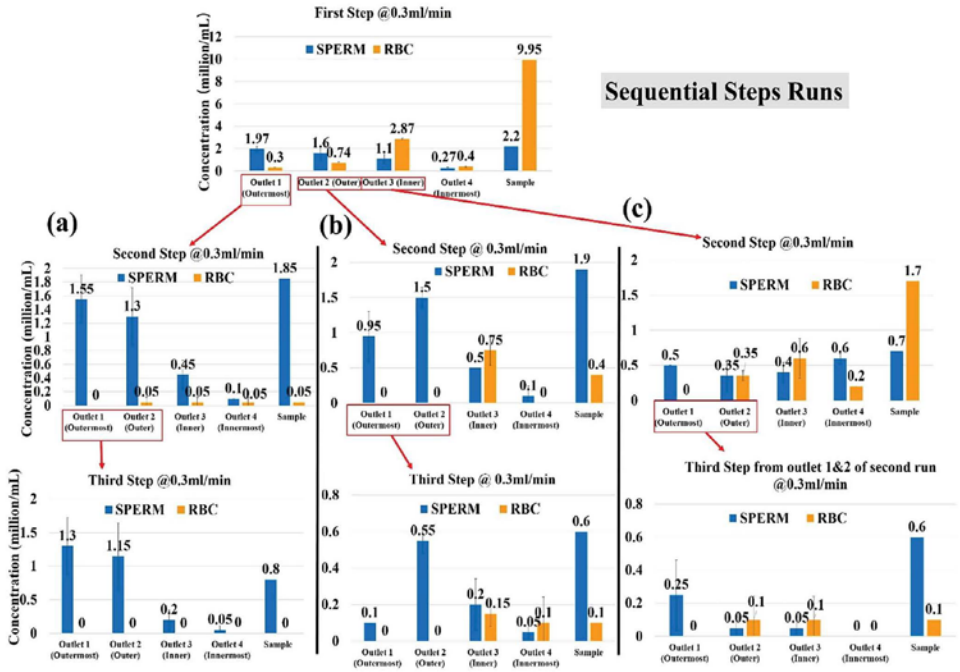

Fig. 7 Sequential step runs to confirm purification of sample use of the spiral channel (a) step runs of 2, 3 with outlet 1 sample of step 1, (b) step runs of 2, 3 with outlet 2 sample of step 1, (c) step runs of 2, 3 with outlet 3 sample of step 1. Note: name of outlet are selected for convenience, outlet 1: outermost, outlet 2: outer, outlet 3: inner, and outlet 4: innermost.

results suggest that there is some randomness associated with the shape factors, and less related to concentration effects, as there were no clear changes at the lower concentrations.

Conclusions

In conclusion, we successfully demonstrated the use of inertial microfluidic technology to purify sperm by focusing particles in a spiral channel flow. Unlike conventional sperm separation techniques, the technique presented here was not dependent upon sperm motility, nor do they require any labels. Modelling of the sperm and RBCs as 5 μm and 9 μm diameter spheres respectively, a set of spiral channel dimensions was selected that adequately separated these cells, though further modelling may suggest better channel geometries for these asymmetric particles. The results corresponded well with previous publications which suggested that inertial microfluidics should be able to generate focused-flow of 5 μm diameter spheres at the outer wall area and focused-flow of 9 μm diameter spheres near the inner wall of the channel.

With sample injection flow rates up to the calculated optimal flow rate (0.52 ml min^{-1}), sperm only and mixed (sperm/RBC) samples run through the spiral channel demonstrated moderate flow focusing of sperm toward the outer wall of the channel and sharper flow-focusing of the RBCs toward the inner wall of channel. 81% of non-motile sperm were recovered at outer wall exits and 99% of RBCs could be recovered at the inner wall outlets for an injection flow rate of 0.52 ml min^{-1}. These results were verified through visualization by acquiring high speed video of cells transiting the channel for a small section of the outer rim of the channel confirming two different focused-flow lines of stained sperm and RBCs within the channel.

Reprocessing of samples showed that 100% removal of RBCs was possible while still collecting a high percentage of sperm. Sperm that were lost in earlier processing runs could also be recovered while removing all of the RBCs using a reprocessing approach. Even with the possibility of losing of sperm cells through multiple step runs, this study showed the possible usefulness of spiral channels in purifying sperm from background cell debris. Application of this approach, which only takes a few minutes, could significantly improve the current processing time of mTESE samples significantly, because 99% of mTESE samples are unwanted cells and debris, and technicians currently spend significant time looking through these samples for sperm. Presenting the technicians with a sample where 99% of the debris has been removed would be a significant improvement.

References

1 J. E. Swain, D. Lai, S. Takayama and G. D. Smith, *Lab Chip*, 2013, **13**, 1213–1224.
2 L. J. Kricka, I. Faro, S. Heyner, W. T. Garside, G. Fitzpatrick, G. McKinnon, J. Ho and P. Wilding, *J. Pharm. Biomed. Anal.*, 1997, **15**, 1443–1447.
3 J. M. Wu, Y. Chung, K. J. Belford, G. D. Smith, S. Takayama and J. Lahann, *Biomed. Microdevices*, 2006, **8**, 99–107.
4 Y.-J. Ko, J.-H. Maeng, B.-C. Lee, S. Lee, S. Y. Hwang and Y. Ahn, *Anal. Sci.*, 2012, **28**, 27–32.
5 R. S. Suh, X. Zhu, N. Phadke, D. A. Ohl, S. Takayama and G. D. Smith, *Hum. Reprod.*, 2006, **21**, 477–483.
6 C. Ainsworth, B. Nixon and R. J. Aitken, *Hum. Reprod.*, 2005, **20**, 2261–2270.
7 C. Ainsworth, B. Nixon, R. P. S. Jansen and R. J. Aitken, *Hum. Reprod.*, 2007, **22**, 197–200.
8 N. Zaninović and P. N. Schlegel, *Atlas of the Human Testis*, Springer-Verlag, London, 2013DOI: 10.1007/978-1-4471-2763-5.
9 S. Shen, C. Ma, L. Zhao, Y. Wang, J.-C. Wang, J. Xu, T. Li, L. Pang and J. Wang, *Lab Chip*, 2014, **14**, 2525–2538.
10 M. G. Lee, J. H. Shin, C. Y. Bae, S. Choi and J. K. Park, *Anal. Chem.*, 2013, **85**, 6213–6218.
11 N. Nivedita and I. Papautsky, *Biomicrofluidics*, 2013, **7**, 054101, DOI: 10.1063/1.4819275.
12 A. A. S. Bhagat, H. W. Hou, L. D. Li, C. T. Lim and J. Han, *Lab Chip*, 2011, **11**, 1870–1878.
13 H. Amini, W. Lee and D. Di Carlo, *Lab Chip*, 2014, **14**, 2739–2761.
14 D. Di Carlo, J. F. Edd, K. J. Humphry, H. A. Stone and M. Toner, *Phys. Rev. Lett.*, 2009, **102**, 1–4.
15 D. Di Carlo, *Lab Chip*, 2009, **9**, 3038–3046.
16 J. Zhou and I. Papautsky, *Lab Chip*, 2013, **13**, 1121–1132.
17 S. S. Kuntaegowdanahalli, A. A. S. Bhagat, G. Kumar and I. Papautsky, *Lab Chip*, 2009, **9**, 2973–2980.
18 J. M. Martel and M. Toner, *Sci. Rep.*, 2013, **3**, 1–8.
19 J. M. Martel and M. Toner, *Phys. Fluids*, 2012, **24**, 032001, DOI: 10.1063/1.3681228.
20 L. Maree, S. S. Du Plessis, R. Menkveld and G. Van Der Horst, *Hum. Reprod.*, 2010, **25**, 1369–1382.
21 M. Diez-Silva, M. Dao, J. Han, C.-T. Lim and S. Suresh, *MRS Bull.*, 2010, **35**, 382–388.

CHAPTER 3

SEPARATION OF SPERM FROM SAMPLES CONTAINING HIGH CONCENTRATIONS OF WHITE BLOOD CELLS USING A SPIRAL CHANNEL

3.1 Introduction

Microfluidic technology provides valuable options for cell sorting and separation and can be used to replace tedious and inefficient conventional protocols[53], [58], [60]–[63]. Of particular interest to us are research efforts related to microfluidic methods for separating sperm from unwanted debris while improving the efficiency of assisted reproductive technologies (ART). In one of the earliest such efforts, a glass microfluidic chip containing multiple microchannels connecting an input reservoir to a collecting reservoir enabled motile sperm to swim to specific reservoirs where they could be collected while removing nonmotile sperm and debris [80], [81]. This technology first demonstrated the value of microfluidic platforms for sperm separation. More recently, a common microfluidics approach for sperm separation has been developed involving parallel laminar fluid streams of media through straight microchannels: One stream consists of a dilute semen sample and the other stream contains sperm media [82], [83]. At the microscale, the two fluid streams do not mix readily, so only motile sperm can travel across the interface between the two parallel streams. The two streams are separated again after a length sufficient to allow motile sperm to cross the boundary in high numbers, generating separation of motile sperm from nonmotile sperm and debris. Following a series of device optimizations, the utility of this technology for ART was verified using sperm collected from the outlet for IVF [23], [84]–[88]. Another novel microfluidic approach to sperm separation utilizes chemotaxis in addition to motility. This approach induces sperm to travel through microchannels toward chemo-attractants which were applied to the bottom surface of the collection reservoirs at the periphery of the device [89]–[91].

Most of the sperm separation approaches utilizing microfluidics rely on sperm motility

for separation with added features through which only highly motile sperm can pass: chemo-attractants, physical obstacles, and microdiffusers [80], [81], [90]–[99]. Thus, these techniques can separate only progressive motile sperm from semen samples, but they lose a significant number of sperm cells including viable nonprogressive motile and nonmotile sperm, and are not feasible for use with immature and nonmotile sperm that may be the only sperm produced by some patients. Thus, a system to recover all sperm, not just motile sperm, is needed. Such as device would serve a wide patient base needing sperm sample preparation.

Recently we demonstrated sperm separations from a simulated microTESE sample, which included sperm cells, blood cells, and other debris [100], using a passive, purely mechanical, label-free microfluidic approach based on inertial microfluidics that separated sperm (regardless of their motility state) from other unwanted cells/debris. The approach did not require any externally applied forces except the movement of the fluid sample through the instrument. The system could recover not only motile sperm, but also viable less-motile and nonmotile sperm with high recovery rates. This study also suggested that a precisely designed spiral channel could generate some flow focusing of sperm, making it a suitable solution for increasing the purity of sperm from semen samples with high concentrations of unwanted particles, such as the high concentration of WBCs in semen samples obtained from leukospermia patients.

Leukospermia is a condition characterized by abnormally high white blood cell (WBC) concentrations in semen (>1 million WBCs/milliliter of semen), which may lead to infertility and render ineffective ART procedures such as Intrauterine Insemination (IUI). As highlighted by Gambera [77]: high concentrations of WBCs in the semen, can cause

disruption during fertilization. To deal with leukospermia, a density gradient centrifugation preparation method is widely utilized in fertility clinics as a WBC separation method. It consists of filtering sperm by centrifugal forces through either one or multiple layers of increasingly concentrated silane-coated silica particles. The process is able to generate a pellet at the bottom of the tube which contains a higher percentage of clean, motile sperm for IUI [78]. Unfortunately, this method can lead to low sperm recovery when the starting sample has a low concentration of sperm [79]. Additionally, it also requires significant time (~1 hr) to prepare the sample, which creates a potentially problematic time gap between sample preparation and insemination. Accordingly, there is a need for a method with a high recovery rate from samples with low sperm concentrations. Additionally, a sample preparation time reduction can provide significant relief to IUI patients who are under stress from the IUI procedure itself.

In this study, we demonstrate the use of inertial microfluidic technology to separate sperm from WBCs, the major contaminant in leukospermia semen samples, by flow focusing sperm and WBCs into different flow exits. This new method could conveniently process semen on site with much shorter processing times ~10 times faster. The results show moderate sperm flow focusing and clear WBC flow focusing, indicating that this method can be used for sperm concentration enrichment even when working with high WBC concentrations or debris-filled semen samples.

3.2 Design and Theory

To enable the most effective and efficient WBC removal from a semen sample using a spiral channel, the appropriate dimensions of the spiral channel can be calculated based on

inertial microfluidics theory: the force ratio (R_f), the ratio of particle diameter and hydraulic diameter (λ), and the aspect ratio of the channel. The force ratio (R_f) is a ratio between the Dean drag force (F_D) and the lift force (F_L), all given by[27], [43]

$$R_f = \frac{F_L}{F_D} \geq \sim 0.08, \tag{3.1}$$

$$F_D = 3\pi\mu U_{Dean} a_p \tag{3.2}$$

$$F_L = 0.05 \frac{a_p^4 \rho U_m^2}{D_h^2} \tag{3.3}$$

where F_D is the force resulting from a secondary vortex that appears on the channel laterally, F_L is a lift force that pushes all particles from the channel walls, μ is fluid viscosity, U_{Dean} is the average Dean velocity, $a_p$is particle diameter, and U_m is maximum fluid velocity. When R_f is higher than 0.08, the flow should able to generate target particle focusing. The ratio λ (Eq 4) should be more than 0.07 to generate optimal particle focus flow [30] and the aspect ratio of the channel should be approximately between 0.5 – 0.25 (height/width)[26], [31],

$$\lambda = \frac{a_p}{D_h} \geq 0.07 \ , \tag{3.4}$$

where D_h is the hydrodynamic diameter for a rectangular channel. The channel length (L_I) required for a particle to reach its equilibrium position can be calculated by [43];

$$L_I = \frac{U_f}{U_L} \times L_M \tag{3.5}$$

where U_f is the flow velocity, U_L is the lateral migration velocity of the particle,

$$U_L = 0.5 \frac{\rho U_m^2 a_p^3}{3\pi\mu D_h^2} \tag{3.6}$$

and L_M is the migration length.

$$L_M = W + H + \frac{3}{4}W \tag{3.7}$$

The target cell's dimensions can be approximated as a sphere having the largest diameter of each cell. WBCs are reported to have an average diameter of 12 μm and the longest sperm head dimension is about 5 μm [102]–[105]. Approximating cells as spheres to simplify calculations is reasonable based on an experimental study involving asymmetrical particle focusing within a microfluidic channel by Hur et al.[50]. This study suggests that the maximum diameter (rotational diameter) of an asymmetrical particle determines the stable position and can be used to predict the movement of asymmetrical particles in spiral channels.

A range of dimensions and flow rates were used in equations (3.1 ~ 4) to find the best conditions for flow focusing (R_f, λ, and aspect ratio) and fabrication convenience. After a series of calculations, we found a set of dimensions which satisfied the design guidelines

(ratio conditions from equation 3.1 and 3.4): height = 50 μm, width = 150 μm, space between channel = 310 μm, initial radius = 700 μm, and final radius = 899 μm. For the selected dimensions, $\lambda = 0.16$ for a 12 μm diameter particle, and $\lambda = 0.067$ for a 5 μm diameter particle. The injection flow rate was selected based on the experimental results of our previous work [100]. The flow rate from the previous study was 0.52 ml/min generating R_f values of 0.40 for 5 μm particles, and 5.63 for 12 μm particles.

3.3 Experimental Methodology

To demonstrate the separation capability of the spiral channel with sperm and WBCs, a series of experiments were designed to show flow focusing of sperm and WBCs.

Fabrication of the designed device was carried out using polydimethylsiloxane (PDMS, Sylgard 184, Dow Corning, MI, USA) with SU-8 (SU-8 3035, Microchem, MA, USA) mold. The SU-8 mold was fabricated on a 100 mm (4 inch) wafer according to the manufacturer's instructions in a clean room environment. 40 ml of uncured PDMS at a 10:1 (PDMS base: curing agent) ratio was poured over the mold and it was placed in an oven at 60° C for at least 6 hours. After curing, the molded PDMS was peeled off from the mold and any excess PDMS removed. Inlets and outlets were cored with a 1.5 mm diameter coring tool. After cleaning the channel side surface of the PDMS piece, a glass slide (Corning 2947-70 X 50 mm) was plasma bonded with the PDMS to form a closed channel.

All sperm and WBC samples were acquired under an Institutional Review Board-approved study, IRB00072239. Written informed consent was obtained from all participants for their samples to be utilized for this study. Sperm samples were prepared from previously frozen semen specimens which were suspended in the sperm media

(Quinn's Advantage media with HEPES (Sage, CT, USA) and 3% of serum protein substitute (Sage, CT, USA)). WBC samples were obtained from donor's whole blood specimens within one week of collection. Note that WBC samples mostly contained WBC and small amount of RBC, because the WBC separation process from whole blood could not separate RBC completely. WBC samples were also suspended in the sperm media. The sperm and WBC samples were diluted using the sperm media to prevent interparticle collision and we experimentally found optimal total cell concentration range from a previous study < 10 million cells/ml[100]. Table 3.1 provides a technical description of each sample type and its label.

Prepared samples were placed within two 1 ml plastic syringes (BD, 1 ml Syringe Luer-lock tip) and each syringe was connected to the spiral channel inlets through platinum-cured silicone tubing (Sani-Tech, Clear Platinum-Cured Silicone Tubing, STHT-062-1) and nylon barbs (Nordson Medical, Straight Through Tube Fitting, N210-1). The outlet sample collection setup was constructed in the same manner as the inlet setup and separated samples from the two outlets were collected into two 1 ml plastic syringes (one for each outlet).

Samples were split into two syringes and injected through two spiral channel inlets using a dual syringe pump. Two inlets were used instead of one because it helped eliminate leaks near the inlet port, according to our previous study [100]. The injection flow rate was close to the calculated flow rate (0.26 ml/min from each syringe, resulting in accumulated flow rate of 0.52 ml/min). To collect equal amounts of sample from each outlet, another set of two syringe pumps pulled sample with a slightly lower flow rate than the injection flow rate (0.2ml/min) to provide a back pressure and prevent gas bubble formation in the

outlet area.

To observe and characterize the behavior of WBCs in the spiral channel, samples were prepared from two different donors and diluted to a concentration of 8.1 million/ml (WBC A sample, Table 3.1). The concentration was selected to simulate high WBC concentrations (WBC: >1 million/ml [77]) in semen samples from leukospermia patients. The prepared WBC A sample was injected at 0.52 ml min^{-1} and collected from two outlets (inner and outer outlets).

Semen A sample was prepared by spiking WBC into semen [77], [105]. Cell concentrations were 2.45 and 8.35 million/ml sperm and WBCs respectively (Semen A sample, Table 3.1). These concentrations were selected to simulate the extreme condition of high WBC contaminated semen with low sperm concentration. Prepared samples were injected at 0.52 ml min^{-1}. After processing with the spiral channel, the eluted material was collected from both outlets and both WBCs and sperm were quantified using a cell counting chamber under a microscope at 200X magnification. The estimated time from sample injection to collection of the processed sample was ~ 5 minutes, which is more than 10 times shorter than current clinical protocols (density gradient centrifugation).

To visualize the flow focusing of WBCs and sperm cells within the spiral channel, a stained Semen A sample was injected at a flow rate of 0.52 ml per min^{-1} and observed under a high speed scanner equipped with a microscope (Nikon AR1 confocal microscope). The stained sperm were prepared by purifying sperm (from semen) using density gradient centrifugation and then stained with DAPI (Sigma, MO, USA). WBCs from Semen A (Table 3.1) were stained with PKH26 (Sigma, MO, USA) according to the manufacturer's instructions separately before spiking into Semen A. The microscope objective was focused

on a location between the end of the 4th ring of the spiral channel and the outlet area (near outlet, Figures 3.1, 3.2). To observe the flow focusing behavior at each ring of the spiral, two individual locations on each ring (as shown in Figure 3.2) were selected for data acquisition. On each acquisition, ~5 sec (840~1050 frames) were collected and analyzed by projecting all frames from each video onto one image using NIS Elements software. The generated projection images were analyzed for fluorescence intensity of stained cells, and the data was plotted to show cell locations in the channel. The raw intensity data was acquired sequentially from the inner wall boundary to the outer wall boundary and plotted. A curved data acquisition line was traced along the inner wall boundary and used as an intensity data collection reference. Intensity data along the curved data acquisition line was totaled to determine an accumulated intensity value at a particular position across the channel width. The *x* axis of the final plot was divided equally into four regions to represent estimated lateral location of the channel (Inner, Mid-inner, Mid-outer, Outer). The peak location of each cell type was identified using the location of the highest intensity point in the raw data. Note that the 4th ring lower location was considered as redundant with the near outlet area, so the near outlet location represents the last location observed on the 4th ring.

3.4 Results and Discussion

3.4.1 WBC Characterization

Experiments with WBC A (Table 3.1) sample showed flow focusing of WBCs within the spiral channel, and this was confirmed by the WBC count from collected samples at spiral channel outlets. The results clearly showed that WBCs can be focused under the

conditions predicted by theory, and has been shown by others [60], [62]. In Table 3.2, the relative percentage of WBCs directed to the inner outlet was 94.8% (5.45 million/ml) or more compared to the outer outlet which was 5% (0.3 million/ml) or less. These results suggest that the WBCs are focusing towards the inner wall with high focusing ability, as relatively few WBCs strayed to the outer outlet.

3.4.2 Semen A Sample Characterization

Characterization results using Semen A showed a clear reduction of WBC concentration from the outer outlet while enhancing sperm concentration from the same outlet (Table 3.3) through clear flow focusing of WBC and partial flow focusing of sperm. WBCs and RBCs primarily exited the inner outlet, while sperm were predominantly driven to the outer outlet. The concentration difference between input and summed outlet samples can be explained by the uncertainty of the cell counting chamber sampling and measurement approach. Detailed results are shown for total concentrations and also percent totals in Table 3.3. The results clearly show that the method is capable of separating out WBCs and RBCs from the majority of sperm cells.

3.4.3 Flow Focusing Observation of WBC and Sperm Near the Outlet

Images of the flow focusing behavior of a stained SEMEN A sample (stained WBC (red) and stained sperm (blue)) at the last ring of the spiral channel are shown in Figure 3.3. A focused stream of WBCs appeared near the inner wall of the channel and a partially focused stream of sperm appeared in the outer half of the channel. Figure 3.3 shows the separate and combined images of the different constituents during flow. The first image

(Figure 3.3(1)) shows both the stained WBCs and the sperm focused near each outlet mostly in parallel paths. Separate fluorescent signals for sperm and WBCs are shown in Figure 3.3(2) and Figure 3.3(3), respectively.

Figure 3.3(4) is a graph of the fluorescence intensity across the width of the channel and integrated across the breadth for the two cell types. The intensity plot of each signal shows the general location of each cell type relative to one another. The blue plot represents the location of DAPI stained sperm which has its highest intensity peak in the mid outer half of the channel. The red plot represents the location of PKH26 stained WBCs, which has its peak at middle of the inner half of the channel. These results show a clear shift between the two cell populations, but they are never completely separate, which is consistent with earlier concentration data showing enrichment of sperm, but not complete separation.

3.4.4 Flow Focusing Observation of WBC and Sperm in All Rings of Channel

The fluorescence images and their intensity profile from locations on all the other rings of the channel are plotted in Figure 3.4. These images allow us to visualize the focusing of the sperm and WBCs through the channel. In location 1, the intensity of WBC and sperm were evenly spread throughout the channel which represents the evenly suspended condition of the input sample. At location 2 the intensity peak of the WBCs begins to narrow in the middle of the channel but there is limited flow focusing of the sperm. Starting at location 3, there is a gradual shifting in signal of the WBC's red fluorescence toward the inner wall of the channel until location 8, and the band narrows initially before broadening out close to the exit. This phenomenon can also be seen in each fluorescent intensity plot for each location (Figure 3.4(2-8)). The blue fluorescent signal from the sperm did not show

specific signs of focusing until location 3, but it is not as highly clustered as the WBC signal at location 3. However, the intensity of the blue fluorescent stream gradually moves toward the outer wall of the channel from location 3 to location 8 (Figure 3.3(3-8)). This transition of the fluorescent intensity of each color (red and blue) give some insight into the physics affecting these particles. The WBCs, being larger in size, focus more quickly and have a shorter focusing distance along the channel. The sperm, being smaller and asymmetric, focus more slowly and do not focus as tightly. The results seem to suggest that the particles reach an equilibrium location by about ring 3, suggesting that the channel could possibly be made shorter. Interestingly, the analysis at the end of the channel and the collected fractions are somewhat different in that the outlet fractions are more fractionated than the images and intensity plots would suggest. Thus, there may be some additional separation that occurs in the brief widening of the channels and split before the outlets.

Equation 3.5 can be used to calculate a predicted required channel length for reaching equilibrium position of the WBCs and sperm cells, and these results can be compared to the data in Figure 3.4. According to these calculations, R_f (force ratio) for a 12 μm diameter sphere (approximating a WBC) becomes higher than 0.08 by location 2: R_f = 2.42, and the equilibrium channel length (L_l) for the 12 μm diameter sphere is 0.41 cm, which is 1/10th the length of the first ring. This value of the equilibrium length for WBCs corresponds to the narrowing of the intensity peak of the WBCs at location 2 where the channel length is 2.15 cm. From location 3 the R_f of 12 μm particles increases from 2.50 to 2.91 until location 8, which means the flow focus of 12 μm particles should be improved along each ring of the channel. Verifying this prediction with R_f, the red fluorescence signal intensity and peak generally became sharper at the middle of the channel from

location 3 to location 6. There are also wider intensity peak profiles at locations 5, 7, and 8. he highest peak in these wider peaks profiles seems to move toward the inner wall.

The shifting phenomenon of focused stream can be caused by Dean flow shifting. Dean force drives the slow-moving fluids near the long face pf the wall inward, while faster-moving fluid in the core is swept outward. The known equilibrium particle positions of a rectangular channel are around the near long face wall middle area. Therefore, the slower inward force of a Dean flow can cause shifting of the focused WBC stream toward the middle of the channel. And this effect may also cause disruption/broadening of focused particle stream.

It has observed that the width of focused streams of WBC is not consistent from location 1 to 8. The most sharpened streams are at locations 4 and 6. And wider focused streams are at locations 3, 5, and 7; these streams are very similar in width. It almost seems that this pulsation is periodic. A plausible explanation for this pulsation of focused streams in Figure 3.4 is deformability of WBCs in the flow. A similar effect was also observed by Nivedta et al. in the flow of red blood cells in spiral channels [59].

A similar equilibrium length analysis of sperm cells (5 μm particle) was carried out using equation 5 and R_f. The analysis showed that R_f is always above 0.08 (R_f: 0.175 ~0.21) from location 1 to location 8 with a flowrate of 0.52 ml/min, which suggests sperm should be focused after location 1 and the flow focusing should improve as sperm pass through later ring locations. The calculated equilibrium length for a 5 μm particle is 5.73 cm, which occurs between location 3 and location 4. The sperm stream appears to reach its maximum focusing level at this point and the peak location gradually slides towards a mid-outer location from location 4 to location 8. However, the intensity plot of location 8

(Figure 3.4(8)) again shows the flow focusing of sperm is not as narrow as the WBC stream.

The analysis of images from Figure 3.4, also provides an understanding of the relationship between particle concentration and flow focusing behavior. This phenomenon can be defined by the number of particles per channel length (length fraction) [25], [27], which is defined following the relation: $\beta = 3WHV_f/4\pi {a_p}^2$. According to Amini et al., for the case of $\beta > 1$, particles cannot be expected to be focused, due to interactions between neighboring particles. Therefore to minimize interaction between neighboring particles, concentrations of particles should be adjusted to appropriate β values. For this work with 5 μm (sperm: 5 million/ml) and 12 μm (WBC: 2 million/ml) diameter particles, $\beta_{5\mu m}$ is 3.6% and $\beta_{12\mu m}$ is 0.6%. For WBC separation by a spiral channel, β is far less than ~50%; which Amini et al. described as the threshold of high length fraction. These calculated $\beta_{5\mu m}$ and $\beta_{12\mu m}$values verify that our initial sample concentration is within the range of the length fraction condition for RBCs (with β_{RBC} = 1.6%). Our previous empirical results on separation of RBCs in spiral channels with β_{RBC} = 1.6% have been reported with good focusing of RBCs [27].

In summary, sperm focusing peaks were less sharp than WBC peaks, which is likely due to to the asymmetrical shape of the sperm. The results suggest that sperm cells cannot be assumed to have the same focusing behavior as 5 μm diameter spherical particles, so their effective size must be considered as something smaller. This relatively poor focusing behavior has been briefly discussed by Hur et al. in the study regarding inertial focusing of nonspherical microparticles [50]. We are currently performing extensive experiments to explain the cause of this behavior. However, sharp flow focusing of WBCs allowed the significant reduction in concentration of WBCs in the

sample and consequently provided a much cleaner (fewer WBCs) final sample than the initial simulated sample of sperm and WBCs.

3.5 Conclusion

In conclusion, we successfully demonstrated the use of inertial microfluidics to significantly reduce WBC concentration by flow focusing of WBCs to a waste channel utilizing inertial microfluidics physics. The estimated sample process time was more rapid (~5 minutes) and less hands-on than the conventional method (gradient centrifuge sperm wash; ~1 hour). A mixture of sperm/WBC was injected as input and 83% of sperm and 93% of WBCs were collected separately from two distinct outlets.

During modeling and design preparations, we assumed a spherical shape for WBCs (12 μm sphere) and sperm cells (5 μm sphere) and found that the WBC results corresponded with a force ratio (R_f) and equilibrium length typical of a 12 μm sphere particle, suggesting that the modeling of WBCs as a sphere was sufficient, but the results for the sperm cells suggested that modeling them as a 5 μm sphere was not accurate, They were still only modestly focused, suggesting that they behave as smaller particles, or that the asymmetrical nature of the sperm cells causes them to not act like a uniform particle set. Despite the fact that generating sharp flow focusing of sperm was not possible under these conditions, most likely due to our current incomplete understanding of how sperm behave in the inertial microfluidic channel, the ability to somewhat focus the sperm while sharply focusing the WBCs led to the significant reduction of WBC concentration in high WBC semen, which should provide a significant advantage over current ART procedures when processing leukospermia samples.

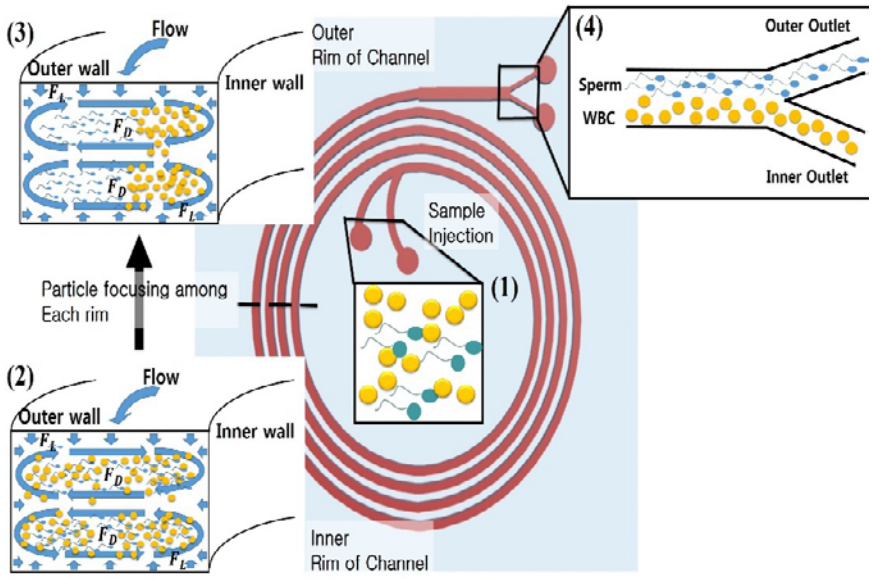

Figure 3.1 Overview of approach: A spiral channel is utilized to separate unwanted bio-molecular from highly contaminated semen samples (high WBC semen). (1) A semen sample with a high concentration of WBCs (yellow) and a low sperm (blue) concentration is injected though the inlets. (2) Evenly distributed cells at the first ring of the spiral. Flow focusing of particles in the channels proceeds as the sample moves through the spiral. (3) The lateral migration of each cell (sperm and WBC) continues until each cell reaches an equilibrium position in the later rings of the spiral. (4) Focused flow cells at the outlet area: most of the WBCs are collected at the inner outlet and the sperm are collected at the outer outlet.

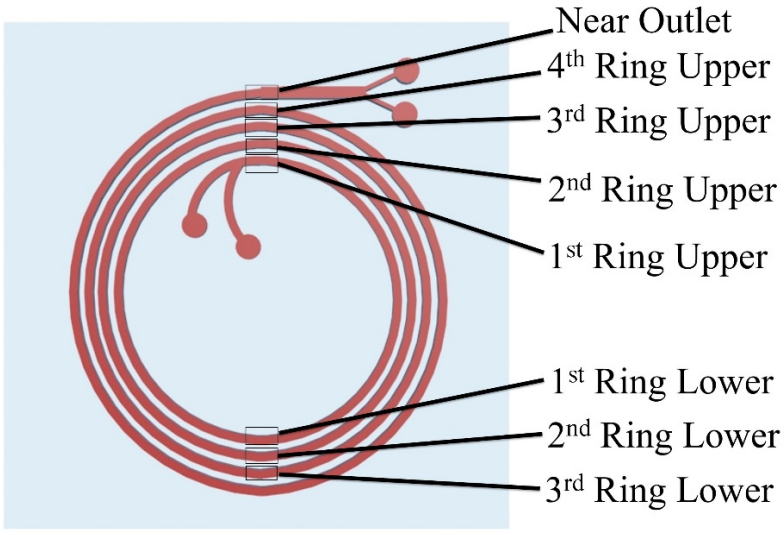

Figure 3.2 High-speed camera image acquisition locations to observe the focusing behavior of the cells and their equilibrium positions along the spiral channel (Top view of the spiral channel). Eight different locations were utilized for image acquisition.

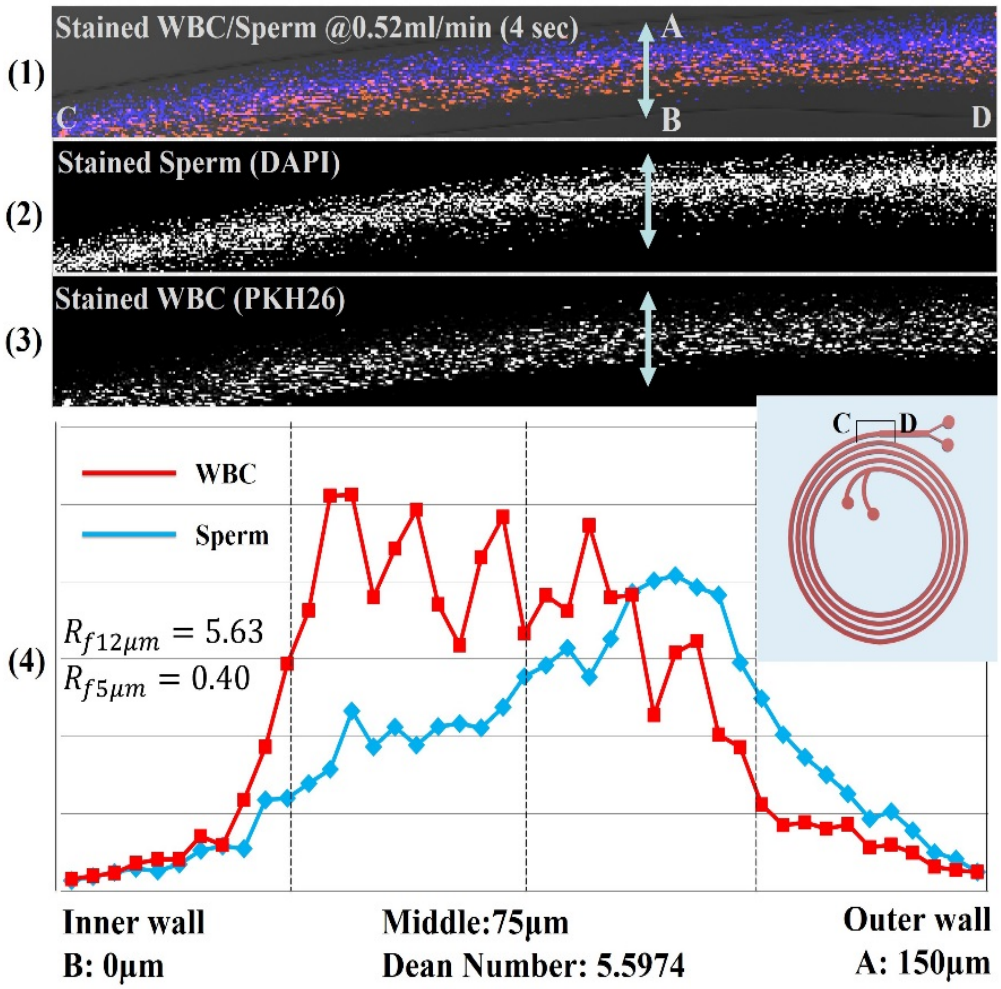

Figure 3.3 Results of WBC and sperm location imaging experiments. Each image is a combined stack of frames obtained by a high speed camera monitoring near the end of the 4th ring of the channel, (1) combined stained sperm and WBC image, (2) DAPI only image showing sperm, (3) PKH26 only image showing WBCs, (4) optical intensity plot across the width of the channel for the stained sperm and WBCs acquired from the obtained images.

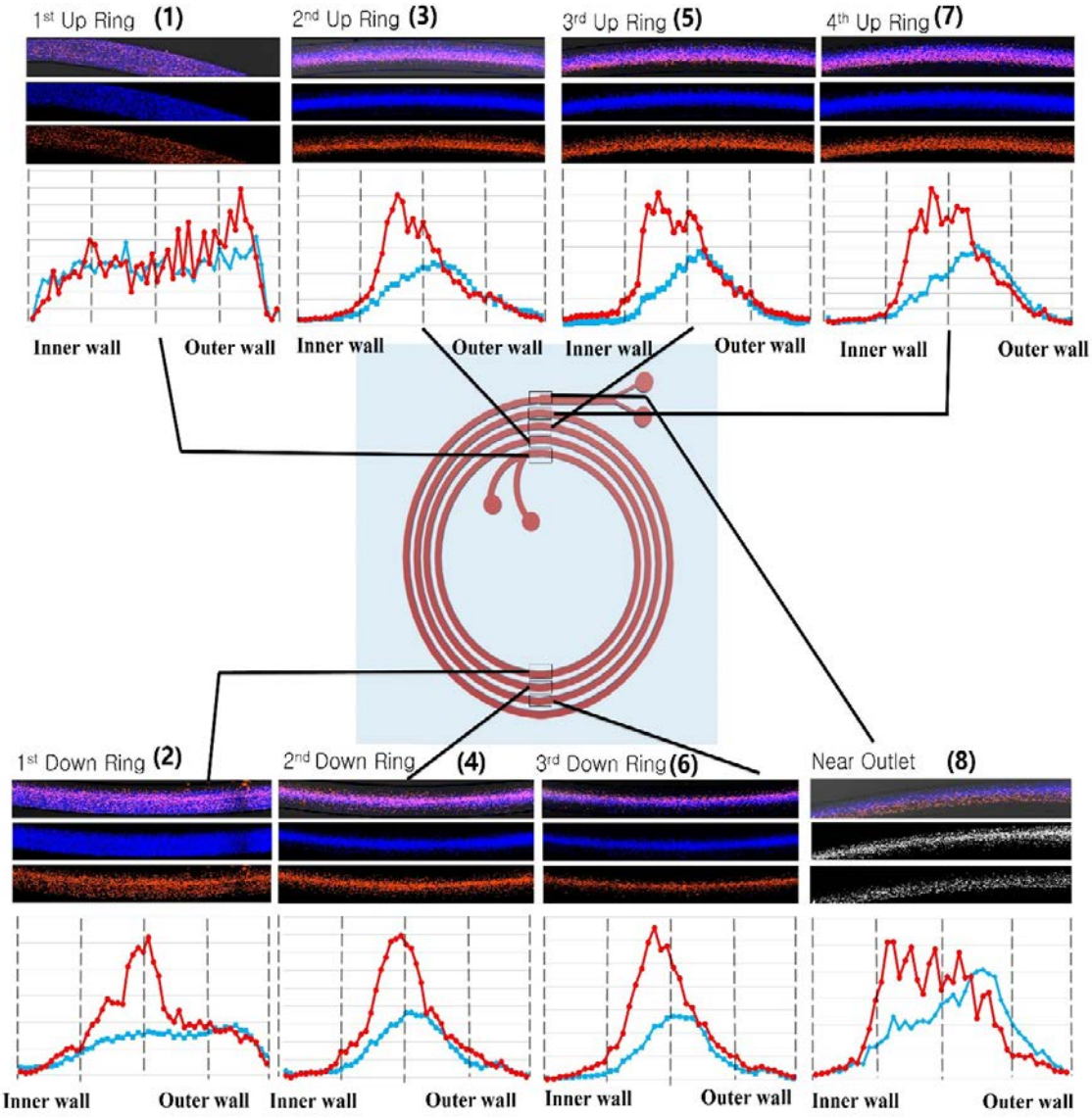

Figure 3.4 Stained WBC and sperm flow stacked images and intensity plots at both the "up" and "down" positions of 1st, 2nd, 3rd, and 4th rings. These positions are expressed as location 1-8.

Table 3.1 Sample details. WBC A sample is for WBC characterization purposes, and Semen A represent a simulated high WBC semen sample

Sample Type	WBC Concentration (million/ml)	*RBC Concentration (million/ml)	Sperm Concentration (million/ml)
WBC A	8.1	1.3	0
Semen A	8.35	1.4	2.45

* RBC count data appeared in the table because WBCs were separated from a whole blood sample. Therefore, there was a small amount of RBCs in the WBC sample.

Table 3.2 WBC A sample behavior at 0.52ml/min within the channel.

Cell Type	Inner Outlet In million/ml (Percent of total)	Outer Outlet In million/ml (Percent of total)	Total In million/ml	Inlet Sample In million/ml
WBC	5.45±0.85 (95%)	0.3±0.1 (5%)	5.75(100%)	8.1±0.8
RBC*	1.15±0.15 (85.2%)	0.2±0.1 (14.8%)	1.35(100%)	1.3

* RBC count data are included because WBCs were contaminated with some RBCs.

Table 3.3 Semen A sample separation results in terms of concentration.

Cell Type	Inner Outlet In million/ml (Percent of total)	Outer Outlet In million/ml (Percent of total)	Total In million/ml	Inlet Sample In million/ml
WBC	7.25±1.63(92%)	0.47±0.08 (8%)	7.72(100%)	8.35±0.43
RBC*	0.69±0.13(87.3%)	0.11±0.05(12.7%)	0.80(100%)	1.4±0.05
Sperm	0.58±0.08(16.8%)	2.81±0.25(83.2%)	3.39(100%)	2.45±0.08

* RBC count data are included because WBCs were contaminated with some RBCs.

3.6 References

[1] G. Velve-Casquillas, M. Le Berre, M. Piel, and P. T. Tran, "Microfluidic tools for cell biological research," *Nano Today*, vol. 5, no. 1, pp. 28–47, Feb. 2010.

[2] S. Cho, D. K. Kang, J. Choo, A. J. deMello, and S. I. Chang, "Recent advances in microfluidic technologies for biochemistry and molecular biology," *BMB Rep.*, vol. 44, no. 11, pp. 705–712, Nov. 2011.

[3] D. C. Duffy, J. C. McDonald, O. J. A. Schueller, and G. M. Whitesides, "Rapid prototyping of microfluidic systems in poly(dimethylsiloxane)," *Anal. Chem.*, vol. 70, no. 23, pp. 4974–4984, Oct. 1998.

[4] K. Ohno, K. Tachikawa, and A. Manz, "Microfluidics: Applicatons analytical purposes in chemistry and biochemistry," *Electrophoresis*, vol. 29, pp. 4443–4453, Nov. 2008.

[5] Y. Zhang *et al.*, "DNA methylation analysis on a droplet-in-oil PCR array," *Lab Chip*, vol. 9, no. 8, pp. 1059–1064, Apr. 2009.

[6] C. Wyatt Shields IV, C. D. Reyes, and G. P. López, "Microfluidic cell sorting: A review of the advances in the separation of cells from debulking to rare cell isolation," *Lab Chip*, vol. 15, no. 5, pp. 1230–1249, Jan. 2015.

[7] H. Andersson and A. Van den Berg, "Microfluidic devices for cellomics: A review," *Sensors Actuators, B Chem.*, vol. 92, no. 3, pp. 315–325, Jul. 2003.

[8] S. M. Kim, S. H. Lee, and K. Y. Suh, "Cell research with physically modified microfluidic channels: A review," *Lab a Chip - Miniaturisation Chem. Biol.*, vol. 8, no. 7, pp. 1015–1023, Jul. 2008.

[9] R. N. Zare and S. Kim, "Microfluidic platforms for single-cell analysis," *Annu. Rev. Biomed. Eng.*, vol. 12, no. 1, pp. 187–201, Apr. 2010.

[10] A. Lenshof and T. Laurell, "Continuous separation of cells and particles in microfluidic systems," *Chem. Soc. Rev.*, vol. 39, no. 3, pp. 1203–1217, Feb. 2010.

[11] D. R. Gossett *et al.*, "Label-free cell separation and sorting in microfluidic systems," *Anal. Bioanal. Chem.*, vol. 397, no. 8, pp. 3249–67, Aug. 2010.

[12] A. A. S. Bhagat, H. Bow, H. W. Hou, S. J. Tan, J. Han, and C. T. Lim, "Microfluidics for cell separation," *Med. Biol. Eng. Comput.*, vol. 48, no. 10, pp. 999–1014, Oct. 2010.

[13] S. Choi and J.-K. Park, "Microfluidic system for dielectrophoretic separation based on a trapezoidal electrode array," *Lab Chip*, vol. 5, no. 10, pp. 1161–1167, Oct.

2005.

[14] A. F. Cowman and B. S. Crabb, “Review invasion of red blood cells by malaria parasites,” *Cell,* pp. 755–766, Feb. 2006.

[15] W. J. Kleijer, M. L. T. van der Sterre, V. H. Garritsen, A. Raams, and N. G. J. Jaspers, “Prenatal diagnosis of the Cockayne syndrome: Survey of 15 years experience,” *Prenat. Diagn.*, vol. 26, no. 10, pp. 980–984, Oct. 2006.

[16] S. Nagrath *et al.*, “Isolation of rare circulating tumour cells in cancer patients by microchip technology,” *Nature*, vol. 450, pp. 1235-1239, December, 2007.

[17] F. Petersson, L. Åberg, A. M. Swärd-Nilsson, and T. Laurell, “Free flow acoustophoresis: Microfluidic-based mode of particle and cell separation,” *Anal. Chem.*, vol. 79, no. 14, pp. 5117–5123, Jun. 2007.

[18] E. L. Tóth, E. Holczer, P. Földesy, K. Iván, and P. Fürjes, “Microfluidic particle sorting system for environmental pollution monitoring applications,” *Procedia Eng.*, vol. 168, pp. 1462–1465, Sep. 2016.

[19] N. Xia *et al.*, “Combined microfluidic-micromagnetic separation of living cells in continuous flow,” *Biomed. Microdevices*, vol. 8, no. 4, pp. 299–308, Dec. 2006.

[20] B. H. Weigl and P. Yager, “Microfluidic diffusion-based separation and detection,” *Science*, vol. 283, no. 5400, p. 346 LP-347, Jan. 1999.

[21] D. W. Inglis, “Efficient microfluidic particle separation arrays,” *Appl. Phys. Lett.*, vol. 94, no. 1, Jan. 2009.

[22] J. Nam, H. Lim, D. Kim, H. Jung, and S. Shin, “Continuous separation of microparticles in a microfluidic channel via the elasto-inertial effect of non-Newtonian fluid,” *Lab Chip*, vol. 12, no. FEBRUARY, p. 1347, Jan. 2012.

[23] J. E. Swain, D. Lai, S. Takayama, and G. D. Smith, “Thinking big by thinking small: Application of microfluidic technology to improve ART,” *Lab Chip*, vol. 13, no. 7, pp. 1213–24, Apr. 2013.

[24] G. Segré and A. Silberberg, “Radial particle displacements in poiseuille flow of suspensions,” *Comput. Geotech.*, vol. 189, no. 4760, pp. 209–210, Jan. 1961.

[25] D. Di Carlo, “Inertial microfluidics,” *Lab Chip*, vol. 9, no. 21, pp. 3038–3046, Nov. 2009.

[26] J. M. Martel and M. Toner, “Inertial focusing dynamics in spiral microchannels,” *Phys. Fluids*, vol. 24, no. 3, p. 32001, Mar. 2012.

[27] H. Amini, W. Lee, and D. Di Carlo, “Inertial microfluidic physics,” *Lab Chip*, vol. 14, no. 15, pp. 2739–61, May. 2014.

[28] E. S. Asmolov, “The inertial lift on a spherical particle in a plane Poiseuille flow at large channel Reynolds number,” *J. Fluid Mech.*, vol. 381, pp. 63–87, Jan. 1999.

[29] D. Di Carlo, J. F. Edd, K. J. Humphry, H. A. Stone, and M. Toner, “Particle segregation and dynamics in confined flows,” *Phys. Rev. Lett.*, vol. 102, no. 9, pp. 1–4, Mar. 2009.

[30] J. Zhou and I. Papautsky, “Fundamentals of inertial focusing in microchannels,” *Lab Chip*, vol. 13, no. 6, pp. 1121–32, Mar. 2013.

[31] J. M. Martel and M. Toner, “Particle focusing in curved microfluidic channels,” *Sci. Rep.*, vol. 3, pp. 1–8, Nov. 2013.

[32] P. G. Saffman, “The lift on a small sphere in a slow shear flow,” *J. Fluid Mech.*, vol. 22, no. 2, pp. 385–400, Fe. 1965.

[33] S. I. Rubinow and J. B. Keller, “The transverse force on a spinning sphere moving in a viscous fluid,” *J. Fluid Mech.*, vol. 11, no. 3, pp. 447–459, Nov. 1961.

[34] B. P. Ho and L. G. Leal, “Migration of rigid spheres in a two-dimensional unidirectional shear flow of a second-order fluid,” *J. Fluid Mech.*, vol. 65, no. 2, pp. 365–400, Aug. 1974.

[35] W. R. Dean, “LXXII. The stream-line motion of fluid in a curved pipe (Second paper),” *London, Edinburgh, Dublin Philos. Mag. J. Sci.*, vol. 5, no. 30, pp. 673–695, Apr. 1928.

[36] S. A. Berger, L. Talbot, and L. S. Yao, “Flow in curved pipes,” *Annu. Rev. Fluid Mech.*, vol. 15, pp. 461–512, Jan. 1983.

[37] D. R. Gossett and D. Di Carlo, “Particle focusing mechanisms in curving confined flows,” *Anal. Chem.*, vol. 81, no. 20, pp. 8459–8465, Sep. 2009.

[38] D. Di Carlo, D. Irimia, R. G. Tompkins, and M. Toner, “Continuous inertial focusing, ordering, and separation of particles in microchannels,” *Proc. Natl. Acad. Sci. U. S. A.*, vol. 104, no. 48, pp. 18892–18897, Nov. 2007.

[39] A. A. S. Bhagat, S. S. Kuntaegowdanahalli, and I. Papautsky, “Continuous particle separation in spiral microchannels using Dean flows and differential migration,” *Lab Chip*, vol. 8, no. 11, pp. 1906–1914, Nov. 2008.

[40] S. Ookawara, R. Higashi, D. Street, and K. Ogawa, “Feasibility study on concentration of slurry and classification of contained particles by microchannel,”

Chem. Eng. J., vol. 101, no. 1–3, pp. 171–178, Aug. 2004.

[41] A. A. S. Bhagat, S. S. Kuntaegowdanahalli, and I. Papautsky, "Enhanced particle filtration in straight microchannels using shear-modulated inertial migration," *Phys. Fluids*, vol. 20, no. 10, 2008.

[42] D. Di Carlo, "Inertial microfluidics," *Lab Chip*, vol. 9, no. 21, pp. 3038–46, Nov. 2009.

[43] F. P. Bretherton, "The motion of rigid particles in a shear flow at low Reynolds number," *J. Fluid Mech.*, vol. 14, no. 2, pp. 284–304, Oct. 1962.

[44] W. E. Uspal, H. Burak Eral, and P. S. Doyle, "Engineering particle trajectories in microfluidic flows using particle shape," *Nat. Commun.*, vol. 4, p. 2666, Apr. 2013.

[45] T. Kaya and H. Koser, "Characterization of hydrodynamic surface interactions of escherichia coli cell bodies in shear flow," *Phys. Rev. Lett.*, vol. 103, no. 13, pp. 1–4, Sep. 2009.

[46] G. B. Jeffery, "The motion of ellipsoidal particles immersed in a viscous fluid," *Math. Phys. Eng. Sci.*, pp. 161–179, Nov. 1922.

[47] C. Y. Wu, K. Owsley, and D. Di Carlo, "Rapid software-based design and optical transient liquid molding of microparticles," *Adv. Mater.*, vol. 27, no. 48, pp. 7970–7978, Oct. 2015.

[48] M. L. Ekiel-Jeżewska and E. Wajnryb, "Hydrodynamic orienting of asymmetric microobjects under gravity," *J. Phys. Condens. Matter*, vol. 21, no. 20, p. 204102, May. 2009.

[49] P. J. A. Janssen, M. D. Baron, P. D. Anderson, J. Blawzdziewicz, M. Loewenberg, and E. Wajnryb, "Collective dynamics of confined rigid spheres and deformable drops," *Soft Matter*, vol. 8, no. 28, pp. 7495–7506, Aug. 2012.

[50] S. C. Hur, S. E. Choi, S. Kwon, and D. Di Carlo, "Inertial focusing of non-spherical microparticles," *Appl. Phys. Lett.*, vol. 99, no. 4, pp. 1–4, Jul. 2011.

[51] J. Elgeti, U. B. Kaupp, and G. Gompper, "Hydrodynamics of sperm cells near surfaces," *Biophysj*, vol. 99, no. 4, pp. 1018–1026, Aug. 2010.

[52] W. Lee, H. Amini, H. A Stone, and D. Di Carlo, "Dynamic self-assembly and control of microfluidic particle crystals," *Proc. Natl. Acad. Sci. U. S. A.*, vol. 107, no. 52, pp. 22413–22418, Dec. 2010.

[53] J. Sun *et al.*, "Double spiral microchannel for label-free tumor cell separation and

enrichment," *Lab Chip*, vol. 12, no. 20, p. 3952, Jul. 2012.

[54] M. Jimenez, B. Miller, and H. L. Bridle, "Efficient separation of small microparticles at high flowrates using spiral channels: Application to waterborne pathogens," *Chem. Eng. Sci.*, vol. 157, pp. 247–254, Jan. 2017.

[55] Z. Wu, B. Willing, J. Bjerketorp, J. K. Jansson, and K. Hjort, "Soft inertial microfluidics for high throughput separation of bacteria from human blood cells," *Lab Chip*, vol. 9, no. 9, pp. 1193–9, May. 2009.

[56] A. J. Mach and D. di Carlo, "Continuous scalable blood filtration device using inertial microfluidics," *Biotechnol. Bioeng.*, vol. 107, no. 2, pp. 302–311, Oct. 2010.

[57] X. Wang, C. Liedert, R. Liedert, and I. Papautsky, "A disposable, roll-to-roll hot-embossed inertial microfluidic device for size-based sorting of microbeads and cells," *Lab Chip*, vol. 16, pp. 1821–1830, May. 2016.

[58] M. G. Lee, J. H. Shin, C. Y. Bae, S. Choi, and J. K. Park, "Label-free cancer cell separation from human whole blood using inertial microfluidics at low shear stress," *Anal. Chem.*, vol. 85, no. 13, pp. 6213–6218, Jun. 2013.

[59] N. Nivedita and I. Papautsky, "Continuous separation of blood cells in spiral microfluidic devices," *Biomicrofluidics*, vol. 7, no. 5, Sep. 2013.

[60] M. E. Warkiani *et al.*, "Slanted spiral microfluidics for the ultra-fast, label-free isolation of circulating tumor cells," *Lab Chip*, vol. 14, no. 1, pp. 128–37, Jan. 2014.

[61] T. H. Kim, H. J. Yoon, P. Stella, and S. Nagrath, "Cascaded spiral microfluidic device for deterministic and high purity continuous separation of circulating tumor cells," *Biomicrofluidics*, vol. 8, no. 6, p. 64117, Dec. 2014.

[62] A. A. S. Bhagat, H. W. Hou, L. D. Li, C. T. Lim, and J. Han, "Pinched flow coupled shear-modulated inertial microfluidics for high-throughput rare blood cell separation," *Lab Chip*, vol. 11, no. 11, pp. 1870–1878, Apr. 2011.

[63] S. Shen *et al.*, "High-throughput rare cell separation from blood samples using steric hindrance and inertial microfluidics," *Lab Chip*, vol. 14, no. 14, pp. 2525–38, Jul. 2014.

[64] D. Di Carlo, J. F. Edd, D. Irimia, R. G. Tompkins, and M. Toner, "Equilibrium separation and filtration of particles using differential inertial focusing," *Anal. Chem.*, vol. 80, no. 6, pp. 2204–2211, Feb. 2008.

[65] J. Boivin, L. Bunting, J. A. Collins, and K. G. Nygren, "International estimates of

infertility prevalence and treatment-seeking: Potential need and demand for infertility medical care," *Hum. Reprod.*, vol. 22, no. 6, pp. 1506–1512, Jun. 2007.

[66] T. G. Cooper *et al.*, "World Health Organization reference values for human semen characteristics," *Hum. Reprod. Update*, vol. 16, no. 3, pp. 231–245, May-Jun. 2009.

[67] R. Samuel *et al.*, "Microfluidics: The future of microdissection TESE?," *Syst. Biol. Reprod. Med.*, vol. 62, no. 3, pp. 161–70, Jun. 2016.

[68] K. Baker and E. Sabanegh, "Obstructive azoospermia: Reconstructive techniques and results," *Clinics*, vol. 68, no. S1, pp. 61–73, Feb. 2013.

[69] I. Craft *et al.*, "Percutaneous epididymal sperm aspiration and intracytoplasmic sperm injection in the management of infertility due to obstructive azoospermia," *Fertil. Steril.*, vol. 63, no. 5, pp. 1038–42, May. 1995.

[70] P. N. Schlegel, "Testicular sperm extraction: Microdissection improves sperm yield with minimal tissue excision," *Hum. Reprod.*, vol. 14, no. 1, pp. 131–135, Jan. 1999.

[71] P. N. Schlegel and L. M. Su, "Physiological consequences of testicular sperm extraction," *Hum. Reprod.*, vol. 12, no. 8, pp. 1688–1692, Aug. 1997.

[72] R. Kumar, "Medical management of non-obstructive azoospermia," *Clinics.* vol. 2013, pp. 75–79, Feb. 2013.

[73] P. Donoso, H. Tournaye, and P. Devroey, "Which is the best sperm retrieval technique for non-obstructive azoospermia? A systematic review," *Hum. Reprod. Update*, vol. 13, no. 6, pp. 539–549, Nov-Dec. 2007.

[74] C. Krausz, "Male infertility: Pathogenesis and clinical diagnosis," *Best Pract. Res. Clin. Endocrinol. Metab.*, vol. 25, no. 2, pp. 271–85, Apr. 2011.

[75] A. Bettegowda and M. F. Wilkinson, "Transcription and post-transcriptional regulation of spermatogenesis," *Philos. Trans. R. Soc. Lond. B. Biol. Sci.*, vol. 365, no. 1546, pp. 1637–1651, May. 2010.

[76] M. Ostad, D. Liotta, Z. Ye, P. N. Schlegel, "Teticular sperm extraction for nonobstructive azoospermia: Results of a multibiopsy approach with optimized tissue dispersion," *Urology*, vol. 4295, no. 98, pp. 692–696, Oct. 1998.

[77] L. Gambera, F. Serafini, G. Morgante, R. Focarelli, V. De Leo, and P. Piomboni, "Sperm quality and pregnancy rate after COX-2 inhibitor therapy of infertile males with abacterial leukocytospermia," *Hum. Reprod.*, vol. 22, no. 4, pp. 1047–1051, Apr. 2007.

[78] C. M. Peterson, A. O. Hammoud, E. Lindley, D. T. Carrell, and K. Wilson, "Assisted Reproductive Technology Practice Management", *Reproductive Endocrinology and Infertility*, D. T. Carrell, C. M. Peterson, Ed. New York: Springer, 2010, pp. 7-37.

[79] M. J. Chen and A. Bongso, "Comparative evaluation of two density gradient preparations for sperm separation for medically assisted conception," *Hum. Reprod.*, vol. 14, no. 3, pp. 759–764, Mar. 1999.

[80] L. J. Kricka *et al.*, "Micromachined analytical devices: Microchips for semen testing," *J. Pharm. Biomed. Anal.*, vol. 15, no. 9–10, pp. 1443–7, Jun. 1997.

[81] S. Tasoglu *et al.*, "Exhaustion of racing sperm in nature-mimicking microfluidic channels during sorting," *Small*, vol. 9, no. 20, pp. 3374–3384, Oct. 2013.

[82] B. S. Cho, T. G. Schuster, X. Zhu, D. Chang, G. D. Smith, and S. Takayama, "Passively driven integrated microfluidic system for separation of motile sperm," *Anal. Chem.*, vol. 75, no. 7, pp. 1671–1675, Feb. 2003.

[83] T. G. Schuster, B. Cho, L. M. Keller, S. Takayama, and G. D. Smith, "Isolation of motile spermatozoa from semen samples using microfluidics," *Reprod. Biomed. Online*, vol. 7, no. 1, pp. 75–81, Jan. 2003.

[84] H. Huang, "Motile human sperm sorting by an integrated microfluidic system," *J. Nanomed. Nanotechnol.*, vol. 5, no. 3, pp. 193-199, May. 2014.

[85] H.-Y. Huang *et al.*, "Isolation of motile spermatozoa with a microfluidic chip having a surface-modified microchannel," *J. Lab. Autom.*, vol. 19, no. 1, pp. 91–9, Feb. 2013.

[86] K. Matsuura, M. Takenami, Y. Kuroda, T. Hyakutake, S. Yanase, and K. Naruse, "Screening of sperm velocity by fluid mechanical characteristics of a cyclo-olefin polymer microfluidic sperm-sorting device," *Reprod. Biomed. Online*, vol. 24, no. 1, pp. 109–15, Jan. 2012.

[87] H. Sano, K. Matsuura, K. Naruse, and H. Funahashi, "Application of a microfluidic sperm sorter to the in-vitro fertilization of porcine oocytes reduced the incidence of polyspermic penetration," *Theriogenology*, vol. 74, no. 5, pp. 863–70, Sep. 2010.

[88] J. M. Wu, Y. Chung, K. J. Belford, G. D. Smith, S. Takayama, and J. Lahann, "A surface-modified sperm sorting device with long-term stability," *Biomed. Microdevices*, vol. 8, no. 2, pp. 99–107, Jun. 2006.

[89] S. Koyama, D. Amarie, H. Soini, M. Novotny, and S. Jacobson, "Chemotaxis assays of mouse sperm on microfluidic devices," *Anal. chem.*, vol. 78, no. 10, pp.

3354–3359, Apr. 2006.

[90] L. Xie *et al.*, "Integration of sperm motility and chemotaxis screening with a microchannel-based device," *Clin. Chem.*, vol. 56, no. 8, pp. 1270–8, Aug. 2010.

[91] Y.-J. Ko, J.-H. Maeng, B.-C. Lee, S. Lee, S. Y. Hwang, and Y. Ahn, "Separation of progressive motile sperm from mouse semen using on-chip chemotaxis," *Anal. Sci.*, vol. 28, no. 1, pp. 27–32, Jan. 2012.

[92] S. S. Suarez and M. Wu, "Microfluidic devices for the study of sperm migration," *Mol. Hum. Reprod.*, pp. 1–8, Apr. 2017.

[93] C.-Y. Chen *et al.*, "Sperm quality assessment via separation and sedimentation in a microfluidic device," *Analyst*, vol. 138, no. 17, pp. 4967–74, Sep. 2013.

[94] S. M. Knowlton, M. Sadasivam, and S. Tasoglu, "Microfluidics for sperm research," *Trends Biotechnol.*, vol. 33, no. 4, pp. 221–229, Apr. 2015.

[95] R. Ma *et al.*, "In vitro fertilization on a single-oocyte positioning system integrated with motile sperm selection and early embryo development," *Anal. Chem.*, vol. 83, no. 8, pp. 2964–2970, Mar. 2011.

[96] Y. Lin, P. Chen, R. Wu, L. Pan, and F. Tseng, "Micro diffuser-type movement inversion sorter for high-efficient sperm sorting," *Int. Conf Nano/Micro Eng. Mol. Syst.*, pp. 7–10, Apr. 2013.

[97] M. D. C. Lopez-Garcia, R. L. Monson, K. Haubert, M. B. Wheeler, and D. J. Beebe, "Sperm motion in a microfluidic fertilization device," *Biomed. Microdevices*, vol. 10, no. 5, pp. 709–718, Oct. 2008.

[98] M. Wheeler and M. Rubessa, "Integration of Microfluidics and Mammalian IVF," *Mol. Hum Regrod,* vol. 23, iss. 4, pp. 248–256, Apr. 2017.

[99] R. S. Suh, X. Zhu, N. Phadke, D. A. Ohl, S. Takayama, and G. D. Smith, "IVF within microfluidic channels requires lower total numbers and lower concentrations of sperm," *Hum. Reprod.*, vol. 21, no. 2, pp. 477–483, Feb. 2006.

[100] J. Son, K. Murphy, R. Samuel, B. Gale, D. Carrell, and J. Hotaling, "Non-motile sperm cell separation using a spiral channel," *Anal. Methods*, iss. 7, pp. 8041-8047, May. 2015.

[101] S. S. Kuntaegowdanahalli, A. A. S. Bhagat, G. Kumar, and I. Papautsky, "Inertial microfluidics for continuous particle separation in spiral microchannels," *Lab Chip*, vol. 9, no. 20, pp. 2973–80, Oct. 2009.

[102] P. R. Wheater, H. G. Burkitt, and V. G. Daniels, *Functional Histology. A Text and*

Colour Atlas. Edinburgh: Churchill, 1979.

[103] M. Diez-Silva, M. Dao, J. Han, C.-T. Lim, and S. Suresh, "Shape and biomechanical characteristics of human red blood cells in health and disease," *MRS Bull.*, vol. 35, no. 5, pp. 382–388, May. 2010.

[104] J. A. Mossman, J. T. Pearson, H. D. Moore, and A. A. Pacey, "Variation in mean human sperm length is linked with semen characteristics," *Hum. Reprod.*, vol. 28, no. 1, pp. 22–32, Jan. 2013.

[105] L. Maree, S. S. Du Plessis, R. Menkveld, and G. Van Der Horst, "Morphometric dimensions of the human sperm head depend on the staining method used," *Hum. Reprod.*, vol. 25, no. 6, pp. 1369–1382, Jun. 2010.

[106] J. E. Lackner, I. Märk, K. Sator, J. Huber, and M. Sator, "Effect of leukocytospermia on fertilization and pregnancy rates of artificial reproductive technologies," *Fertil. Steril.*, vol. 90, no. 3, pp. 869–871, Sep. 2008.

[107] N. Nivedita and I. Papautsky, "Continuous separation of blood cells in spiral microfluidic devices," *Biomicrofluidics*, vol. 7, no. 5, pp. 1–14, Sep. 2013.

[108] J.-P. Frimat *et al.*, "Make it spin: Individual trapping of sperm for analysis and recovery using micro-contact printing," *Lab Chip*, vol. 14, no. 15, pp. 2635–41, Aug. 2014.

[109] C. Ainsworth, B. Nixon, R. P. S. Jansen, and R. J. Aitken, "First recorded pregnancy and normal birth after ICSI using electrophoretically isolated spermatozoa," *Hum. Reprod.*, vol. 22, no. 1, pp. 197–200, Sep. 2007.

[110] R. Zeggari, B. Wacogne, C. Pieralli, C. Roux, and T. Gharbi, "A full micro-fluidic system for single oocyte manipulation including an optical sensor for cell maturity estimation and fertilisation indication," *Sensors Actuators, B Chem.*, vol. 125, no. 2, pp. 664–671, Aug. 2007.

[111] A. A. El-Ghobashy and C. R. West, "The human sperm head: A key for successful fertilization," *J. Androl.*, vol. 24, no. 2, pp. 232–8, Mar-Apr. 2003.

[112] WHO, *Examination and processing of human semen*, 5th ed, WHO, Geneva: Swiss. 2010.

[113] M. Ionescu *et al.*, "Enhanced biocompatibility of PDMS (polydimethylsiloxane) polymer films by ion irradiation," *Nucl. Inst. Methods Phys. Res. B*, vol. 273, pp. 161–163, Feb. 2012.

[114] C. Garrett, D. Y. Liu, R. I. McLachlan, and H. W. G. Baker, "Time course of changes in sperm morphometry and semen variables during testosterone-induced

suppression of human spermatogenesis," *Hum. Reprod.*, vol. 20, no. 11, pp. 3091–3100, Nov. 2005.

[115] N. Guz, M. Dokukin, V. Kalaparthi, and I. Sokolov, "If cell mechanics can be described by elastic modulus: Study of different models and probes used in indentation experiments," *Biophys. J.*, vol. 107, no. 3, pp. 564–575, Aug. 2014.

[116] X. Zhang *et al.*, "Lensless imaging for simultaneous microfluidic sperm monitoring and sorting," *Lab Chip*, vol. 11, no. 15, pp. 2535–2540, Aug. 2011.

[117] L. I. Segerink, A. J. Sprenkels, P. M. ter Braak, I. Vermes, and A. van den Berg, "On-chip determination of spermatozoa concentration using electrical impedance measurements," *Lab Chip*, vol. 10, no. 8, pp. 1018–24, Apr. 2010.

CHAPTER 4

THE BIOLOGICAL AND PHYSICAL EFFECTS ON SPERM PROCESSED IN A PDMS SPIRAL CHANNEL

4.1 Introduction

Microfluidic technologies can provide valuable options for cell sorting/separation and there have been various attempts to eliminate the tedium and imprecision of procedures associated with conventional protocols [6], [7], [9], [11], [12], [16], [22]. There have also been many microfluidic attempts to separate sperm from unwanted debris and to improve the efficiency and the effectiveness of assisted reproductive technology (ART). Recently, we have reported a sperm separation method utilizing inertial microfluidic technology that showed clear evidence of sperm separation from unwanted debris, such as red blood cells (RBC) [70] and white blood cells (WBC) [107], without relying on sperm motility. Because this approach showed substantial evidence of sperm enrichment in a highly contaminated sperm sample, there is promise for this approach to be used clinically. Before clinical trials can begin, the physical and biological effects of the process on live sperm need to be understood and evaluated in order to provide assurance of clinical safety.

Previous microfluidic approaches for ART applications [81], [85], [87]–[91], [94], [108]–[110] have been heavily reliant on the motility of sperm and have typically utilized relatively slow, gravity-driven flow (~ few µl/min). In these systems, gravity is the major influencing force for sperm cells during the operation of the device, which does not have any known significant effects reported on the sperm cells. Therefore, the major source of possible damage from these methods was mostly the sample contacting elements such as the inner surface of the device and the buffer. Accordingly, comprehensive testing of the materials contacting the samples is needed to ensure biocompatibility. Unlike previous methods, our recent sperm separation method utilized a syringe pump for injecting samples into a spiral channel device [100]. Also, the injection flow rate was significantly higher

(~1000 times) than previous devices (~ml/min V.S. ~μl/min), which generates significantly higher pressures, shear stress, and centrifugal forces throughout the channel relative to previous microfluidic sperm separation devices [81], [85], [87]–[91], [94], [108]–[110]. Since these effects may cause physical or biological damage to sperm cells, a study quantifying sperm damage is necessary to verify clinical utility of the spiral channel.

Commonly utilized verification methods from previous ART-supporting microfluidic technologies were sperm motility assays, sperm viability (live/dead), the TUNEL assay, fertilization rate, and sperm recovery tests. Among these tests, the motility and the viability tests have been the most common clinical methods to verify sperm quality. Through these tests the difference between the dead and live sperm count and between the initial sperm sample viability and the processed sample viability can indicate if there are significant defects generated in the spiral chip-processed sperm samples. In addition, the sperm recovery rate is also a critical trait to consider, since one of the goals of the spiral channel device is to separate sperm from microdissection testicular sperm extraction (mTESE) samples that only contain extremely small numbers of sperm.

In this work, we performed viability, toxicity, and recovery tests using the proposed sperm separation method. These tests should provide initial verification of clinical usefulness. To show the effectiveness and safety of the device when used with a large number of samples, dozens of sperm samples were acquired randomly from the andrology clinic at the University of Utah and these samples were utilized in each test. All test results show promising evidence that the proposed sperm separation method doesn't significantly affect the sperm when the spiral channel device system is operated under the regular process protocol.

4.2 Spiral Channel Design and Influence on Processed Sperm Cells

The design of the spiral channel determines the optimal injection flow rate, the pressure on sperm cells, and the centrifugal force on sperm cells. Therefore, it is crucial to determine appropriate dimensions because those factors can directly influence the target cells by induced forces during flow.

The optimal dimensions of the spiral channel need to be precisely calculated based on inertial microfluidics theory: the force ratio (R_f), the ratio of particle diameter and hydraulic diameter (λ), and the aspect ratio of the channel. The force ratio (R_f) is a ratio between the Dean drag force (F_D) and the lift force (F_L), where F_D generates a secondary vortex which appears in the channel laterally and F_L is the net lift force comprising the combination of the wall induced lift force and the shear gradient induced lift force that pushes particles away from the walls and center of the channel. The ratio λ should be more than 0.07 to generate optimal particle focusing flow [30] and the aspect ratio of the channel should be approximately between 0.5 - 0.25 (height/width) [26]. The ratio R_f should be higher than 0.08 in order to generate flow focusing of the target particle. The equations describing each of these variables (F_D, F_L, R_f, λ) follow [27]:

$$F_D = 3\pi\mu U_{Dean} a_p \tag{4.1}$$

$$F_L = 0.05 \frac{a_p^4 \rho U_m^2}{D_h^2} \tag{4.2}$$

$$R_f = \frac{F_L}{F_D} \geq \sim 0.08 \tag{4.3}$$

$$\lambda = \frac{a_p}{D_h} \geq 0.07 \ . \tag{4.4}$$

In these equations μ is the fluid viscosity, U_{Dean} is the average Dean velocity, a_p is the target particle diameter, U_m is the maximum fluid velocity, and D_h is the hydrodynamic diameter for a rectangular channel.

In spite of the nonspherical nature of the target cells, the dimensions can be simplified as a sphere having the largest diameter of each cell or its rotational diameter [50]. The longest sperm head diameter is 5μm [104], [105]. Substitution of this value for the target diameter (a_p) in order to simplify calculations is justified based on an experimental study involving asymmetrical particle focusing within a microfluidic channel by Hur et al.[50], which suggests that the maximum diameter of an asymmetrical particle determines the stable position and can be used to predict the flowing behavior of the asymmetrical particles.

A range of dimensions and flow rates were used in the equations (Equation 4.1-4) to find the optimal condition of flow focusing (R_f, λ, and aspect ratio) and fabrication convenience was also considered. Through these calculations, we found a set of optimal dimensions which satisfied all ratio conditions above. The selected dimensions are as follows: height— 50 μm, width— 150 μm, space between channel— 310 μm, initial radius- 700 μm, and final radius— 899 μm. For the selected dimensions, λ for a 5 μm diameter particle is 0.067. The injection flow rate was selected based on the results of our previous report [100]. The flow rate from the previous study was 0.52 ml/min generating R_f values of 0.40 for 5 μm particles. From the selected dimension, the device and the

selected flow rate (0.52 ml/min) can generate high injection pressure and high centrifugal force. The measured injection pressure had an average pressure of 2.25 psi and a maximum pressure of 7 psi.

The maximum calculated centrifugal force/acceleration from the spiral channel was 4.19×10^{-12} N (19.45 g). The maximum value was calculated from the steepest curvature of the spiral channel (the first ring) with the centrifugal force equation (4.5),

.

$$F_c = \mathrm{M}\omega^2 r \tag{4.5}$$

where M is the mass of the particle, ω is the speed of the particle, and r is the radius of the channel. The calculated maximum centrifugal force from the spiral channel was still considerably lower than the force from clinical centrifuges which is ~500 g, or 1.083e-10 N [112].

The shear stress (T) was also calculated with (4.6) for a Newtonian fluid.

$$\mathrm{T(y)} = \mu\frac{\mathrm{du}}{\mathrm{dy}} \tag{4.6}$$

where μ is the dynamic viscosity, u is the flow velocity along the boundary, and y is the height above the boundary. The dynamic viscosity of the working fluid was selected as water (8.90×10^{-4} *Pa*) and a plane flow velocity profile was obtained from a finite element simulation of the first ring structure of the spiral using COMSOL. The plane of the velocity profile was acquired from the half point of the first ring, which should have the fastest flow velocity. The velocity sampling pattern was a crucifix shape in the middle of the acquired

plane of raw velocity data. The calculated shear stress profile of the channel was plotted in Figure 4.1. The maximum shear stress was $1.9\times10^{-3}Pa$ among all calculated values of the sampled velocity plane.

4.3 Fabrication of the Device and Possible Effects

Fabrication of the designed device was carried out using polydimethylsiloxane (PDMS, Sylgard 184, Dow Corning, MI, USA) with an SU-8 (SU-8 3035, Microchem, MA, USA) mold. The SU-8 mold was fabricated on a 100 mm (4 inch) wafer according to the manufacturer's instructions in a clean room environment. 40 ml of uncured PDMS at a 10:1 (polymer: curing agent) ratio was poured over the mold, and it was placed in an oven at 60° C for at least 6 hours. The molded PDMS was peeled off from the mold and any excess PDMS removed. Inlets and outlets were cored with a 1.5mm diameter coring tool. After cleaning the surface of the PDMS, a glass slide (Corning 2947-70 X 50 mm) was plasma bonded with the PDMS to form closed channels.

To complete the spiral channel device, two 1 ml clear polycarbonate syringes (BD, 1 ml Syringe Luer-lock tip) were utilized to connect the spiral channel inlets through platinum-cured silicone tubing (Sani-Tech, Clear Platinum-Cured Silicone Tubing, STHT-062-1) and nylon barbs (Nordson Medical, Straight Through Tube Fitting, N210-1). The outlet sample collection setup was constructed in the same manner as described previously (Figure 4.2).

Even though all the materials (PMDS, glass, and polymers) in the device are well known for minimal toxic effects on live samples[113], the fabricated spiral channel device and connected components needed to be tested for overall biocompatibility, in order to

show the clinical safety of the method. The possible source of damage to the sperm is the inner surface of the completed system, which includes the spiral channel, connecting barbs, tubes, and syringes.

4.4 Experimental Methodology

The purpose of the study was to find effects on sperm caused by the spiral channel device and its operating protocols. Therefore, a series of viability and toxicity tests were conducted to see the change in the number of live/normal sperm before the process and after the process. Recovery tests were also conducted to measure the possible sample loss during the process.

4.4.1 Sample Preparation Protocol

All sperm samples were acquired under an Institutional Review Board-approved study, IRB00072239. Frozen and fresh samples were acquired from the University of Utah Andrology lab. Written, informed consent was obtained from all participants for their tissues to be utilized for this study. Sperm samples were prepared from freshly collected specimens from the clinic and previously frozen semen specimens were suspended in sperm media (Quinn's Advantage media with HEPES Sage, CT, USA). The sperm concentration was adjusted depending on experimental needs through dilution with sperm media. Prepared samples were placed within two 1 ml syringes. The outlet sample collection setup was constructed in the same manner as the inlet setup and separated samples from the two outlets were collected into 1 ml plastic syringes at each outlet.

4.4.2 Sperm Viability Study

In this study, we utilized 17 freshly collected semen samples to represent the universal influence of the device system and operation protocols. Samples were collected on different occasions due to the difficulty of getting consented donations from clinic patients. Within an hour of collection time, prepared samples were split into two syringes and injected into each spiral channel inlet using one dual syringe pump. Two inlets were used, rather than one, because having two inlets helps eliminate leaks near the inlet port, which was shown to be effective from our previous report[100]. The injection flow rate was 0.26 ml/min from each syringe, resulting in accumulated flow rate of 0.52 ml/min. To collect an equal amount of sample from the outlet, another dual syringe pump pulled sample with a slightly lower flow rate than the injection flow rate (0.2ml/min), which is also shown effective from our previous report.

Collected samples in the syringes from each outlet were transferred to separate sample tubes (Corning plastic 10 ml sample tube). Then sample slides were made for the viability and the morphology test. The sample reading process was designed to be a blinded test in which each sample was labeled with a coded name. For making control references, two sample slides were prepared before the experiment.

The sperm viability staining was conducted according to World Health Organization (WHO) guidelines [112]. The preparation proceeded as follows: several drops (~80 µl) of a mixture of Eosin Y (Sigma #E6003) and Nigrosin (Sigma #N4754) were applied with a drop (~40 µl) of well-suspended collected sample on a glass slide, then drops were mixed well to make a thin smear for microscopic examination. After the sample slides are completely dried, we randomly observed 100 sperm, including stained and unstained

sperm, under the microscope with 200X magnification. The standard protocol [112] for sample reading states that magnification should be 1000X with oil and count number should be 200. However, we reduced the magnification to 200X and the random sperm count to 100 because finding a set of 200 random sperm cells in low sperm concentration samples can be difficult.. The reading reference for stained (dead) and unstained (live) cells followed the WHO standard [112] which states: Eosin Y will penetrate the cell membrane of dead or membrane defective sperm so the head will appear pink on the smear. In contrast, sperm with normal membrane function will resist eosin penetration and will appear white against the purple nigrosin background (Figure 4.3).

Sperm morphology testing was also conducted according to WHO guidelines [112]. To prepare sperm morphology slides, a well-suspended drop (~40 µl) from the collected sample is smeared on a glass slide. Then the slide is stained using the standard hematoxylin-eosin[112] method and then coverslipped for microscopic examination. Hematoxylin will stain the nucleic elements of cells (the sperm head) and eosin will stain the cytoplasmic or basic elements of cells (the sperm tail). With stained sample slides, a total number of 100 sperm were randomly counted under the microscope at 1000X magnification. The reading reference for morphology of head and tail of sperm were WHO guidelines, which contains seven types of head shape to be categorized as normal morphology sperm, both head and tail shape should be within the normal boundary.

4.4.3 Sperm Toxicology Study

To understand the influence on sperm in terms of toxicology, the time-dependent toxicology study included exposures to the inner surface of the spiral device system of 5

min, 30 min, 1 hour, and 2 hours. Twenty semen samples were used to represent the universal toxic influence of the device system. To find possible effect differences between fresh and frozen samples, there were 10 frozen samples and 10 fresh samples within the 20 samples. The selected time interval exposures were as follows: 5 min (regular operation time), 30 min, 1 hour, and 2 hours. Within 30 min of collection time, semen samples were split into two syringes and loaded into a spiral device system. For the 5 min. exposure time tests, sample loaded syringes were injected into each spiral channel device inlets using the same injection and collection protocol from the viability study. For rest of the time intervals (30 min, 1 hour, and 2 hours), the sample was injected halfway (0.25ml) and then the device system (one spiral device, four tubes, and four syringes) was placed in an incubator at 37°C. After the end of each time interval, the half of the sample remaining in the input syringes was injected into the device to push the exposed, earlier half of the sample into collection syringes (Figure 4.4).

Collected samples were transferred to individual sample tubes and the sample was measured for motility of sperm under 200X microscope magnification. The motility of sperm was categorized as progressive motile, nonprogressive motile, and nonmotile, as defined by WHO standards [112]. Randomly selected couple sets of 100 sperm cells were analyzed and each set's motility was recorded. For the live/dead sample reading, a drop of the well-suspended collected sample (~40 μl) was applied and smeared for viability tests using WHO's standard stain procedures. To make viability (live/dead) control references, two sample slides were prepared before the experiment. After prepared viability (live/dead) sample sides were completely dried, we randomly counted a total number of 100 sperm, including stained and unstained sperm, under the microscope with 200X magnification.

The reading reference for stained (dead) and unstained (live) followed the WHO standard.

4.4.4 Sperm Recovery Study

To demonstrate the improvement of sample recovery rate from conventional methods of sperm collection from the high WBC semen sample and the mTESE sample, the device system needs to demonstrate high sperm sample yield after the operation. To prevent possible cell sticking on microchannel walls, the whole inside of the device system was soaked with 5% BSA on DI water (diluted from Bovine serum albumin, approx. 99%, SIGMA). 1ml of BSA was loaded up in each injection syringe then injected into the device with a flow rate of 0.1ml/min until the syringe reached half of the initial volume (0.5 ml). The BSA filled system sat at room temperature for 30 min and was then flushed out with a flow rate of 0.1 ml/min.

The recovery tests performed with low concentration range (0.1, 1.1, 1.3, 6.5 million/ml) sperm samples were conducted to determine yield for samples with limited numbers of sperm. Samples were injected with a flow rate of 0.52ml/min and two outlets were connected to one syringe to minimize sample transfers. Samples were pulled with a slightly lower flow rate (0.4 ml/min) to maintain a backpressure. After collection, the sample was transferred to a sample tube (Corning plastic 10 ml sample tube) and a measured concentration of sperm under the microscope with 200X magnification. To represent the extremely low sperm concentration case, a batch of samples were made by serial dilutions. After using the dilution technique, the sperm number of the sample should be around 20 sperm/ml. The collected volume (~1.5ml) was concentrated by the in-house, custom-made microfluidic volume concentrator using a hollow fiber membrane tube

(MicroKros® and MidiKros® hollow fiber membranes, Spectrum Labs). The concentrated sample (~80µl) was placed on a glass slide and observed by an inverted microscope with 400X magnification (Figure 4.5).

4.5 Results and Discussion

4.5.1 Viability Study

The viability of collected sperm samples were verified by the viability stain (live/dead stain) test and the morphology test. The purpose of these tests was to show possible changes caused by the spiral channel device system and the operational protocol. According to the paired *t* test of the collected live/dead sample slides reading data, it shows higher *p* value between control and collected samples (Figure 4.6). This means there is no statistical difference between the control and the collected samples (inner and outer) in terms of the live sperm count. The paired *t* test of the morphology sample slides reading result (Figure 4.6) also shows that there is no statistical difference in the normal sperm count between the control and collected samples (inner and outer). These two plots (Figure 4.6) and statistical test results demonstrate that the spiral channel system and the operational protocol do not significantly affect the viability of sperm.

Figure 4.6 also shows a higher number of live sperm on the outer outlet than the inner outlet. Figure 4.6 also shows that the normal morphology count of the outer outlet is higher than the inner outlet count. This number difference could be caused by the size-dependent nature of the particle sorting mechanism. Because the spiral channel was designed to generate flow focusing of 5 µm diameter sphere, similar size sperm cells such as normal head shape sperm (5 µm long, 3 µm width ellipse) should be separated toward the outer

outlet. If this effect can be optimized, automated sorting of normal head shaped sperm can be achieved.

4.5.2 Time-Dependent Toxicology Study

The toxicology study with four different time intervals verified the effect of the spiral channel device system to sperm samples exposed to the inner surface of the system such as the spiral channel, syringes, connectors, and connection tubing. Figure 4.7(1) shows the results of the live sperm count and the sperm progressive motility count of the regular protocol time (5-min exposure time). The *p* value from the paired *t* test suggests that there is no significant difference of live sperm count between the control samples and sperm recovered from the outer outlet. However, there is a slight change of live sperm count between control and inner outlet. This difference between inner and outer outlet can be explained by the flow focusing trend of sperm toward the outer outlet. Because the spiral channel is designed to separate sperm to the outer outlet, the outer outlet should have more live and progressively motile sperm than the inner outlet. These data are consistent with the finding that more morphologically normal cells are present in the outer outlet. In Figure 4.7(2), the *p* value of motility data shows that statistical difference between control and outlet collected samples are significant but the difference is an only slight difference from control count.

Figures 4.8, 4.9, and 4.10 show that the difference between control and collected outlet samples from the 30-min, 1-hour, and 2-hour exposure tests are significant. The motility test results also show that there are significant statistical differences between the control and collected outlet samples (except 30 minutes live sperm count between control and outer

outlet). This means longer exposure (30 min, 1-hour, and 2-hour) can cause negative effects on sperm samples. The motility statistical comparison results of 2-hours between the control and outer outlet is insignificant, which might be a statistical glitch due to lack of data plots for paired *t*-test. This can be improved by more data plots. The clear appearance of the negative effects from 30 min, 1 hour, and 2 hours also may be caused by the different temperature inductions between the device system and the control sample tube during incubation. Due to the multiple components of the system, the incubation heat couldn't be conducted as quickly as that of the control sample tube. This may cause different rates of decay of viability and motility of sperm between the control and collected samples [114]. Overall, these data show that regular operation time exposure wouldn't affect a sperm sample significantly until 30 min of exposure time, however, there was clear decay of live sperm count and sperm motility count from the 1-hour exposure case and the 2-hour exposure case (Figures 4.9, 4.10).

4.5.3 Sperm Recovery Study

The recovery test results show a high recovery rate with low concentration samples (0.1, 1.1, 1.3, 6.5 million/ml) from 96% to 85% (Figure 4.11). In the case of the extremely low concentration sample, recovery results also show promising evidence of high recovery capability as shown in Table 4.1. Note that the size of the concentration may explain ~10% of the relatively lower recovery rate of 0.1 million/ml sample case. In the extremely low sperm concentration case (Table 4.1), sperm recovery results are promising, even though there is always the high possibility of sample loss during sample transfer for every sample measurement. The sample counts are close (19 and 24 sperm) to the expected initial sample

counts (~20 sperm). The recovery data for the extremely low concentration case provides valuable evidence that this spiral channel device system may sucessfully extract sperm cells from actual mTESE samples, which may contain an extremly low number of sperm.

4.6 Conclusion

In conclusion, we successfully tested the biological effects and sample recovery capability of a spiral microfluidic device system with several sperm samples. Possible causes of biological damage were high injection pressures, shear stress, and centrifugal forces throughout the channel. To investigate the influence of the spiral channel device and the operation protocols on sperm, a series of tests were conducted including viability, time interval toxicity, and recovery tests. The results from the viability test show clear evidence of statistically insignificant changes in the number of live sperm between control and collected samples during regular operation. The live sperm data suggest that the spiral channel device system and the operation protocols would not significantly reduce the number of live sperm. The viability study also shows insignificant changes in the number of normal morphology sperm between the control and collected sample. The normal morphology sperm data suggest the spiral channel device system and the proposed protocols would not physically damage sperm significantly during regular operation time.

The time interval toxicity test results show evidence of minimum change between the control and collected samples (inner and outer) within 30 min of operation time. Even though there are clear live and progressive motile sperm count differences between the control and collected samples during longer time cases (1-2 hours), the results from the 5-min and 30-min tests show promising evidence of almost no effect after the operation,

which suggests the designed spiral channel device and the operational protocols would not cause a significant negative effect during those operation times. There is also the possibility of reducing the statistical difference between the control and collected sample count by adding more data points.

The sperm recovery test results showed evidence of minimum sample loss during the operation. The recovery capability for the low concentration (0.1, 1.1, 1.3, 6.5 million/ml) sample case was relatively high (up to 96%), for the extremely low number of sperm (~20 sperm). In conclusion, the negative biological and physical effects of the spiral channel device system and the operational protocols are shown to be minimal according to viability, toxicity, and recovery test results. Therefore, the system may improve the clinical procedures of the sperm sample purification process without significant sperm loss and damage.

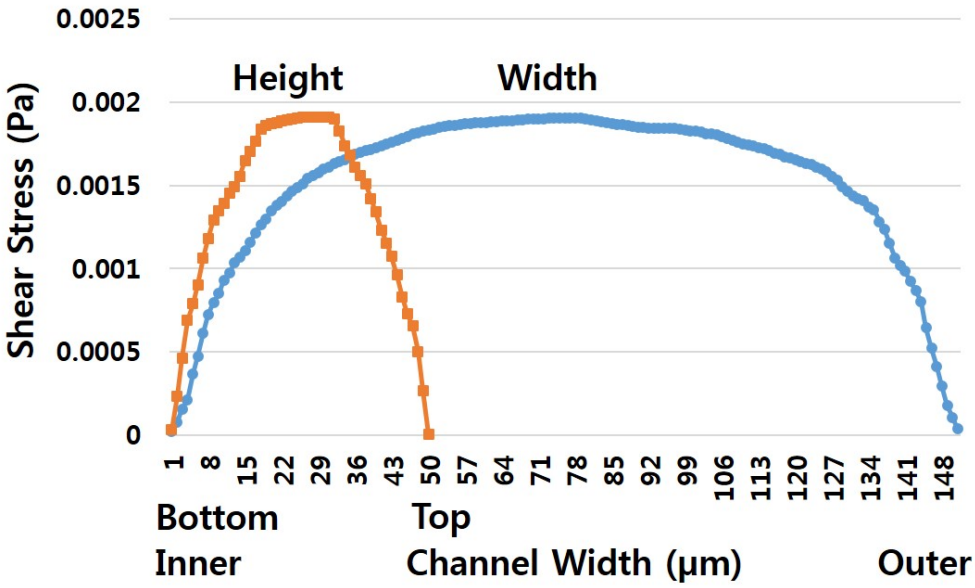

Figure 4.1 Calculated shear stress profile of height and width of the first ring of the spiral channel. (Orange) Shear stress profile across the height cross section, (Blue) Shear stress profile across the width.

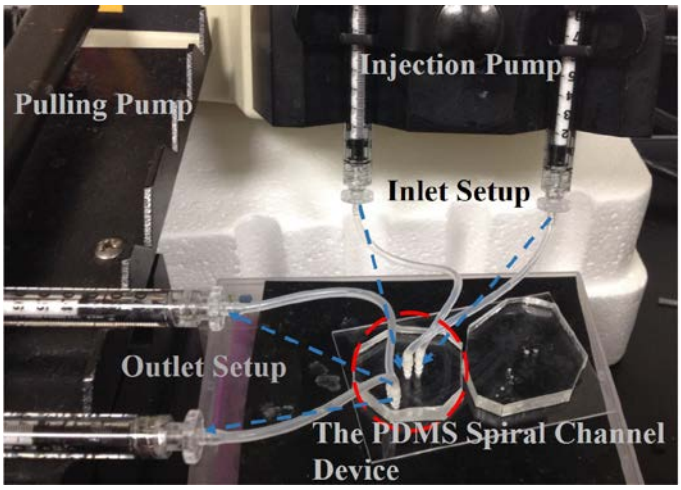

Figure 4.2 The PDMS spiral channel device system setup with two syringe pumps

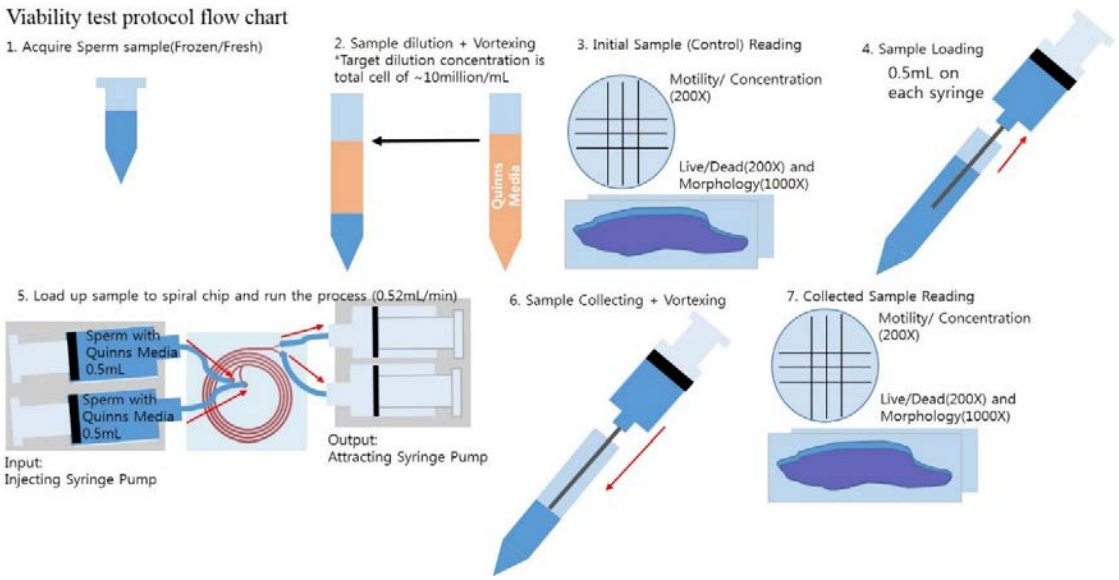

Figure 4.3. Protocol flow chart of sperm viability test.

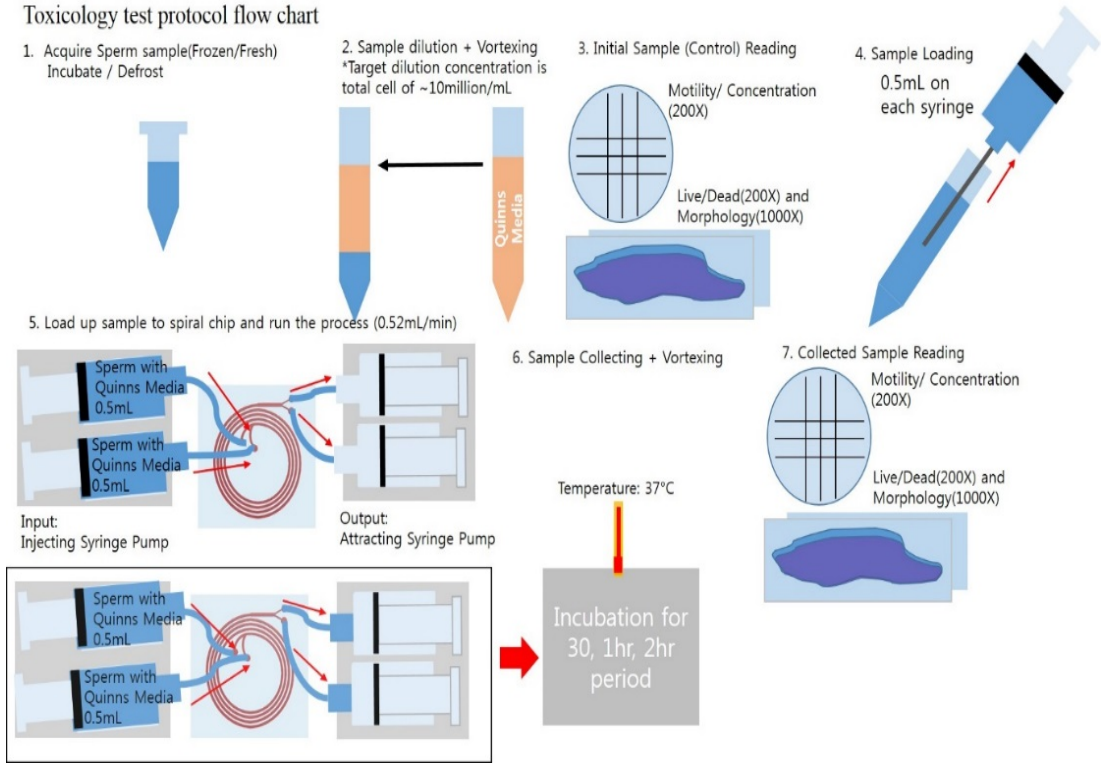

Figure 4.4 Protocol flow chart of sperm toxicology test

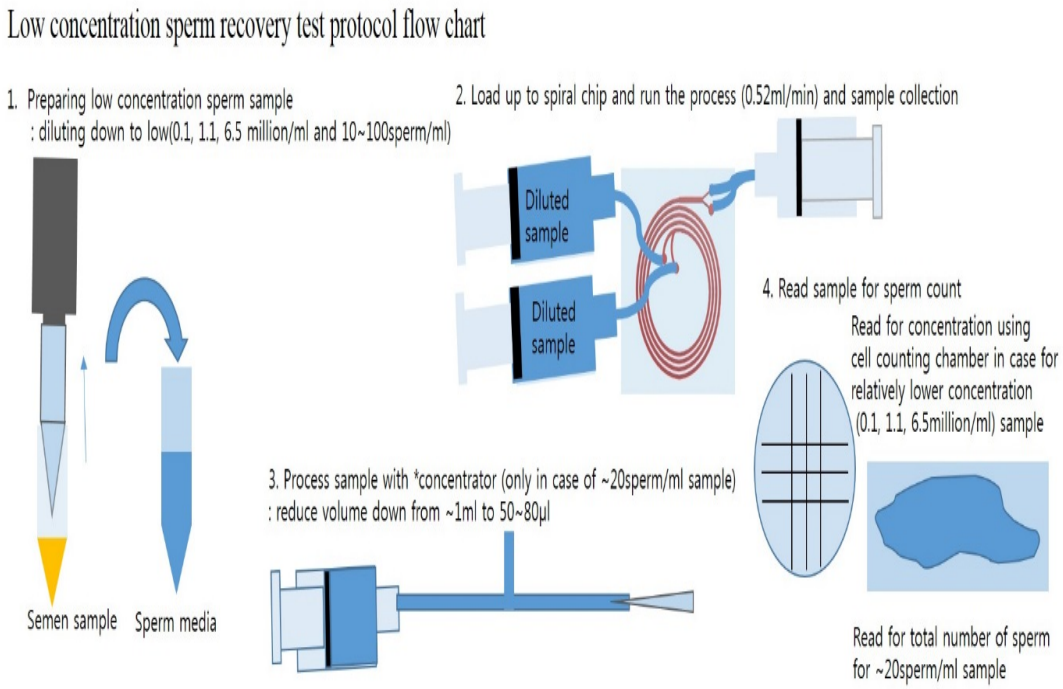

Figure 4.5 Protocol flow chart of sperm recovery test steps (1~4) with low sample concentration (0.1, 1.1, 6.5million/ml) and extremely low concentration(~20sperm/ml). * In-house custom-made microfluidic volume concentrator using a hollow fiber membrane tube.

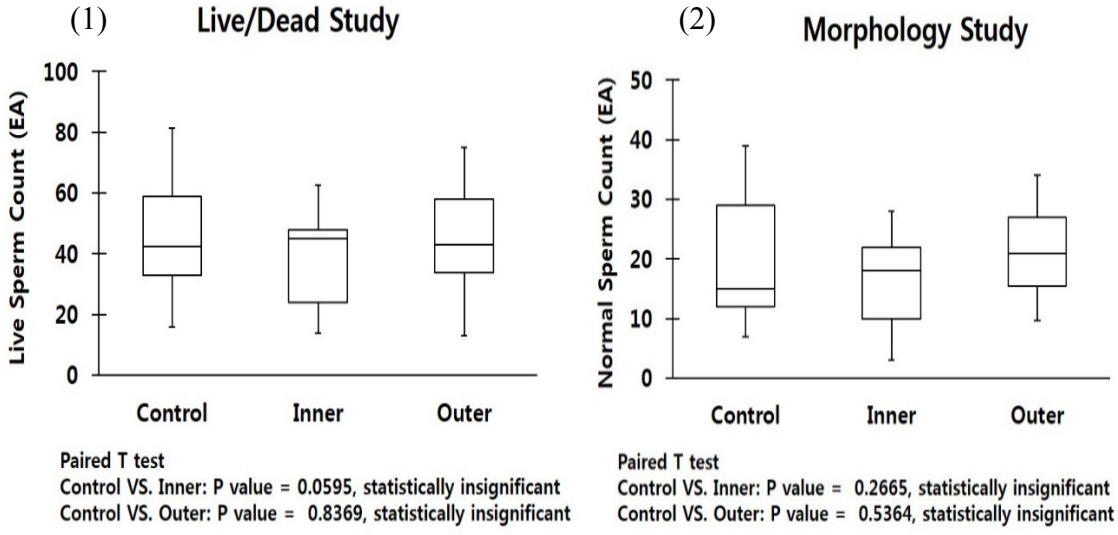

Figure 4.6 Viability study plots. (1) viability stain result for live sperm, (2) morphology results for normally shaped sperm.

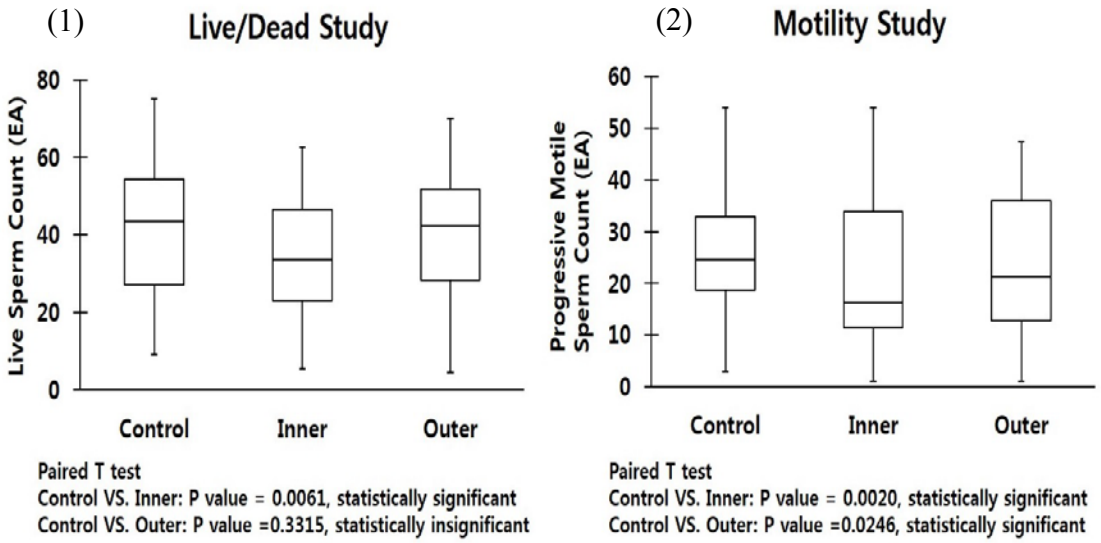

Figure 4.7 Toxicology study of regular exposure time (5 min). (1) live sperm reading, (2) motility reading.

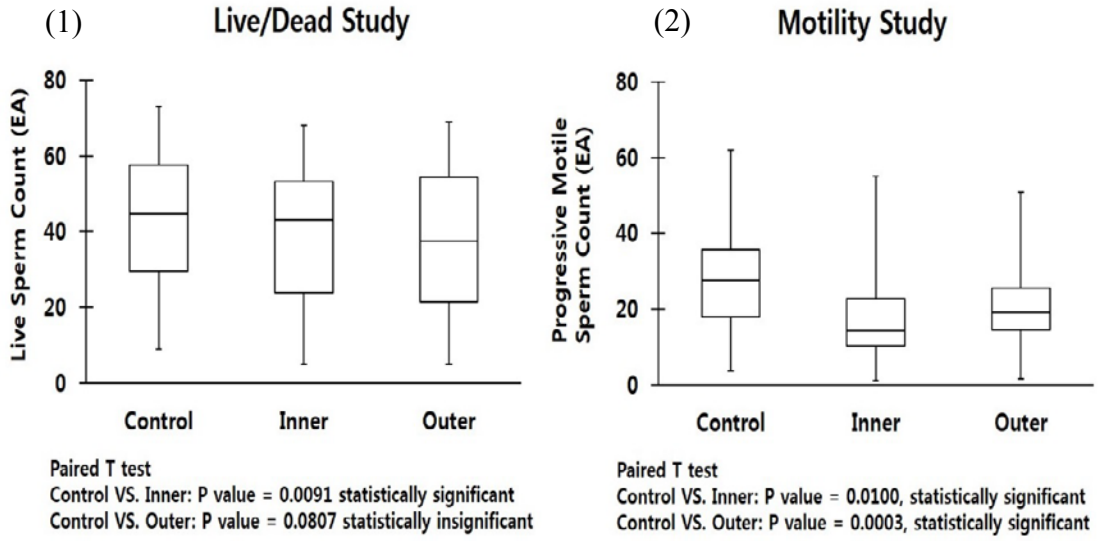

Figure 4.8 Toxicology study of 30 min exposure time. (1) live sperm reading, (2) motility reading.

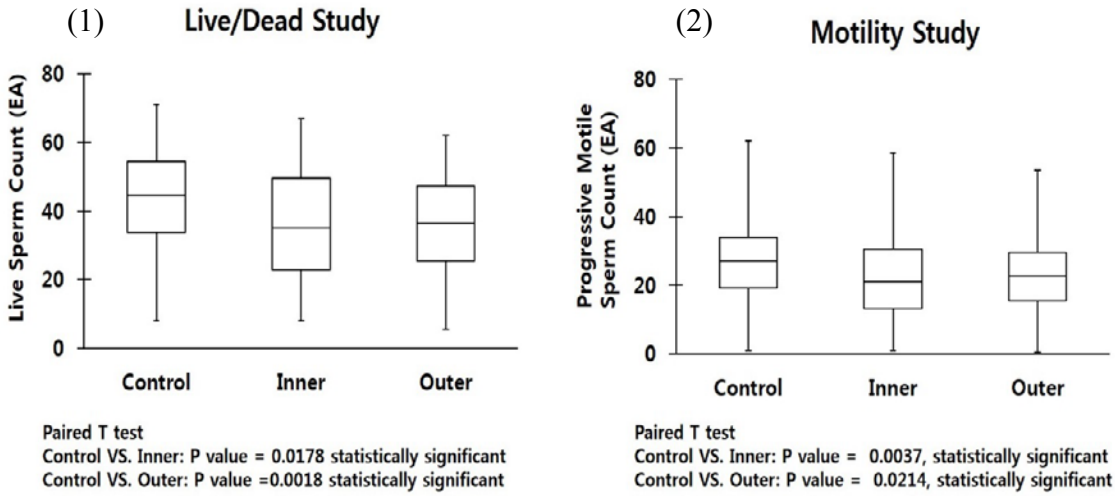

Figure 4.9. Toxicology study of 1 hour exposure time. (1) live sperm reading, (2) motility reading.

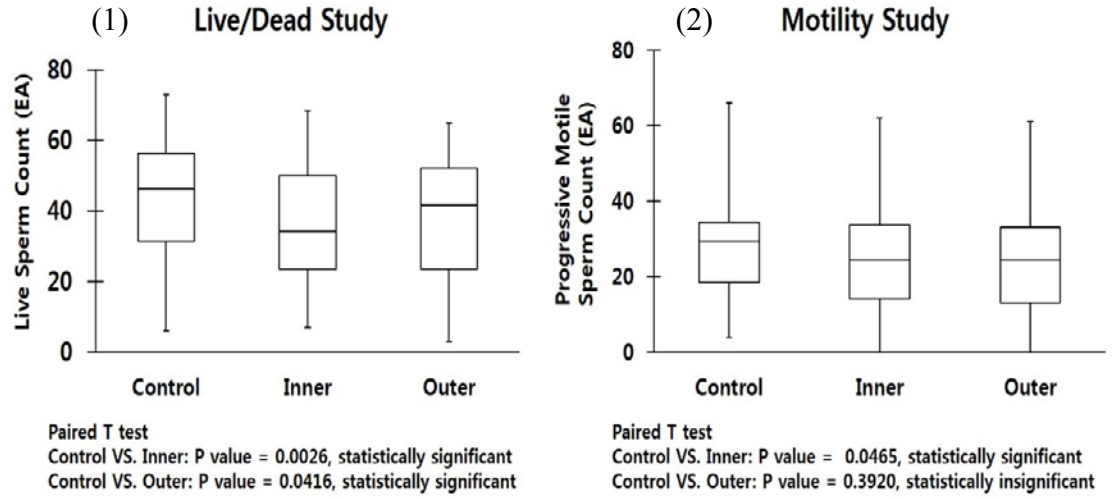

Figure 4.10. Toxicology study of 2-hour exposure time. (1) live sperm reading, (2) motility reading.

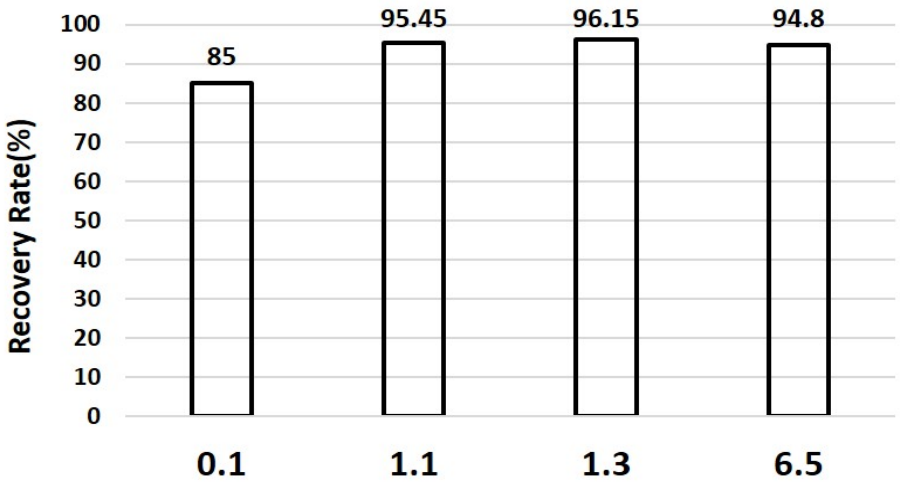

Figure 4.11 Sperm recovery test for the spiral channel

Table 4.1. Extremely low concentration recovery test results (~20sperm/ml)

Sample Number	Initial Sample Estimated Sperm Count (sperm/ml)	Collected Sample Hard Count from ~1ml of Collected Sample
1	~20	19
2	~20	24

4.7 References

[1] G. Velve-Casquillas, M. Le Berre, M. Piel, and P. T. Tran, "Microfluidic tools for cell biological research," *Nano Today*, vol. 5, no. 1, pp. 28–47, Feb. 2010.

[2] S. Cho, D. K. Kang, J. Choo, A. J. deMello, and S. I. Chang, "Recent advances in microfluidic technologies for biochemistry and molecular biology," *BMB Rep.*, vol. 44, no. 11, pp. 705–712, Nov. 2011.

[3] D. C. Duffy, J. C. McDonald, O. J. A. Schueller, and G. M. Whitesides, "Rapid prototyping of microfluidic systems in poly(dimethylsiloxane)," *Anal. Chem.*, vol. 70, no. 23, pp. 4974–4984, Oct. 1998.

[4] K. Ohno, K. Tachikawa, and A. Manz, "Microfluidics: Applicatons analytical purposes in chemistry and biochemistry," *Electrophoresis*, vol. 29, pp. 4443–4453, Nov. 2008.

[5] Y. Zhang *et al.*, "DNA methylation analysis on a droplet-in-oil PCR array.," *Lab Chip*, vol. 9, no. 8, pp. 1059–1064, Apr. 2009.

[6] C. Wyatt Shields IV, C. D. Reyes, and G. P. López, "Microfluidic cell sorting: A review of the advances in the separation of cells from debulking to rare cell isolation," *Lab Chip*, vol. 15, no. 5, pp. 1230–1249, Jan. 2015.

[7] H. Andersson and A. Van den Berg, "Microfluidic devices for cellomics: A review," *Sensors Actuators, B Chem.*, vol. 92, no. 3, pp. 315–325, Jul. 2003.

[8] S. M. Kim, S. H. Lee, and K. Y. Suh, "Cell research with physically modified microfluidic channels: A review," *Lab a Chip - Miniaturisation Chem. Biol.*, vol. 8, no. 7, pp. 1015–1023, Jul. 2008.

[9] R. N. Zare and S. Kim, "Microfluidic platforms for single-cell analysis," *Annu. Rev. Biomed. Eng.*, vol. 12, no. 1, pp. 187–201, Apr. 2010.

[10] A. Lenshof and T. Laurell, "Continuous separation of cells and particles in microfluidic systems," *Chem. Soc. Rev.*, vol. 39, no. 3, pp. 1203–1217, Feb. 2010.

[11] D. R. Gossett *et al.*, "Label-free cell separation and sorting in microfluidic systems," *Anal. Bioanal. Chem.*, vol. 397, no. 8, pp. 3249–67, Aug. 2010.

[12] A. A. S. Bhagat, H. Bow, H. W. Hou, S. J. Tan, J. Han, and C. T. Lim, "Microfluidics for cell separation," *Med. Biol. Eng. Comput.*, vol. 48, no. 10, pp. 999–1014, Oct. 2010.

[13] S. Choi and J.-K. Park, "Microfluidic system for dielectrophoretic separation based on a trapezoidal electrode array," *Lab Chip*, vol. 5, no. 10, pp. 1161–1167, Oct.

2005.

[14] A. F. Cowman and B. S. Crabb, “Review invasion of red blood cells by malaria parasites,” *Cell,* pp. 755–766, Feb. 2006.

[15] W. J. Kleijer, M. L. T. van der Sterre, V. H. Garritsen, A. Raams, and N. G. J. Jaspers, “Prenatal diagnosis of the Cockayne syndrome: Survey of 15 years experience,” *Prenat. Diagn.*, vol. 26, no. 10, pp. 980–984, Oct. 2006.

[16] S. Nagrath *et al.*, “Isolation of rare circulating tumour cells in cancer patients by microchip technology,” *Nature*, vol. 450, pp. 1235-1239, December, 2007.

[17] F. Petersson, L. Åberg, A. M. Swärd-Nilsson, and T. Laurell, “Free flow acoustophoresis: Microfluidic-based mode of particle and cell separation,” *Anal. Chem.*, vol. 79, no. 14, pp. 5117–5123, Jun. 2007.

[18] E. L. Tóth, E. Holczer, P. Földesy, K. Iván, and P. Fürjes, “Microfluidic particle sorting system for environmental pollution monitoring applications,” *Procedia Eng.*, vol. 168, pp. 1462–1465, Sep. 2016.

[19] N. Xia *et al.*, “Combined microfluidic-micromagnetic separation of living cells in continuous flow,” *Biomed. Microdevices*, vol. 8, no. 4, pp. 299–308, Dec. 2006.

[20] B. H. Weigl and P. Yager, “Microfluidic diffusion-based separation and detection,” *Science*, vol. 283, no. 5400, p. 346 LP-347, Jan. 1999.

[21] D. W. Inglis, “Efficient microfluidic particle separation arrays,” *Appl. Phys. Lett.*, vol. 94, no. 1, Jan. 2009.

[22] J. Nam, H. Lim, D. Kim, H. Jung, and S. Shin, “Continuous separation of microparticles in a microfluidic channel via the elasto-inertial effect of non-Newtonian fluid,” *Lab Chip*, vol. 12, no. FEBRUARY, p. 1347, Jan. 2012.

[23] J. E. Swain, D. Lai, S. Takayama, and G. D. Smith, “Thinking big by thinking small: Application of microfluidic technology to improve ART,” *Lab Chip*, vol. 13, no. 7, pp. 1213–24, Apr. 2013.

[24] G. Segré and A. Silberberg, “Radial particle displacements in poiseuille flow of suspensions,” *Comput. Geotech.*, vol. 189, no. 4760, pp. 209–210, Jan. 1961.

[25] D. Di Carlo, “Inertial microfluidics,” *Lab Chip*, vol. 9, no. 21, pp. 3038–3046, Nov. 2009.

[26] J. M. Martel and M. Toner, “Inertial focusing dynamics in spiral microchannels,” *Phys. Fluids*, vol. 24, no. 3, p. 32001, Mar. 2012.

[27] H. Amini, W. Lee, and D. Di Carlo, “Inertial microfluidic physics,” *Lab Chip*, vol. 14, no. 15, pp. 2739–61, May. 2014.

[28] E. S. Asmolov, “The inertial lift on a spherical particle in a plane Poiseuille flow at large channel Reynolds number,” *J. Fluid Mech.*, vol. 381, pp. 63–87, Jan. 1999.

[29] D. Di Carlo, J. F. Edd, K. J. Humphry, H. A. Stone, and M. Toner, “Particle segregation and dynamics in confined flows,” *Phys. Rev. Lett.*, vol. 102, no. 9, pp. 1–4, Mar. 2009.

[30] J. Zhou and I. Papautsky, “Fundamentals of inertial focusing in microchannels,” *Lab Chip*, vol. 13, no. 6, pp. 1121–32, Mar. 2013.

[31] J. M. Martel and M. Toner, “Particle focusing in curved microfluidic channels,” *Sci. Rep.*, vol. 3, pp. 1–8, Nov. 2013.

[32] P. G. Saffman, “The lift on a small sphere in a slow shear flow,” *J. Fluid Mech.*, vol. 22, no. 2, pp. 385–400, Fe. 1965.

[33] S. I. Rubinow and J. B. Keller, “The transverse force on a spinning sphere moving in a viscous fluid,” *J. Fluid Mech.*, vol. 11, no. 3, pp. 447–459, Nov. 1961.

[34] B. P. Ho and L. G. Leal, “Migration of rigid spheres in a two-dimensional unidirectional shear flow of a second-order fluid,” *J. Fluid Mech.*, vol. 65, no. 2, pp. 365–400, Aug. 1974.

[35] W. R. Dean, “LXXII. The stream-line motion of fluid in a curved pipe (Second paper),” *London, Edinburgh, Dublin Philos. Mag. J. Sci.*, vol. 5, no. 30, pp. 673–695, Apr. 1928.

[36] S. A. Berger, L. Talbot, and L. S. Yao, “Flow in curved pipes,” *Annu. Rev. Fluid Mech.*, vol. 15, pp. 461–512, Jan. 1983.

[37] D. R. Gossett and D. Di Carlo, “Particle focusing mechanisms in curving confined flows,” *Anal. Chem.*, vol. 81, no. 20, pp. 8459–8465, Sep. 2009.

[38] D. Di Carlo, D. Irimia, R. G. Tompkins, and M. Toner, “Continuous inertial focusing, ordering, and separation of particles in microchannels,” *Proc. Natl. Acad. Sci. U. S. A.*, vol. 104, no. 48, pp. 18892–18897, Nov. 2007.

[39] A. A. S. Bhagat, S. S. Kuntaegowdanahalli, and I. Papautsky, “Continuous particle separation in spiral microchannels using Dean flows and differential migration,” *Lab Chip*, vol. 8, no. 11, pp. 1906–1914, Nov. 2008.

[40] S. Ookawara, R. Higashi, D. Street, and K. Ogawa, “Feasibility study on concentration of slurry and classification of contained particles by microchannel,”

Chem. Eng. J., vol. 101, no. 1–3, pp. 171–178, Aug. 2004.

[41] A. A. S. Bhagat, S. S. Kuntaegowdanahalli, and I. Papautsky, "Enhanced particle filtration in straight microchannels using shear-modulated inertial migration," *Phys. Fluids*, vol. 20, no. 10, 2008.

[42] D. Di Carlo, "Inertial microfluidics," *Lab Chip*, vol. 9, no. 21, pp. 3038–46, Nov. 2009.

[43] F. P. Bretherton, "The motion of rigid particles in a shear flow at low Reynolds number," *J. Fluid Mech.*, vol. 14, no. 2, pp. 284–304, Oct. 1962.

[44] W. E. Uspal, H. Burak Eral, and P. S. Doyle, "Engineering particle trajectories in microfluidic flows using particle shape," *Nat. Commun.*, vol. 4, p. 2666, Apr. 2013.

[45] T. Kaya and H. Koser, "Characterization of hydrodynamic surface interactions of escherichia coli cell bodies in shear flow," *Phys. Rev. Lett.*, vol. 103, no. 13, pp. 1–4, Sep. 2009.

[46] G. B. Jeffery, "The motion of ellipsoidal particles immersed in a viscous fluid," *Math. Phys. Eng. Sci.*, pp. 161–179, Nov. 1922.

[47] C. Y. Wu, K. Owsley, and D. Di Carlo, "Rapid software-based design and optical transient liquid molding of microparticles," *Adv. Mater.*, vol. 27, no. 48, pp. 7970–7978, Oct. 2015.

[48] M. L. Ekiel-Jeżewska and E. Wajnryb, "Hydrodynamic orienting of asymmetric microobjects under gravity," *J. Phys. Condens. Matter*, vol. 21, no. 20, p. 204102, May. 2009.

[49] P. J. A. Janssen, M. D. Baron, P. D. Anderson, J. Blawzdziewicz, M. Loewenberg, and E. Wajnryb, "Collective dynamics of confined rigid spheres and deformable drops," *Soft Matter*, vol. 8, no. 28, pp. 7495–7506, Aug. 2012.

[50] S. C. Hur, S. E. Choi, S. Kwon, and D. Di Carlo, "Inertial focusing of non-spherical microparticles," *Appl. Phys. Lett.*, vol. 99, no. 4, pp. 1–4, Jul. 2011.

[51] J. Elgeti, U. B. Kaupp, and G. Gompper, "Hydrodynamics of sperm cells near surfaces," *Biophysj*, vol. 99, no. 4, pp. 1018–1026, Aug. 2010.

[52] W. Lee, H. Amini, H. A Stone, and D. Di Carlo, "Dynamic self-assembly and control of microfluidic particle crystals," *Proc. Natl. Acad. Sci. U. S. A.*, vol. 107, no. 52, pp. 22413–22418, Dec. 2010.

[53] J. Sun *et al.*, "Double spiral microchannel for label-free tumor cell separation and

enrichment," *Lab Chip*, vol. 12, no. 20, p. 3952, Jul. 2012.

[54] M. Jimenez, B. Miller, and H. L. Bridle, "Efficient separation of small microparticles at high flowrates using spiral channels: Application to waterborne pathogens," *Chem. Eng. Sci.*, vol. 157, pp. 247–254, Jan. 2017.

[55] Z. Wu, B. Willing, J. Bjerketorp, J. K. Jansson, and K. Hjort, "Soft inertial microfluidics for high throughput separation of bacteria from human blood cells," *Lab Chip*, vol. 9, no. 9, pp. 1193–9, May. 2009.

[56] A. J. Mach and D. di Carlo, "Continuous scalable blood filtration device using inertial microfluidics," *Biotechnol. Bioeng.*, vol. 107, no. 2, pp. 302–311, Oct. 2010.

[57] X. Wang, C. Liedert, R. Liedert, and I. Papautsky, "A disposable, roll-to-roll hot-embossed inertial microfluidic device for size-based sorting of microbeads and cells," *Lab Chip*, vol. 16, pp. 1821–1830, May. 2016.

[58] M. G. Lee, J. H. Shin, C. Y. Bae, S. Choi, and J. K. Park, "Label-free cancer cell separation from human whole blood using inertial microfluidics at low shear stress," *Anal. Chem.*, vol. 85, no. 13, pp. 6213–6218, Jun. 2013.

[59] N. Nivedita and I. Papautsky, "Continuous separation of blood cells in spiral microfluidic devices," *Biomicrofluidics*, vol. 7, no. 5, Sep. 2013.

[60] M. E. Warkiani *et al.*, "Slanted spiral microfluidics for the ultra-fast, label-free isolation of circulating tumor cells," *Lab Chip*, vol. 14, no. 1, pp. 128–37, Jan. 2014.

[61] T. H. Kim, H. J. Yoon, P. Stella, and S. Nagrath, "Cascaded spiral microfluidic device for deterministic and high purity continuous separation of circulating tumor cells," *Biomicrofluidics*, vol. 8, no. 6, p. 64117, Dec. 2014.

[62] A. A. S. Bhagat, H. W. Hou, L. D. Li, C. T. Lim, and J. Han, "Pinched flow coupled shear-modulated inertial microfluidics for high-throughput rare blood cell separation," *Lab Chip*, vol. 11, no. 11, pp. 1870–1878, Apr. 2011.

[63] S. Shen *et al.*, "High-throughput rare cell separation from blood samples using steric hindrance and inertial microfluidics," *Lab Chip*, vol. 14, no. 14, pp. 2525–38, Jul. 2014.

[64] D. Di Carlo, J. F. Edd, D. Irimia, R. G. Tompkins, and M. Toner, "Equilibrium separation and filtration of particles using differential inertial focusing," *Anal. Chem.*, vol. 80, no. 6, pp. 2204–2211, Feb. 2008.

[65] J. Boivin, L. Bunting, J. A. Collins, and K. G. Nygren, "International estimates of

infertility prevalence and treatment-seeking: Potential need and demand for infertility medical care," *Hum. Reprod.*, vol. 22, no. 6, pp. 1506–1512, Jun. 2007.

[66] T. G. Cooper *et al.*, "World Health Organization reference values for human semen characteristics," *Hum. Reprod. Update*, vol. 16, no. 3, pp. 231–245, May-Jun. 2009.

[67] R. Samuel *et al.*, "Microfluidics: The future of microdissection TESE?," *Syst. Biol. Reprod. Med.*, vol. 62, no. 3, pp. 161–70, Jun. 2016.

[68] K. Baker and E. Sabanegh, "Obstructive azoospermia: Reconstructive techniques and results," *Clinics*, vol. 68, no. S1, pp. 61–73, Feb. 2013.

[69] I. Craft *et al.*, "Percutaneous epididymal sperm aspiration and intracytoplasmic sperm injection in the management of infertility due to obstructive azoospermia," *Fertil. Steril.*, vol. 63, no. 5, pp. 1038–42, May. 1995.

[70] P. N. Schlegel, "Testicular sperm extraction: Microdissection improves sperm yield with minimal tissue excision," *Hum. Reprod.*, vol. 14, no. 1, pp. 131–135, Jan. 1999.

[71] P. N. Schlegel and L. M. Su, "Physiological consequences of testicular sperm extraction," *Hum. Reprod.*, vol. 12, no. 8, pp. 1688–1692, Aug. 1997.

[72] R. Kumar, "Medical management of non-obstructive azoospermia," *Clinics.* vol. 2013, pp. 75–79, Feb. 2013.

[73] P. Donoso, H. Tournaye, and P. Devroey, "Which is the best sperm retrieval technique for non-obstructive azoospermia? A systematic review," *Hum. Reprod. Update*, vol. 13, no. 6, pp. 539–549, Nov-Dec. 2007.

[74] C. Krausz, "Male infertility: Pathogenesis and clinical diagnosis," *Best Pract. Res. Clin. Endocrinol. Metab.*, vol. 25, no. 2, pp. 271–85, Apr. 2011.

[75] A. Bettegowda and M. F. Wilkinson, "Transcription and post-transcriptional regulation of spermatogenesis," *Philos. Trans. R. Soc. Lond. B. Biol. Sci.*, vol. 365, no. 1546, pp. 1637–1651, May. 2010.

[76] M. Ostad, D. Liotta, Z. Ye, P. N. Schlegel, "Teticular sperm extraction for nonobstructive azoospermia: Results of a multibiopsy approach with optimized tissue dispersion," *Urology*, vol. 4295, no. 98, pp. 692–696, Oct. 1998.

[77] L. Gambera, F. Serafini, G. Morgante, R. Focarelli, V. De Leo, and P. Piomboni, "Sperm quality and pregnancy rate after COX-2 inhibitor therapy of infertile males with abacterial leukocytospermia," *Hum. Reprod.*, vol. 22, no. 4, pp. 1047–1051, Apr. 2007.

[78] C. M. Peterson, A. O. Hammoud, E. Lindley, D. T. Carrell, and K. Wilson, "Assisted Reproductive Technology Practice Management", *Reproductive Endocrinology and Infertility*, D. T. Carrell, C. M. Peterson, Ed. New York: Springer, 2010, pp. 7-37.

[79] M. J. Chen and A. Bongso, "Comparative evaluation of two density gradient preparations for sperm separation for medically assisted conception," *Hum. Reprod.*, vol. 14, no. 3, pp. 759–764, Mar. 1999.

[80] L. J. Kricka *et al.*, "Micromachined analytical devices: Microchips for semen testing," *J. Pharm. Biomed. Anal.*, vol. 15, no. 9–10, pp. 1443–7, Jun. 1997.

[81] S. Tasoglu *et al.*, "Exhaustion of racing sperm in nature-mimicking microfluidic channels during sorting," *Small*, vol. 9, no. 20, pp. 3374–3384, Oct. 2013.

[82] B. S. Cho, T. G. Schuster, X. Zhu, D. Chang, G. D. Smith, and S. Takayama, "Passively driven integrated microfluidic system for separation of motile sperm," *Anal. Chem.*, vol. 75, no. 7, pp. 1671–1675, Feb. 2003.

[83] T. G. Schuster, B. Cho, L. M. Keller, S. Takayama, and G. D. Smith, "Isolation of motile spermatozoa from semen samples using microfluidics," *Reprod. Biomed. Online*, vol. 7, no. 1, pp. 75–81, Jan. 2003.

[84] H. Huang, "Motile human sperm sorting by an integrated microfluidic system," *J. Nanomed. Nanotechnol.*, vol. 5, no. 3, pp. 193-199, May. 2014.

[85] H.-Y. Huang *et al.*, "Isolation of motile spermatozoa with a microfluidic chip having a surface-modified microchannel," *J. Lab. Autom.*, vol. 19, no. 1, pp. 91–9, Feb. 2013.

[86] K. Matsuura, M. Takenami, Y. Kuroda, T. Hyakutake, S. Yanase, and K. Naruse, "Screening of sperm velocity by fluid mechanical characteristics of a cyclo-olefin polymer microfluidic sperm-sorting device," *Reprod. Biomed. Online*, vol. 24, no. 1, pp. 109–15, Jan. 2012.

[87] H. Sano, K. Matsuura, K. Naruse, and H. Funahashi, "Application of a microfluidic sperm sorter to the in-vitro fertilization of porcine oocytes reduced the incidence of polyspermic penetration," *Theriogenology*, vol. 74, no. 5, pp. 863–70, Sep. 2010.

[88] J. M. Wu, Y. Chung, K. J. Belford, G. D. Smith, S. Takayama, and J. Lahann, "A surface-modified sperm sorting device with long-term stability," *Biomed. Microdevices*, vol. 8, no. 2, pp. 99–107, Jun. 2006.

[89] S. Koyama, D. Amarie, H. Soini, M. Novotny, and S. Jacobson, "Chemotaxis assays of mouse sperm on microfluidic devices," *Anal. chem.*, vol. 78, no. 10, pp.

3354–3359, Apr. 2006.

[90] L. Xie *et al.*, "Integration of sperm motility and chemotaxis screening with a microchannel-based device," *Clin. Chem.*, vol. 56, no. 8, pp. 1270–8, Aug. 2010.

[91] Y.-J. Ko, J.-H. Maeng, B.-C. Lee, S. Lee, S. Y. Hwang, and Y. Ahn, "Separation of progressive motile sperm from mouse semen using on-chip chemotaxis," *Anal. Sci.*, vol. 28, no. 1, pp. 27–32, Jan. 2012.

[92] S. S. Suarez and M. Wu, "Microfluidic devices for the study of sperm migration," *Mol. Hum. Reprod.*, pp. 1–8, Apr. 2017.

[93] C.-Y. Chen *et al.*, "Sperm quality assessment via separation and sedimentation in a microfluidic device," *Analyst*, vol. 138, no. 17, pp. 4967–74, Sep. 2013.

[94] S. M. Knowlton, M. Sadasivam, and S. Tasoglu, "Microfluidics for sperm research," *Trends Biotechnol.*, vol. 33, no. 4, pp. 221–229, Apr. 2015.

[95] R. Ma *et al.*, "In vitro fertilization on a single-oocyte positioning system integrated with motile sperm selection and early embryo development," *Anal. Chem.*, vol. 83, no. 8, pp. 2964–2970, Mar. 2011.

[96] Y. Lin, P. Chen, R. Wu, L. Pan, and F. Tseng, "Micro diffuser-type movement inversion sorter for high-efficient sperm sorting," *Int. Conf Nano/Micro Eng. Mol. Syst.*, pp. 7–10, Apr. 2013.

[97] M. D. C. Lopez-Garcia, R. L. Monson, K. Haubert, M. B. Wheeler, and D. J. Beebe, "Sperm motion in a microfluidic fertilization device," *Biomed. Microdevices*, vol. 10, no. 5, pp. 709–718, Oct. 2008.

[98] M. Wheeler and M. Rubessa, "Integration of Microfluidics and Mammalian IVF," *Mol. Hum Regrod,* vol. 23, iss. 4, pp. 248–256, Apr. 2017.

[99] R. S. Suh, X. Zhu, N. Phadke, D. A. Ohl, S. Takayama, and G. D. Smith, "IVF within microfluidic channels requires lower total numbers and lower concentrations of sperm," *Hum. Reprod.*, vol. 21, no. 2, pp. 477–483, Feb. 2006.

[100] J. Son, K. Murphy, R. Samuel, B. Gale, D. Carrell, and J. Hotaling, "Non-motile sperm cell separation using a spiral channel," *Anal. Methods*, iss. 7, pp. 8041-8047, May. 2015.

[101] S. S. Kuntaegowdanahalli, A. A. S. Bhagat, G. Kumar, and I. Papautsky, "Inertial microfluidics for continuous particle separation in spiral microchannels," *Lab Chip*, vol. 9, no. 20, pp. 2973–80, Oct. 2009.

[102] P. R. Wheater, H. G. Burkitt, and V. G. Daniels, *Functional Histology. A Text and*

Colour Atlas. Edinburgh: Churchill, 1979.

[103] M. Diez-Silva, M. Dao, J. Han, C.-T. Lim, and S. Suresh, "Shape and biomechanical characteristics of human red blood cells in health and disease," *MRS Bull.*, vol. 35, no. 5, pp. 382–388, May. 2010.

[104] J. A. Mossman, J. T. Pearson, H. D. Moore, and A. A. Pacey, "Variation in mean human sperm length is linked with semen characteristics," *Hum. Reprod.*, vol. 28, no. 1, pp. 22–32, Jan. 2013.

[105] L. Maree, S. S. Du Plessis, R. Menkveld, and G. Van Der Horst, "Morphometric dimensions of the human sperm head depend on the staining method used," *Hum. Reprod.*, vol. 25, no. 6, pp. 1369–1382, Jun. 2010.

[106] J. E. Lackner, I. Märk, K. Sator, J. Huber, and M. Sator, "Effect of leukocytospermia on fertilization and pregnancy rates of artificial reproductive technologies," *Fertil. Steril.*, vol. 90, no. 3, pp. 869–871, Sep. 2008.

[107] N. Nivedita and I. Papautsky, "Continuous separation of blood cells in spiral microfluidic devices," *Biomicrofluidics*, vol. 7, no. 5, pp. 1–14, Sep. 2013.

[108] J.-P. Frimat *et al.*, "Make it spin: Individual trapping of sperm for analysis and recovery using micro-contact printing," *Lab Chip*, vol. 14, no. 15, pp. 2635–41, Aug. 2014.

[109] C. Ainsworth, B. Nixon, R. P. S. Jansen, and R. J. Aitken, "First recorded pregnancy and normal birth after ICSI using electrophoretically isolated spermatozoa," *Hum. Reprod.*, vol. 22, no. 1, pp. 197–200, Sep. 2007.

[110] R. Zeggari, B. Wacogne, C. Pieralli, C. Roux, and T. Gharbi, "A full micro-fluidic system for single oocyte manipulation including an optical sensor for cell maturity estimation and fertilisation indication," *Sensors Actuators, B Chem.*, vol. 125, no. 2, pp. 664–671, Aug. 2007.

[111] A. A. El-Ghobashy and C. R. West, "The human sperm head: A key for successful fertilization," *J. Androl.*, vol. 24, no. 2, pp. 232–8, Mar-Apr. 2003.

[112] WHO, *Examination and processing of human semen*, 5th ed, WHO, Geneva: Swiss. 2010.

[113] M. Ionescu *et al.*, "Enhanced biocompatibility of PDMS (polydimethylsiloxane) polymer films by ion irradiation," *Nucl. Inst. Methods Phys. Res. B*, vol. 273, pp. 161–163, Feb. 2012.

[114] C. Garrett, D. Y. Liu, R. I. McLachlan, and H. W. G. Baker, "Time course of changes in sperm morphometry and semen variables during testosterone-induced

suppression of human spermatogenesis," *Hum. Reprod.*, vol. 20, no. 11, pp. 3091–3100, Nov. 2005.

[115] N. Guz, M. Dokukin, V. Kalaparthi, and I. Sokolov, "If cell mechanics can be described by elastic modulus: Study of different models and probes used in indentation experiments," *Biophys. J.*, vol. 107, no. 3, pp. 564–575, Aug. 2014.

[116] X. Zhang *et al.*, "Lensless imaging for simultaneous microfluidic sperm monitoring and sorting," *Lab Chip*, vol. 11, no. 15, pp. 2535–2540, Aug. 2011.

[117] L. I. Segerink, A. J. Sprenkels, P. M. ter Braak, I. Vermes, and A. van den Berg, "On-chip determination of spermatozoa concentration using electrical impedance measurements," *Lab Chip*, vol. 10, no. 8, pp. 1018–24, Apr. 2010.

CHAPTER 5

STUDY OF SPERM-LIKE-PARTICLE (SLP) BEHAVIOR IN CURVED MICROFLUIDIC CHANNELS AND ITS APPLICATION TO INERTIAL MICROFLUIDICS PRINCIPLES

5.1 Introduction

In recent biological studies, focus has shifted from genetic analysis to cell biology as individual cells are considered to be the basic component of biological understanding. In molecular analysis demands, there have been challenges to make measurements at the single cell level, because cell samples are highly complex, containing many different species at widely different abundance levels [6]–[8]. Therefore, the ability to sort and separate individual cells or cell types has become particularly important and using microfluidic technology has proven a favorable solution due its inherent capabilities for automation and high throughput[6], [11], [12], [16], [22]. Microfluidic approaches have been applied specifically in male fertility studies in order to separate sperm from unwanted debris and to improve the efficiency of assisted reproductive technologies (ART) [23]. A current popular microfluidic approach for sperm separation utilizes parallel laminar fluid streams of media through a straight microchannel: one stream consisting of a dilute semen sample, and the other stream consisting of sperm media [82], [83]. At the micro scale, the two fluid streams do not mix readily such that only motile sperm, chemically attracted towards the sperm media, can travel across the interface between the two parallel streams. The two streams are separated again after a sufficient length to allow motile sperm to separate from non-motile sperm and debris. This, and all other microfluidic sperm separation approaches to date, have been heavily reliant on sperm motility, employing microchannel features such as: chemo-attractants[89]–[91], physical obstacles[99], and micro-diffusers[96]. Since these methods were only designed to separate progressive motile sperm cells from semen samples, they lose a significant number of viable sperm cells including nonprogressive, motile and nonmotile sperm cells. Therefore, for patients

with low quantities of low quality sperm, these approaches are not optimal as they select against the patient's immature and nonmotile sperm cells despite the fact that those cells could have the potential for conception using ART.

Recently we demonstrated sperm separation utilizing a spiral channel for simulated testicular sperm extraction (TESE) and microdissection testicular sperm extraction (mTESE) samples which include not only sperm cells, but also red blood cells (RBC), white blood cells (WBC), and other contaminating debris [100]. This study showed purely mechanical, label-free separation of sperm from a simulated mTESE sample using inertial microfluidics. The approach did not require any externally applied forces except the movement of the fluid sample through the instrument. Using this method, we were able to recover not only motile sperm, but also viable less-motile and nonmotile sperm at a high recovery rate. This separation was achieved primarily by generating a sharp flow focusing RBCs for separating the unwanted cells away from the sperm cells, while only generating a slight trend of sperm flow focusing. Although performing the separation in this way was an important step forward, and represented a significant contribution to the field, an optimized microfluidic inertial focusing system would generate sharp flow focusing of both RBCs and sperm cells. This type of system would be more capable of handling samples such as extremely low concentrations of sperm with high concentrations of contaminating cells (such as mTESE samples).

Our hypothesis was that sharp flow focusing of sperm cells was possible and that a better understanding of sperm behavior in the curved channel was critical. Specifically, we hypothesized that an improved understanding of the dynamic forces felt by the nonspherical sperm cells was necessary in order to more reliably predict and control their

behavior. The separation of particles utilizing inertial microfluidics principles builds on the foundational assumption that the shape of the target particle is a spherical shape. However, live cell samples such as sperm cells, RBCs, and WBCs [18]–[20] are not always spherically shaped. There has been a study to understand the behavior of nonspherical shaped particles within the microchannel [50]. This study has attempted to characterize focusing behavior of different nonspherical particles, utilizing its rotating diameter.

In this study, we present an improved model of sperm cell behavior in curved channels based on both 2D COMSOL ® simulations and experimental studies (Figure 5.1). The purpose of the study is to find the behavior of a sperm-like-particle (SLP) within a curved channel and propose an improved model of the SLP for generating a clear flow focusing of sperm. Our results show that an SLP has clear alignment behaviors toward direction of primary flow. The alternative modeling from the understanding of SLP behavior can be utilized to calculate new optimal conditions for significantly improving flow focusing of sperm within the previously designed spiral channel [100]. The results show promising evidence that the proposed method should able to generate more precise sperm separation for mTESE samples.

5.2 Known Design Principle and Challenges

Previous studies of inertial effects have presented the physical design guidelines for generating flow focusing of target particles in a spiral channel [26], [27], [30], [31]. The guidelines include the following group of nondimensional parameters: the force ratio (R_f), the ratio of particle diameter and channel hydraulic diameter (λ), and the aspect ratio of the channel.

The force ratio (R_f) is a ratio between the Dean drag force (F_D) and the net lift force (F_L), where F_D is the force resulting from a secondary vortex that appears laterally on the curved channel and F_L represents the combination of wall effect lift and shear gradient lift force [26], [27], [30], [31]. According to the guidelines, R_f should be greater than 0.08 (5.1) and λ should be more than 0.07 (5.6). The aspect ratio of the channel should be between approximately 1:2 and 1:4 (height:width). The following equations show details of nondimensional values, and their constituent elements:

$$R_f = \frac{F_L}{F_D} \geq \sim 0.08 \tag{5.1}$$

$$F_D = 3\pi\mu U_{Dean} a_p \tag{5.2}$$

$$F_L = 0.05 \frac{a_p^4 \rho U_m^2}{D_h^2} \tag{5.3}$$

$$U_{Dean} = 1.8 \times 10^{-2} De^{1.63} \tag{5.4}$$

$$De = \frac{\rho U_f D_h}{\mu} \tag{5.5}$$

$$\lambda = \frac{a_p}{D_h} \geq 0.07\,, \tag{5.6}$$

In these equations, μ is fluid viscosity, U_{Dean} is the average Dean velocity, a_p is particle diameter, *De* is Dean number, ρ is the density of the fluid (water), U_f is flow

velocity, D_h hydraulic diameter, μ is viscosity of the fluid, and U_m is the maximum fluid velocity.

While this theory is well established, it is built exclusively for spherical particles, and when used with nonspherical particles (such as many types of cells) requires the assumption of a representative diameter. Since this simplification has a significant impact on design, it been a critical consideration for the channel design guideline. Hur et al. [50] suggested the use of the rotational diameter of the particle since most particles rotate while they travel through the microchannel in laminar flow, and reported that the rotational diameter of the particle (regardless of its cross-section shape) could determine the final focused position in most cases. In other words, the focused position of a spherical particle will be similar to the final focused position of a nonspherical particle with the same rotational diameter. Based on this finding, the behavior of symmetrical, nonspherical cells has been approximated using the rotational diameter or the largest diameter of the cell [56], [58], [62].

In our previous report, we also utilized Hur's suggestion, using the rotational diameter to predict the focusing of target particles in inertial equations [101]. The sperm cell, which is in actuality composed of an ellipsoid head (~5 μm length, ~3.12 μm width) and a tail (36-49 μm length), was assumed to behave as a rotating sphere of diameter 5 μm [104]. RBCs, which are in actuality flat disks of ~9 μm diameter, were assumed to behave as rotating spheres of diameter 9 μm [102][103]. Due to irregularities, these dimensions are based on average measurements of a finite number of cell samples. The longest dimension of the normal morphology sperm head (5 μm) was utilized as a simplified sphere diameter, while 9 μm and 12 μm diameter spheres were utilized as models for RBC and WBC

respectively. After a series of calculations, selected dimensions which meet required design guidelines, were selected as follows: channel height = 50 μm, channel width = 150 μm, space between channels = 310 μm, initial radius of the spiral = 700 μm, final radius of the spiral = 899 μm.

As previously explained, while this spiral channel was able to generate clear, sharp flow focusing of RBCs, the sharp flow focusing of sperm didn't appear. The successful flow focusing of RBCs, imply that the spherical model did accurately predict the behavior of RBC, but the lack of definitive focusing of sperm cells implies that the modeling of sperm cells wasn't accurate. The lack of focusing of sperm can be improved by a recent study of aligning behavior of uneven doublet particle [44]. In Uspal's study, an example of uneven double particles showed alignment of particle movement toward the primary flow in the microfluidic channel. Through the particle aligning phenomenon, we were able to predict the aligning behavior of sperm while it travels through the curved microfluidic channel due to the morphologic similarities. This behavior should be a good foundation to improve the modeling and focusing of sperm cells.

5.3 Methodology

In this work, we demonstrated that sperm cell alignment is the explanatory particle behavior mechanism. The sperm cell alignment behavior was validated through COMSOL simulation and observational data. With validation we developed an improved modeling of SLPs. We also showed the improved sperm focusing by new optimum condition from improved sperm modeling. We also included experiments using simulated mTESE samples in order to show a potential application of this newly discovered phenomenon.

5.3.1 Sample Preparation

Depending on experimental necessity, three types of particles were used: sperm cells, red blood cells, and beads. Sperm cells and red blood cells were acquired and prepared (DAPI, PKH26 stain) as explained previously[100]. We also utilized 5 μm (Bangs laboratories, Fluorescent Carboxyl Polymer Microbeads, Red) and 3 μm (Polysciences, Fluoresbrite, Yellow Green) fluorescent microbeads. During device operation, all particles were suspended in Quinn's media at various concentrations (sperm & microbeads:0.1-1 million/ml, mTESE:-10 million/ml)

5.3.2 Device Protocol and Operation

Syringes, manipulated at a rate controlled with syringe pumps, were used to inject and withdraw samples from the spiral channel device whose fabrication and operation was explained extensively in a previous chapter [100].

5.3.3 COMSOL Simulation

Two dimensional (2D) finite element software simulations of SLP dynamics were performed using COMSOL Multiphysics®. 2D simulations were utilized due to the simplicity of the study and the limited computational power that it requires. Although 2D models neglect the Dean force induced secondary vortex flow, according to the Dean force Dean velocity equations (Equation 5.2 and 5.4), the lateral particle migration velocity imposed by the Dean force is relatively insignificant compared to the primary flow velocity in terms of magnitude, as the Dean velocity is thousands of times less than the primary flow velocity. In other words, net lift forces induced lateral particle migration is more

significant than Dean force induced lateral particle migration effect. Therefore, the 2D model should provide an appropriate representation of an SLP behavior under the curved channel.

The SLP was geometrically identical to an ideal sperm cell, and contained an ellipsoid head (5 μm length, 3 μm width), and extended tail (30 μm long, 1 μm thick). To represent the flexibility of real cells, a Young's modulus of 1.6 kPa was applied to the SLP, which is similar to Young's modulus of the average cell membrane [115]. As the behavior of the SLP is most interesting in the initial part of the channel (before it has reached its focus location), only a small, initial portion of the channel was simulated, and the behavior of the particle across this length was used to draw conclusions about the SLP as it travelled the length of the channel. Specifically, channel dimensions were obtained from the first $1/16^{th}$ of the innermost ring of the spiral channel. Thus the simulated length was 2.86 mm and 150 μm wide. The no-slip condition was applied on the fluid boundaries. Through the input, fluid (water) was injected with a velocity of 0.14m/sec while the SLP was already inside of the channel near the inlet (Figure 5.2).

To understand the behavior of an SLP with any initial condition, a total of seven simulations were completed, each of which had an SLP placed in the channel with a unique combination of location and orientation. These two variables were parameterized by the initial location of the head (as measured from the inner wall) and the orientation of the head (as measured by the alignment relative to the direction of the primary flow). In Figure 5.3, the eight different cases, which were simulated, are shown. These include seven different SLP positions/orientations and a sperm-head-like particle in the curved channel. The elliptical sperm-head-like particle provided an important background against which to

compare the results of the SLP simulations.

We also quantified the movement of the SLPs through the length of the channel across the following variables: total travel time, number of 360° flips completed, percent of the time (and distance) that the particle spent rotating, and the percent of the time (and distance) that the particle spent aligned. The final alignment and location of the particle were also quantified with the same metrics that quantified the SLPs' initial position.

An additional case (Case 8) was added to compare the behavior of SLPs with the behavior of common nonspherical particle shapes. In this case, a sperm head like particle was simulated as simply an ellipse.

5.3.4 Experimental Verification of the Simulation

To verify COMSOL simulation results, a series of experiments were designed to experimentally observe the alignment behavior of SLPs. The experiment method was tracking individual sperm cells in the channel while injecting sperm through a spiral channel system. Using the high speed scanning capability of the microscope, we were able to confirm behavior of SLP which was identified from 2D simulation.

To observe the alignment of various sperm cells, a Nikon AR1 inverted microscope with a high-speed scanner (230 frames/sec) was utilized to observe the alignment of various sperm cells (Figure 5.1(2)). The selected area near the outlet of the spiral channel was recorded while DAPI stained sperm were injected through the channel. The sperm sample concentration was between 0.1 and 1 million/ml. The injection flow rate was 0.3 ml/min, which was the highest possible flow rate that allowed sperm identification in a frame. The recorded files were accumulated over 5 minutes. The DAPI blue stained sperm head and

tail were clear identification factors allowing us to distinguish sperm from other particles. From the videos, 102 sperm cells were identified for alignment angle measurement. ImageJ was used to measure the estimated alignment angle between sperm cells and primary flow direction.

5.3.5 Experimental Verification of the New SLP Model

With the experimental confirmation of SLPs' alignment behavior, we found enhanced understanding of SLP behavior for sperm modeling. With new modeling, we calculated improved optimum condition of sperm focusing. Without changing channel dimension and condition of media (viscosity and density), we found new focusing flow rate for sperm cells. With this new flow rate, we conducted a series of experiments to confirm the flow focusing improvement of sperm, using a DAPI stained sperm sample, fluorescent microbeads and a stained simulated mTESE sample.

The simulation study and the experimental confirmation provide new understanding and evidence of the SLP self-alignment behavior within the spiral channel and show that sperm do not continuously rotate as do the other nonspherical particles as reported as Hur's study [50]. The observed behavior of the SLP give us an idea of how to change the target particle modeling, specifically by selecting a new representative particle diameter (a_p). Since SLPs are mostly aligned in either a head lead or tail lead position, the two essential lateral particle migrating forces (F_D and F_L) will mostly effect the nonrotating side surface of the sperm heads and is not well-modeled by a 5μm diameter sphere. This estimation predicts reduction of the lateral force effect surface area of the particle, which means applying a new smaller value of a_p in the force equations (5.2)(5.3).

Since the new sperm cell model requires reduced force effect area of the sperm head compared to the previous estimation method, the width of the sperm head (3.12 μm) can be selected as a more conservative particle model diameter (a_p) than the length of the sperm head (5 μm). Therefore, the head width dimension was taken as a new a_p and applied to the two force equations (5.2)(5.3). With a new a_p and the current spiral channel dimensions, a set of calculations provided the minimum flow rate to reach $R_f > 0.08$ for sperm cells. The calculated flow rate was 1.725 ml/min.

A set of experiments was designed to verify the new optimum condition that was determined for the new sperm particle model. The experiments included tests of three types of particles (DAPI stained sperm, 5 μm (Red), and 3 μm (Green) fluorescent microbeads) at three different flow rates: 0.52, 1.04, and 1.7 ml/min. These tests allowed us to observe the changes in flow focusing of each particle with varied flow velocities. The utilized flow rate of 1.7ml/min was slightly lower than the calculated flow rate of 1.725 ml/min, but was utilized to prevent possible damage of the experimental setup due to the high pressure required. The two sizes of microbeads represent the two models of the sperm head. Specifically, the red 5 μm bead represents a rotating sperm cell using the longest head length and the green 3 μm bead represents the nonrotating sperm using the sperm head width as the diameter of the spherical particle models. The flow rate of 0.52 ml/min represents the flow rate calculated from ~5 μm sphere modeling and the flow rate of 1.7 ml/min represented calculated flow rate based on ~3 μm sphere modeling. The flow rate of 1.04 ml/min is added to show the flow focusing pattern change of each particle while the flow rate is increased. With the same high-speed scanner microscopy (Nikon AR-1) from our previous work [100] videos were recorded for 6-8 sec (~1800 frames) and all

frames of videos were projected into an image to show traces of all particles. As before, videos were taken near the outlet of the spiral channel. The intensity profile of each projected image was extracted by NIS Elements software and plotted in Excel

5.3.6 Application of the New SLP Model for mTESE

To demonstrate the usefulness of this new method for mTESE sample, a set of experiments were designed to verify the focusing improvement effect of the new flow rate condition with simulated mTESE samples. Utilizing the same sets of flow rate conditions above (0.52, 1.04, and 1.7 ml/min), these tests allowed us to observe the changes in flow focusing of sperm cells and RBCs with varied flow velocities. The flow rate of 0.52 ml/min represents the flow rate calculated from ~5 μm sphere modeling and the flow rate of 1.7 ml/min represented the calculated flow rate based on ~3 μm sphere modeling. The flow rate of 1.04 ml/min is added to show the flow focusing pattern change of each particle while the flow rate is increased. And the of data acquisition protocols of simulated mTESE sample test were the same as the sperm and microbeads characterization study above, except for the number of frames used for projection images. The total concentration of sperm cells and RBCs which was much higher (~10 million/ml) than stained sperm and microbeads test samples above (0.1-1 million/ml). To present changing of flow focusing of cells properly, only ~100 frames were utilized in all flow rate cases.

5.3.7 Clinical Safety Verification

As data from this study were used to propose a tool that is meant for clinical application, we needed to identify the potential biological and physical damage to any sperm that were

processed through the device. We performed both a live/dead test and morphology test (the most common clinical methods to verify sperm quality) on processed sperm. For both tests we utilized the standard WHO protocol [112] for test and sperm sample reading protocols. Samples from two different patients were used.

5.4 Results and Discussion

5.4.1 Simulation Results: Sperm Alignment

Our simulations verify that unlike the rotational behavior of nonspherical particles which have been previously studied [50], the SLP have a tendency to align with the primary flow in either a tail lead or head lead position and with a strong resistance to rotation. Aligned particle behavior was observed during almost the entirety of every SLP's travel through the channel (84-100%) and was not observed at all in the case of the tail-less particle (Case 8). In terms of rotations, two cases (Case 3 and 6) showed no flips and in cases where the SLP did rotate, rotations were quicker and shorter than in the tailless particle case (Figure 5.3, case 8). Even in Case 1 where three flips were observed, these flips happened over just 13% of the channel's distance. This is as opposed to the tailless particle which tumbled throughout the entirety of its travel through the curved channel. The possible cause for the rotation is a combination of the parabolic flow velocity profile of the channel and wall induced lift force (Figure 5.4). When an SLP is located between multiple boundaries of clearly different velocity fields (Figure 5.3, Case 1, Case 2, Case 4, Case 5, and Case 7), the higher velocity pushes the closest edge of the SLP, which causes a rotation (Figure 5.2(2) 5.2(3)) or a self-alignment. In every case, the length of the channel that the particle spent rotating was very short compared to the overall particle travel

distance (Table 5.1).

The alignment phenomenon can also be explained in terms of the particle's location and orientation relative to the flow velocity profile. When the particle is located mostly in the higher velocity field (Figure 5.3, red color velocity profile area) in the middle of the channel (Figure 5.3, Case 3, Case 6), the particle alignment is maintained as the particle is exposed to a minimal difference between neighboring streamlines across the edges of the particle. This type of particle behavior should be more dominant in the later rings of the spiral channel, because particles should migrate to a stable equilibrium area (upper and bottom middle are of the channel, Figure 5.1(1) of the rectangular channel as the shear gradient lift force and wall effect lift force balance [27]. This also means that there shouldn't be any rotation of SLPs after the focused flow of the particle length around later rings of the spiral channel.

5.4.2 Experimental Confirmation of SLP Alignment Behavior

Using the inverted microscope, we were able to image individual sperm cells as they travelled through the channel. In Figure 5.5(1), a polar plot is used to represent the alignment of each measured sperm cell, and Figure 5.5(2) and 5.5(3) shows two example images from which sperm cells were identified (among 102 cases). The results show a strong preference towards alignment and a weak preference towards the tail lead (Figure 5.5(1)). Since the chance of having clearly identified sperm in each frame was entirely random, the alignment data collection can be used to reliably represent general behavior of the SLP. This result demonstrates that the self-alignment of sperm is a genuine phenomenon.

5.4.3 Improved Focusing Behavior: Microbeads and Sperm Cells

With the three flow rates of 0.52 ml/min, 1.04 ml/min, and 1.7ml/min flow focusing behavior of 3 μm microbeads, 5 μm microbeads, and DAPI stained sperm, was observed near the outlet of the spiral channel; the images and intensity plots are shown in Figure 5.6. At the lowest flow speed, only the 5 um beads are focused, and increasing the flow rate increases the focusing of the 3 um beads and sperm cells, whose peaks appear sequentially from the inner to outer wall. This data appears to validate our hypothesis that the alignment behavior of the sperm cells in the channel would cause them to focus in a manner more similar to smaller particles. This is true both in terms of their location and the flow rate required to focus them.

In Figure 5.6(A), the intensity percentile plot clearly shows different flow focusing behavior among the three different particles. Consistent with the theory, the 5 um beads are found to be focused into a tight stream. Quantitatively, the 5 um beads are found to focus at a position about 25% of the way across the channel into a tight peak that occupies less than 10% of the channel width (quantified at half-mast). The 3 um beads and sperm cells show a minimal tendency towards focusing, with a peak width spanning greater than 40% of the width in both cases. Essentially, we would observe that the 3 um beads and sperm cells are not focused at this lowest flow rate (Table 5.2(1)).

Figure 5.6(B) shows the focusing of particles at the flow rate of 1.04 ml/min, which demonstrated an improvement of flow focusing of all particle cases relative to the slower flow rate of 0.52 ml/min. The most distinct improvement in flow focusing is in the 3 um beads, whose stream width is now only ~10% of the channel's width, nearly a 2X improvement in flow focusing (Figure 5.6(B4)) (Table 5.2(2)) . This data implies that the

forces created at this flow rate have led to a flow focusing tendency in the 3 um beads, although they have not led to complete flow focusing which occurs only at a higher flow rate (Figure 5.6(C)). The flow focusing of sperm cells also improves at this higher flow rate, although the improvement is slight, with the new stream width occupying ~37% of the channel. The focused stream of 5 um beads is nearly identical in both width and position to the stream at the lower flow rate (~22% of the way across the channel, ~7% of the channel width) (Table 5.2(2)). Although the flow focusing is not as evident in this case, as in the faster case the ordering of the beads in terms of size can already be seen, and is the mechanism by which separation is achieved. Here though, the ordering of the peaks can also be used as evidence that, from the perspective of the flow, the sperm cells are acting like particles that are smaller than the 3 um beads, which is especially interesting because the sperm cell's smallest dimension is ~3 um.

Figure 5.6(C) shows the behavior of the three particles at the increased flow rate of 1.7 ml/min. As predicted by the theory, the flow focusing of 3 um beads is very precise at the higher flow rate with a width equivalent to only ~7% of the channel width (Table 5.2(3)). With the flow rate increased to focus smaller particles, the sperm cells have also focused much more tightly. Quantitatively, the width of the sperm cell stream is 25% of the channel width, which represents nearly a 2X improvement in focusing relative to the base case of 0.52 ml/min (Table 5.2(3)). Although the flow focusing of the 5 um beads has diminished slightly with the increased flow rate, the stream width is still only ~12% of the channel width, and is still tight enough to separate the 5 um beads from other particles (Table 5.2(3)). The sequential peaks, that move from the inner to outer wall as the apparent particle diameter decreases, are even more apparent at the higher flow rate (Figure 5.6(A4),

5.6(B4), 5.6(C4)).This observation implies that approximating the sperm cells as a sphere for use with present Dean flow theory requires using a representative diameter smaller than 3 um, which would present an even faster velocity to achieve flow focusing. We were not able to perform experiments at higher flow rates, as the induced pressure was found to cause failure in our devices.

5.4.4 Improved Focusing Utility: Simulated mTESE

The application that drove our interest in this problem is the separation of sperm cells from digested testicular biopsy samples that are obtained as part of a treatment for infertile men. The goal of improving the flow focusing of sperm cells was twofold: (1) improve the separation by selecting a smaller portion of the RBCs, and (2) increase the concentration of sperm cells in the final output by selecting a smaller portion of the total channel width. The optimal device operation would result in two sharp, well separated streams—one of RBCs and one of sperm cells. The results of this work helped us move much closer to this type of performance, as we increased the operational flow rate from 0.52 ml/min to 1.7 ml/min.

In the 0.52 ml/min case, RBCs were focused in a sharp stream near the inner wall area of the channel (Figures 5.7(A1), 5.7(A3)) that occupies less than 6% of the channel width (measured at half-mast). However, sperm cells did not show a clear noticeable flow focusing trend (Figures 5.7(1), 5.7(2)), with a stream width of sperm greater than 40% of the channel width (Table 5.3(1)), as before. This behavior is consistent with our previous result and leads to an operation in which, instead of selecting for the sperm cells, we select for and remove the RBCs. The RBCs advantageously focused to an inner middle portion

of the channel where a waste selection can be made on the inner 35% of the channel to remove the vast majority of the RBCs (the small secondary peak impedes our ability to remove all of the RBCs). In this operation, it may be possible to flow the waste portion of the first run through the device again to try to recover the small quantity of sperm cells that would be selected in this stream, but this would only exacerbate the problem inherent in this operation: The sperm are of necessity suspended in a very large volume at a very low concentration.

At a flow rate of 1.04 ml/min, the trend of flow focusing of sperm cells was improved relative to the 0.52ml/min case, although the ability to separate this stream from the stream of RBCs was diminished (Figure 5.7(A), 5.7(B)). The stream width of sperm cells is reduced to less than 30% of the channel width (Table 5.3(2)), reduced by over a quarter width from the results at a lower flow rate (Figure 5.7(B1), 5.7(B2), 5.7(B4)). The sperm cells focus into two peaks near the middle of the channel, the higher of which is located ~60% of the way towards the outer wall of the channel. Meanwhile, the focused stream of RBC has shifted toward the middle area of the channel and the secondary peak has become more pronounced (Figure 5.7(B1), 5.7(B3), 5.7(B4)). Overall, the stream width has increased to ~20% of the channel, and the stream is now centered about 46% of the way across the channel. This leads to quite considerable and disadvantageous overlap between the streams of RBCs and sperm cells. This flow rate is found to be too high to tightly focus RBCs, and not high enough to create flow focusing of sperm cells.

In the 1.7 ml/min case (Figure 5.7(C)), the focused stream of sperm cells was significantly improved compared to the previous flow rate cases. The stream width of sperm cells was ~22% of the channel width, about half of the width of the original

unfocused stream width from the 0.52 ml/min case (Table 5.3(1), 5.3(3)). The highest signal intensity is measured 60% of the way across the channel, although a fairly distinct secondary peak is present near the middle of the channel. The RBCs focused into a tight stream occupying ~7% of the channel width and located ~44% of the way across the channel, although a much smaller secondary peak appeared close to middle outer area of the channel (Figure 5.7(C4)).

The new particle model based method clearly improved the flow focusing of sperm cells. However, the newly calculated flow rate also caused the focused stream to shift toward the middle of the channel. The shift could be caused by a combination of Dean drag force and the particle's drive to reach an equilibrium position between where the shear gradient lift force and wall induced lift force are balanced (Figure 5.1(1), two equilibrium positions middle of near long face wall of rectangular shape channel). By considering this shift, it is possible to determine a much improved protocol which relies on the improvements offered by the improved focusing behavior reported here.

5.4.5 Sperm Viability Test Results

We were also able to verify that operating the spiral device at the higher flow rates suggested by this work does not impose increased biological or physical damage to the cells. This is true both in terms of sperm viability (live/dead) and sperm morphology. In terms of the live sperm count (Figure 5.8(1)), there is only a small, insignificant difference (-11 sperm and +1 sperm) between the control and processed samples. This difference is especially minor when compared with the natural decay of sperm cells during the clinical process [115]. In terms of morphology, both the normal sperm head and normal sperm tail

counts (Figure 5.8(2), 5.8(3)) demonstrate that the device does not impose excessive physical damage to the sperm cells. The morphological differences between the control and processed samples, both in terms of the head and tail morphologies, can be considered minor from the clinical perspective due to the high variability inherent in the morphology test's manual cell count methodology. The counts provide evidence that the new protocol did not damage the sperm during processing. Overall, viability and morphology tests successfully showed valuable evidence that the device operation with new increased flow rate has only caused a minor defect.

5.5 Conclusion

In conclusion, we proposed a modeling approach of sperm which allowed us to demonstrate the alignment behavior of sperm in the spiral channel. The modeling was completed with 2D COMSOL ® simulation and experimental studies of SLP behavior under a curved channel verified these results. The SLP behavior study showed that the particle would not continuously rotate while it was traveling through the curved channel and that the particle is mostly aligned with the primary flow direction either in a tail lead or a head lead position. This behavior was also confirmed by observing the alignment angle of all recognizable sperm cells with high speed imaging near the outlet area of the spiral channel. The new understanding of the SLP led the lateral migration inducing forces (F_L and F_D) to act over a smaller effective surface than is suggested by the rotating particle model.

A series of experiments with sperm cells and microbeads showed a clear improvement between the new model approach and the previous approach. Analysis of projection images

from recorded high-speed videos confirmed that the flow focusing behavior (in required flow rate and position) was more similar to the 3 μm microbeads than to the 5 um beads, and that the sperm cells may act like particles even smaller than the 3 um beads. This new approach also improved separation of sperm from simulated mTESE samples. The flow focusing of sperm cells and RBCs were significantly improved as confirmed by analysis of the projection image from recorded videos. The focused sperm cells stream appeared in the middle area of the channel and the focused RBCs stream appeared at the mid-inner wall area of the channel. However, there was still a trend of slight overlapping between sperm cells and RBCs focused stream, which would prevent complete separation.

A biocompatibility test shows the biological/physical effects of the new approach. Two semen samples were utilized to conduct survival and morphology tests according to WHO guidelines. The live and normal shape sperm count results show that there were only minor changes in the quantities of living and normal sperm cells between control and processed samples. This means there was almost no significant negative effect from the new approach. Overall, the new understanding of SLP behavior under the curved channel provides improved sperm modeling, allowing for sharper flow focusing of sperm cells. This new approach can provide more precise sperm separation from mTESE samples, which may significantly reduce sperm searching efforts compared to the conventional method. The simple biocompatibility study also gives us promising evidence that the approach can be used clinically.

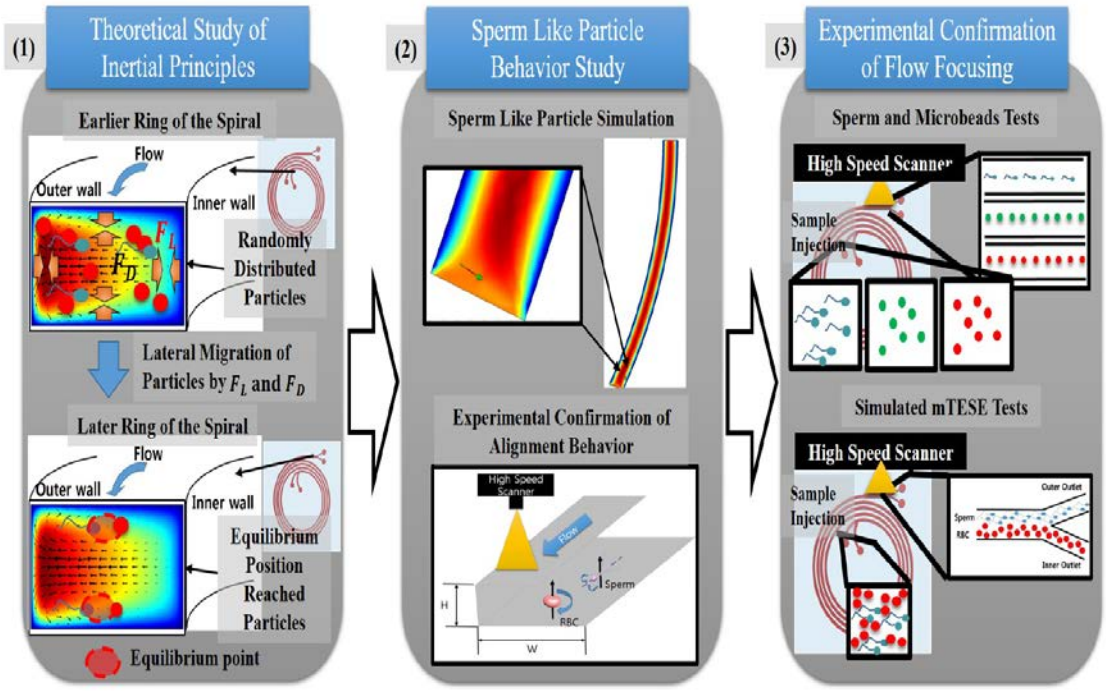

Figure 5.1. Overview of the study. (1) Understanding impact of the particle behavior within inertial microfluidics principles. (2) SLP behavior study utilizing COMSOL and experimental confirmation studies. Then find improved solution of SLP modeling. (3) Experimental confirmation studies utilizing sperm, microbeads, and simulated mTESE samples to show the improvement of flow focusing of sperm cells.

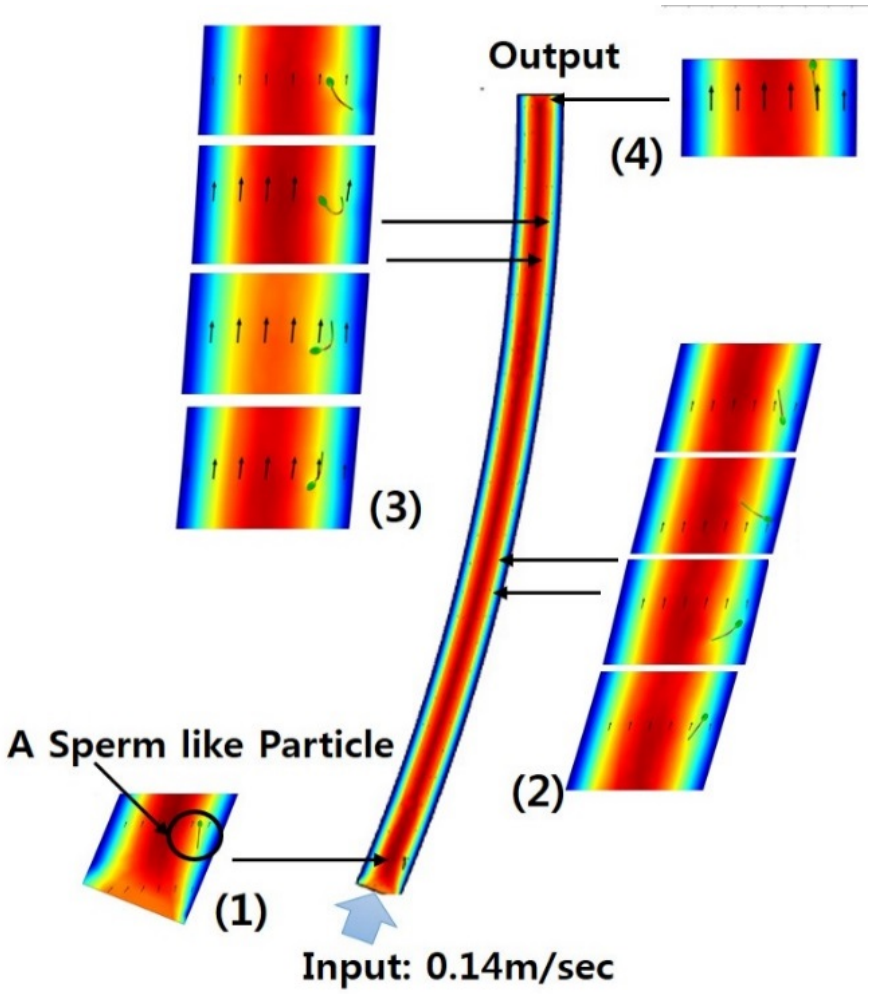

Figure 5.2 An example of 2D COMSOL® simulation, (1) initial position of the SLP, (2) the first rotation of the SLP, (3) the second rotation of the SLP, and (4) the final position of the SLP.

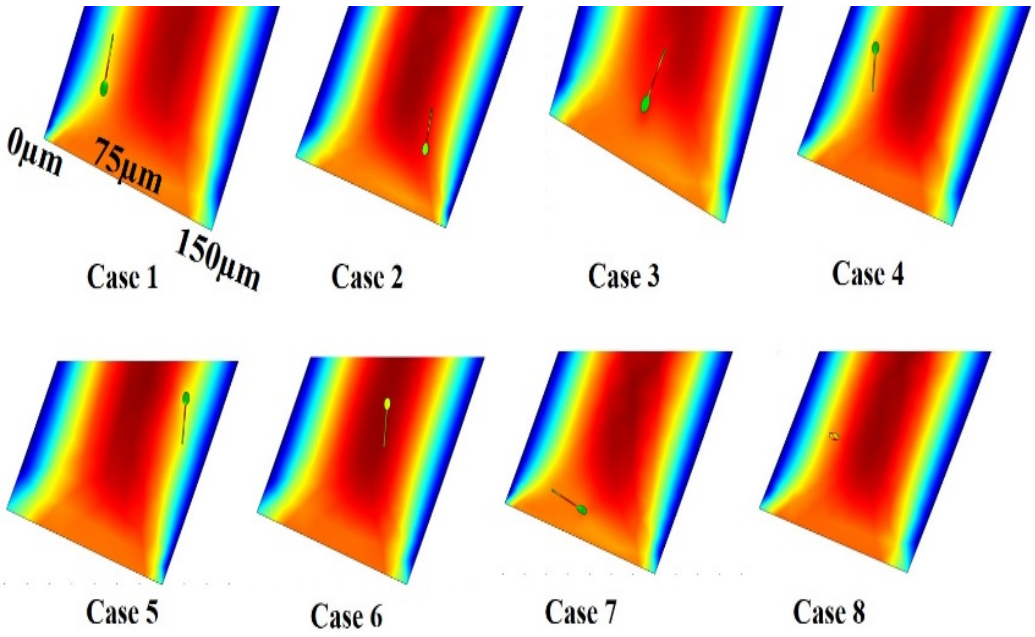

Figure 5.3 Eight different initial position cases for 2D COMSOL simulation study

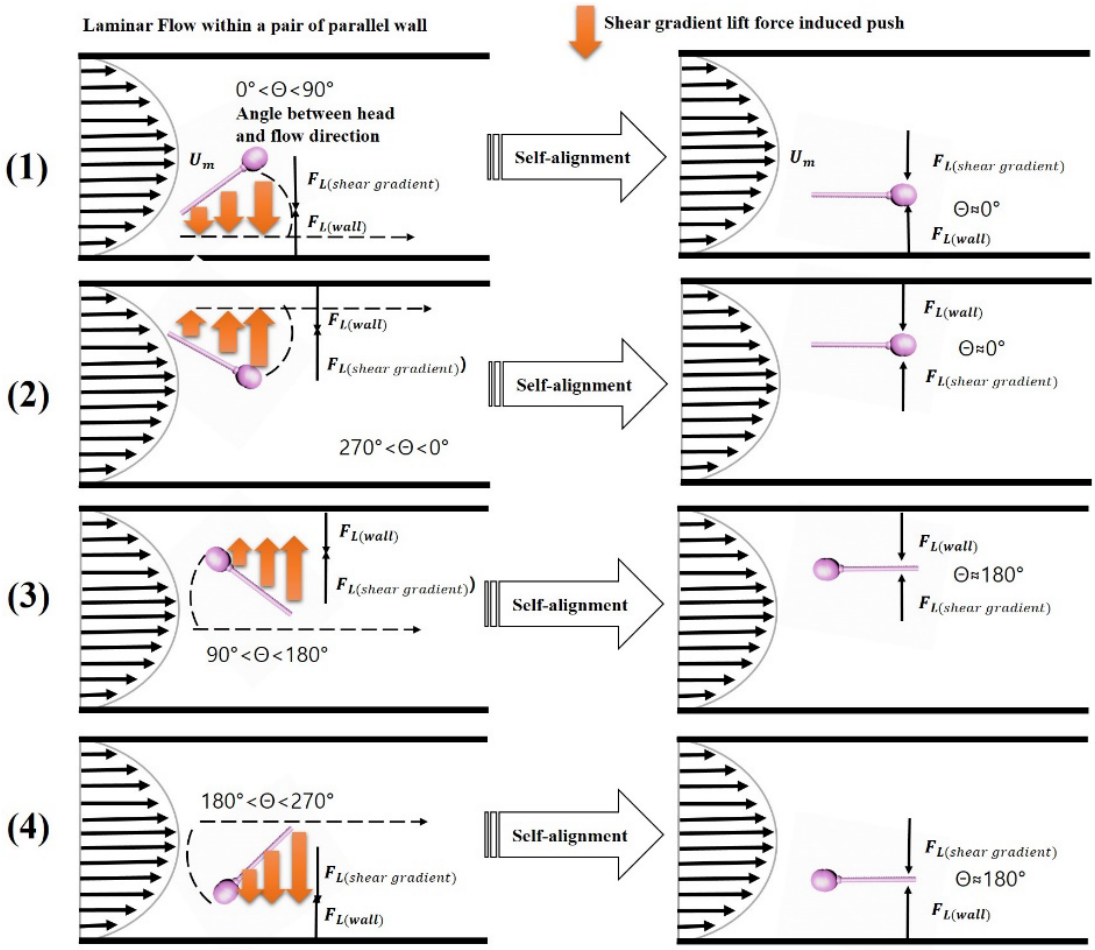

Figure 5.4 SLP alignment behavior summary within a pair of parallel wall (1) head leading with flow direction case, $0° < \Theta < 45°$; (2) head leading with flow direction case, $310° < \Theta < 0°$; (3) tail leading with flow direction case, $135° < \Theta < 180°$; (4) tail leading with flow direction case, $180° < \Theta < 225°$.

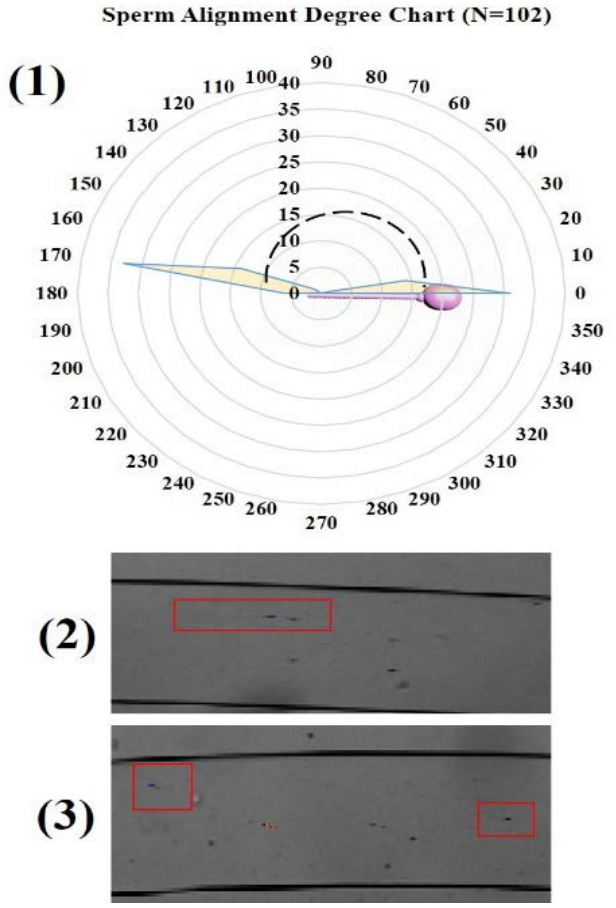

Figure 5.5 Sperm alignment measurement results from 100 sperm image captures (1) The polar plot of sperm alignment within the spiral channel, (2-3) identified sperm cell samples from a single frame of recorded high-speed video.

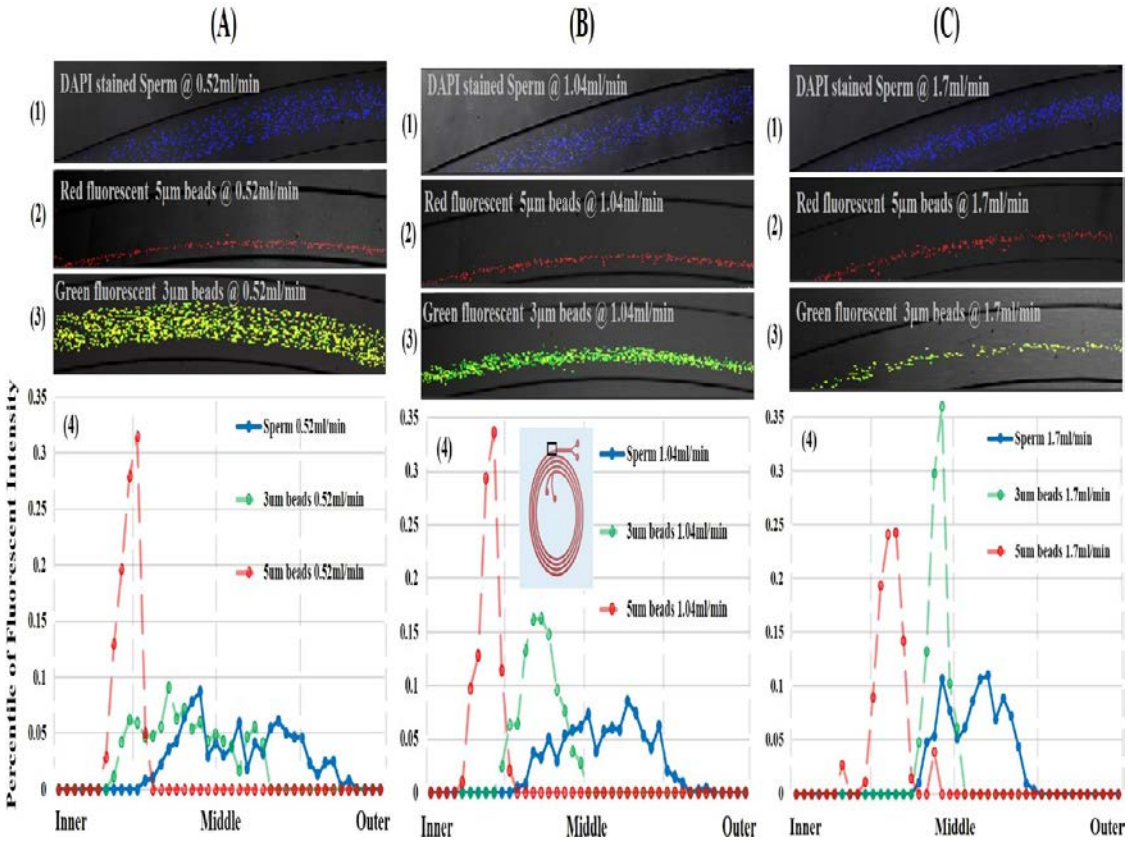

Figure 5.6 Characteristics of DAPI stained sperm, ~5µm, and ~3µm diameter microbeads at a flow rate of 0.52ml/min (A), 1.04ml/min (B), and 1.7ml/min (C). (1) projection image of DAPI stained sperm, (2) projection image of 5µm fluorescent microbeads, (3) projection image of 3µm fluorescent microbeads, (4) fluorescent intensity percentile plot of all three types particle.

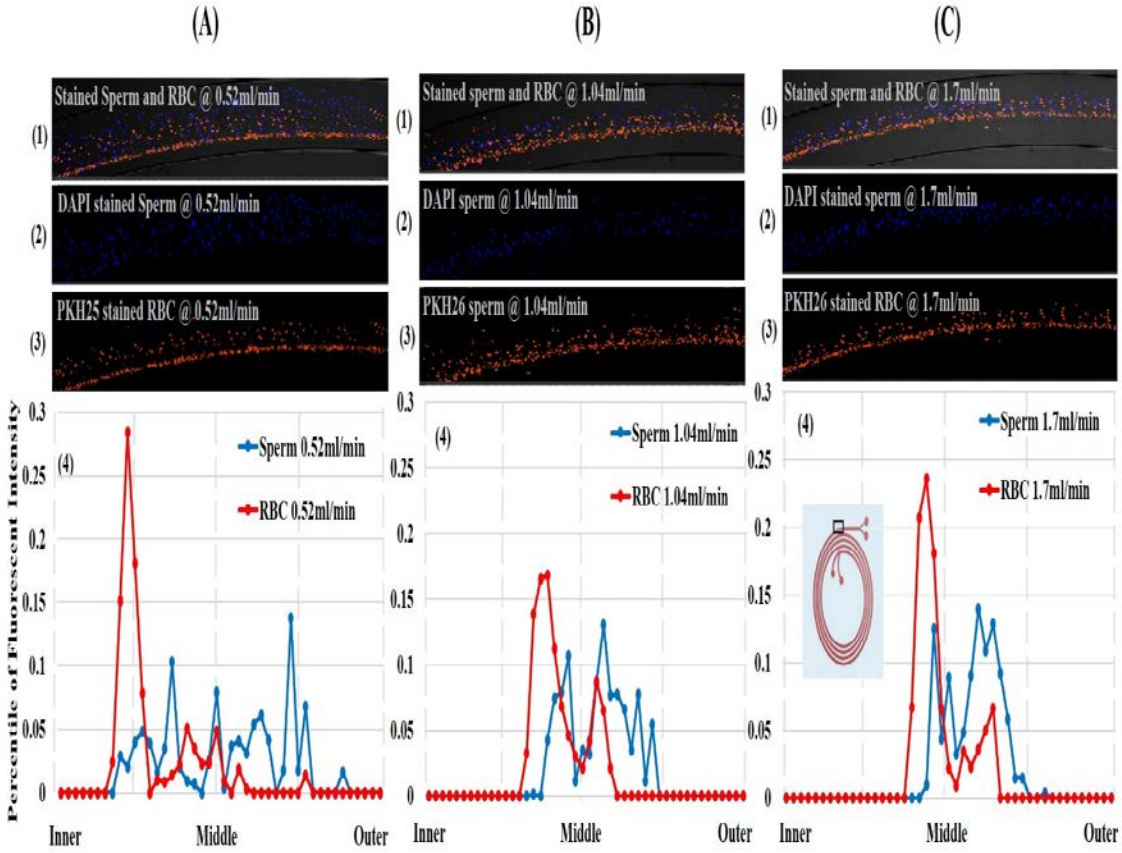

Figure 5.7 Characteristics of stained simulated mTESE (A) at a flow rate of 0.52ml/min, (B) 1.04 ml/min, (C) and 1.7 ml/min. (1) Projection image of DAPI stained sperm and PKH26 stained RBC, (2) Sperm projection image, (3) RBC projection image.

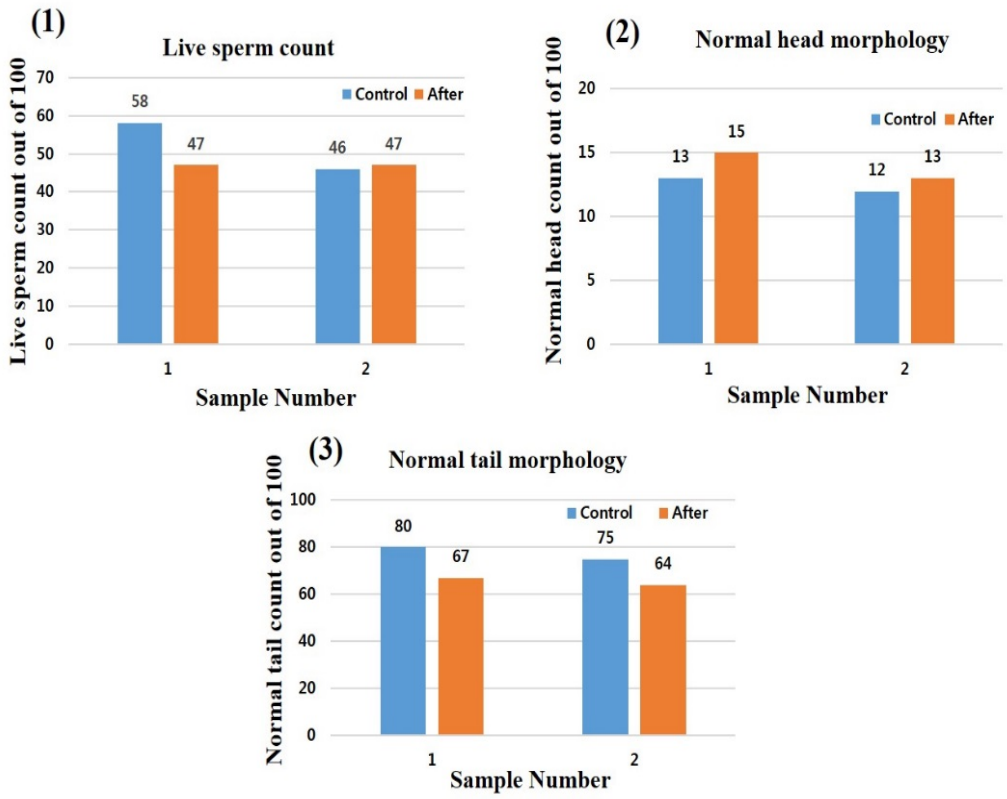

Figure 5.8 Plot results for the biological influence of the device operation protocol, (1) live sperm count from viability (live/dead) test of two different samples, (2) normal head morphology count from morphology test of two different samples, (3) normal tail morphology count from morphology test of two different samples.

Table 5.1 2D simulation summary table. The simulation of the SLP with different initial positions (Case1-Case8). * The particle location is the distance from the inner wall. ** The angle "Θ" is the angle between the primary flow direction and the SLP (Figure 5.4).

Case #	**Case 1**	**Case 2**	**Case 3**	**Case 4**	**Case 5**	**Case 6**	**Case 7**	**Case 8**
Initial location of head* (μm)	30	100	72	30	110	75	75	35
Initial alignment with θ** ◦	Tail lead 190	Tail lead 190	Tail lead 175	Head lead 10	Head lead 10	Head lead 10	Perpendicular 90	Sperm head N/A
Total travel time (sec)	0.593	0.542	0.523	0.560	0.584	0.518	0.532	0.619
Number of flips	3	1	0	2	2	0	0.5	11
Rotation time ratio (distance)%	11.8 (13)	4.1 (7.6)	0 (0)	10.7 (11.1)	3.9 (8)	0 (0)	47.7 (~16)	N/A Tumbling
Aligned time ratio (distance)	89 (87)	96 (93.4)	100 (100)	89.3 (88.9)	96.1 (92)	100 (100)	52.3 (~84)	N/A Tumbling
Final alignment with θ**◦	Head lead ~10	Head lead ~2	Tail lead ~10	Heard lead ~1	Head lead ~10	Head lead 0	Head lead ~20	N/A
Final location of head(μm)*	60	105	70	35	110	77	47	15

Table 5.2. Intensity profile plot analysis of sperm, and microbeads when injection flowrate is 0.52ml/min, 1.04ml/min, and 1.7ml/min. *The peak width is the number of points measured from the left initial location with half intensity of the highest intensity peak value to the final half intensity value of right end. The total points were there to show span width compare to total width of the channel. ** The value in ( ) is the total number points of each plot from inner wall to outer wall.

0.52ml/min Case (1)	**PEAK WIDTH***	**HIGHEST PEAK POSITION****	**PEAKS MIDDLE POSITION****
Sperm	17/42	19^{th}/42	23.5^{th}/42
3µm bead	18/42	15^{th}/42	17.5^{th}/42
5µm bead	4/42	11^{th}/42	10^{th}/42
1.04ml/min Case (2)			
Sperm	15/41	26^{th}/41	23.5^{th}/41
3µm bead	4.5/41	15^{th}/41	15^{th}/41
5µm bead	3/41	9^{th}/41	8.5^{th}/41
1.7ml/min Case (3)			
Sperm	11/43	26^{th}/43	24.3^{th}/43
3µm bead	3/43	20^{th}/43	19.5^{th}/43
5µm bead	5/43	14^{th}/43	13.5^{th}/43

Table 5.3 Intensity profile plot analysis of simulated mTESE sample test when injection flowrate is 0.52ml/min, 1.04 ml/min, and 1.7 ml/min. *The peak width is the number of points measured from the left initial location with half intensity of the highest intensity peak value to the final half intensity value of right end. The total points shows span width compare to total width of the channel. ** The value in () is the total number points of each plot from inner wall to outer wall.

0.52 ML/MIN Case (1)	**PEAK WIDTH***	**HIGHEST PEAK POSITION****	**PEAKS MIDDLE POSITION****
Sperm	18.5/(44)	32^{th}/(44)	25.7^{th}/(44)
RBC	2.5/(44)	10^{th}/(44)	10^{th}/(44)
1.04 ml/min Case (2)			
Sperm	13/(46)	26^{th}/(46)	23^{th}/(46)
RBC	9.5/(46)	18^{th}/(46)	21.5^{th}/(46)
1.7 ml/min Case (3)			
Sperm	10/(45)	27^{th}/(45)	25^{th}/(45)
RBC	3/(45)	20^{th}/(45)	20^{th}/(45)

5.6 References

[1] G. Velve-Casquillas, M. Le Berre, M. Piel, and P. T. Tran, "Microfluidic tools for cell biological research," *Nano Today*, vol. 5, no. 1, pp. 28–47, Feb. 2010.

[2] S. Cho, D. K. Kang, J. Choo, A. J. deMello, and S. I. Chang, "Recent advances in microfluidic technologies for biochemistry and molecular biology," *BMB Rep.*, vol. 44, no. 11, pp. 705–712, Nov. 2011.

[3] D. C. Duffy, J. C. McDonald, O. J. A. Schueller, and G. M. Whitesides, "Rapid prototyping of microfluidic systems in poly(dimethylsiloxane)," *Anal. Chem.*, vol. 70, no. 23, pp. 4974–4984, Oct. 1998.

[4] K. Ohno, K. Tachikawa, and A. Manz, "Microfluidics: Applicatons analytical purposes in chemistry and biochemistry," *Electrophoresis*, vol. 29, pp. 4443–4453, Nov. 2008.

[5] Y. Zhang *et al.*, "DNA methylation analysis on a droplet-in-oil PCR array.," *Lab Chip*, vol. 9, no. 8, pp. 1059–1064, Apr. 2009.

[6] C. Wyatt Shields IV, C. D. Reyes, and G. P. López, "Microfluidic cell sorting: A review of the advances in the separation of cells from debulking to rare cell isolation," *Lab Chip*, vol. 15, no. 5, pp. 1230–1249, Jan. 2015.

[7] H. Andersson and A. Van den Berg, "Microfluidic devices for cellomics: A review," *Sensors Actuators, B Chem.*, vol. 92, no. 3, pp. 315–325, Jul. 2003.

[8] S. M. Kim, S. H. Lee, and K. Y. Suh, "Cell research with physically modified microfluidic channels: A review," *Lab a Chip - Miniaturisation Chem. Biol.*, vol. 8, no. 7, pp. 1015–1023, Jul. 2008.

[9] R. N. Zare and S. Kim, "Microfluidic platforms for single-cell analysis," *Annu. Rev. Biomed. Eng.*, vol. 12, no. 1, pp. 187–201, Apr. 2010.

[10] A. Lenshof and T. Laurell, "Continuous separation of cells and particles in microfluidic systems," *Chem. Soc. Rev.*, vol. 39, no. 3, pp. 1203–1217, Feb. 2010.

[11] D. R. Gossett *et al.*, "Label-free cell separation and sorting in microfluidic systems," *Anal. Bioanal. Chem.*, vol. 397, no. 8, pp. 3249–67, Aug. 2010.

[12] A. A. S. Bhagat, H. Bow, H. W. Hou, S. J. Tan, J. Han, and C. T. Lim, "Microfluidics for cell separation," *Med. Biol. Eng. Comput.*, vol. 48, no. 10, pp. 999–1014, Oct. 2010.

[13] S. Choi and J.-K. Park, "Microfluidic system for dielectrophoretic separation based on a trapezoidal electrode array," *Lab Chip*, vol. 5, no. 10, pp. 1161–1167, Oct.

2005.

[14] A. F. Cowman and B. S. Crabb, “Review invasion of red blood cells by malaria parasites,” *Cell,* pp. 755–766, Feb. 2006.

[15] W. J. Kleijer, M. L. T. van der Sterre, V. H. Garritsen, A. Raams, and N. G. J. Jaspers, “Prenatal diagnosis of the Cockayne syndrome: Survey of 15 years experience,” *Prenat. Diagn.*, vol. 26, no. 10, pp. 980–984, Oct. 2006.

[16] S. Nagrath *et al.*, “Isolation of rare circulating tumour cells in cancer patients by microchip technology,” *Nature*, vol. 450, pp. 1235-1239, December, 2007.

[17] F. Petersson, L. Åberg, A. M. Swärd-Nilsson, and T. Laurell, “Free flow acoustophoresis: Microfluidic-based mode of particle and cell separation,” *Anal. Chem.*, vol. 79, no. 14, pp. 5117–5123, Jun. 2007.

[18] E. L. Tóth, E. Holczer, P. Földesy, K. Iván, and P. Fürjes, “Microfluidic particle sorting system for environmental pollution monitoring applications,” *Procedia Eng.*, vol. 168, pp. 1462–1465, Sep. 2016.

[19] N. Xia *et al.*, “Combined microfluidic-micromagnetic separation of living cells in continuous flow,” *Biomed. Microdevices*, vol. 8, no. 4, pp. 299–308, Dec. 2006.

[20] B. H. Weigl and P. Yager, “Microfluidic diffusion-based separation and detection,” *Science*, vol. 283, no. 5400, p. 346 LP-347, Jan. 1999.

[21] D. W. Inglis, “Efficient microfluidic particle separation arrays,” *Appl. Phys. Lett.*, vol. 94, no. 1, Jan. 2009.

[22] J. Nam, H. Lim, D. Kim, H. Jung, and S. Shin, “Continuous separation of microparticles in a microfluidic channel via the elasto-inertial effect of non-Newtonian fluid,” *Lab Chip*, vol. 12, no. FEBRUARY, p. 1347, Jan. 2012.

[23] J. E. Swain, D. Lai, S. Takayama, and G. D. Smith, “Thinking big by thinking small: Application of microfluidic technology to improve ART,” *Lab Chip*, vol. 13, no. 7, pp. 1213–24, Apr. 2013.

[24] G. Segré and A. Silberberg, “Radial particle displacements in poiseuille flow of suspensions,” *Comput. Geotech.*, vol. 189, no. 4760, pp. 209–210, Jan. 1961.

[25] D. Di Carlo, “Inertial microfluidics,” *Lab Chip*, vol. 9, no. 21, pp. 3038–3046, Nov. 2009.

[26] J. M. Martel and M. Toner, “Inertial focusing dynamics in spiral microchannels,” *Phys. Fluids*, vol. 24, no. 3, p. 32001, Mar. 2012.

[27] H. Amini, W. Lee, and D. Di Carlo, “Inertial microfluidic physics,” *Lab Chip*, vol. 14, no. 15, pp. 2739–61, May. 2014.

[28] E. S. Asmolov, “The inertial lift on a spherical particle in a plane Poiseuille flow at large channel Reynolds number,” *J. Fluid Mech.*, vol. 381, pp. 63–87, Jan. 1999.

[29] D. Di Carlo, J. F. Edd, K. J. Humphry, H. A. Stone, and M. Toner, “Particle segregation and dynamics in confined flows,” *Phys. Rev. Lett.*, vol. 102, no. 9, pp. 1–4, Mar. 2009.

[30] J. Zhou and I. Papautsky, “Fundamentals of inertial focusing in microchannels,” *Lab Chip*, vol. 13, no. 6, pp. 1121–32, Mar. 2013.

[31] J. M. Martel and M. Toner, “Particle focusing in curved microfluidic channels,” *Sci. Rep.*, vol. 3, pp. 1–8, Nov. 2013.

[32] P. G. Saffman, “The lift on a small sphere in a slow shear flow,” *J. Fluid Mech.*, vol. 22, no. 2, pp. 385–400, Fe. 1965.

[33] S. I. Rubinow and J. B. Keller, “The transverse force on a spinning sphere moving in a viscous fluid,” *J. Fluid Mech.*, vol. 11, no. 3, pp. 447–459, Nov. 1961.

[34] B. P. Ho and L. G. Leal, “Migration of rigid spheres in a two-dimensional unidirectional shear flow of a second-order fluid,” *J. Fluid Mech.*, vol. 65, no. 2, pp. 365–400, Aug. 1974.

[35] W. R. Dean, “LXXII. The stream-line motion of fluid in a curved pipe (Second paper),” *London, Edinburgh, Dublin Philos. Mag. J. Sci.*, vol. 5, no. 30, pp. 673–695, Apr. 1928.

[36] S. A. Berger, L. Talbot, and L. S. Yao, “Flow in curved pipes,” *Annu. Rev. Fluid Mech.*, vol. 15, pp. 461–512, Jan. 1983.

[37] D. R. Gossett and D. Di Carlo, “Particle focusing mechanisms in curving confined flows,” *Anal. Chem.*, vol. 81, no. 20, pp. 8459–8465, Sep. 2009.

[38] D. Di Carlo, D. Irimia, R. G. Tompkins, and M. Toner, “Continuous inertial focusing, ordering, and separation of particles in microchannels,” *Proc. Natl. Acad. Sci. U. S. A.*, vol. 104, no. 48, pp. 18892–18897, Nov. 2007.

[39] A. A. S. Bhagat, S. S. Kuntaegowdanahalli, and I. Papautsky, “Continuous particle separation in spiral microchannels using Dean flows and differential migration,” *Lab Chip*, vol. 8, no. 11, pp. 1906–1914, Nov. 2008.

[40] S. Ookawara, R. Higashi, D. Street, and K. Ogawa, “Feasibility study on concentration of slurry and classification of contained particles by microchannel,”

Chem. Eng. J., vol. 101, no. 1–3, pp. 171–178, Aug. 2004.

[41] A. A. S. Bhagat, S. S. Kuntaegowdanahalli, and I. Papautsky, "Enhanced particle filtration in straight microchannels using shear-modulated inertial migration," *Phys. Fluids*, vol. 20, no. 10, 2008.

[42] D. Di Carlo, "Inertial microfluidics," *Lab Chip*, vol. 9, no. 21, pp. 3038–46, Nov. 2009.

[43] F. P. Bretherton, "The motion of rigid particles in a shear flow at low Reynolds number," *J. Fluid Mech.*, vol. 14, no. 2, pp. 284–304, Oct. 1962.

[44] W. E. Uspal, H. Burak Eral, and P. S. Doyle, "Engineering particle trajectories in microfluidic flows using particle shape," *Nat. Commun.*, vol. 4, p. 2666, Apr. 2013.

[45] T. Kaya and H. Koser, "Characterization of hydrodynamic surface interactions of escherichia coli cell bodies in shear flow," *Phys. Rev. Lett.*, vol. 103, no. 13, pp. 1–4, Sep. 2009.

[46] G. B. Jeffery, "The motion of ellipsoidal particles immersed in a viscous fluid," *Math. Phys. Eng. Sci.*, pp. 161–179, Nov. 1922.

[47] C. Y. Wu, K. Owsley, and D. Di Carlo, "Rapid software-based design and optical transient liquid molding of microparticles," *Adv. Mater.*, vol. 27, no. 48, pp. 7970–7978, Oct. 2015.

[48] M. L. Ekiel-Jeżewska and E. Wajnryb, "Hydrodynamic orienting of asymmetric microobjects under gravity," *J. Phys. Condens. Matter*, vol. 21, no. 20, p. 204102, May. 2009.

[49] P. J. A. Janssen, M. D. Baron, P. D. Anderson, J. Blawzdziewicz, M. Loewenberg, and E. Wajnryb, "Collective dynamics of confined rigid spheres and deformable drops," *Soft Matter*, vol. 8, no. 28, pp. 7495–7506, Aug. 2012.

[50] S. C. Hur, S. E. Choi, S. Kwon, and D. Di Carlo, "Inertial focusing of non-spherical microparticles," *Appl. Phys. Lett.*, vol. 99, no. 4, pp. 1–4, Jul. 2011.

[51] J. Elgeti, U. B. Kaupp, and G. Gompper, "Hydrodynamics of sperm cells near surfaces," *Biophysj*, vol. 99, no. 4, pp. 1018–1026, Aug. 2010.

[52] W. Lee, H. Amini, H. A Stone, and D. Di Carlo, "Dynamic self-assembly and control of microfluidic particle crystals," *Proc. Natl. Acad. Sci. U. S. A.*, vol. 107, no. 52, pp. 22413–22418, Dec. 2010.

[53] J. Sun *et al.*, "Double spiral microchannel for label-free tumor cell separation and

enrichment," *Lab Chip*, vol. 12, no. 20, p. 3952, Jul. 2012.

[54] M. Jimenez, B. Miller, and H. L. Bridle, "Efficient separation of small microparticles at high flowrates using spiral channels: Application to waterborne pathogens," *Chem. Eng. Sci.*, vol. 157, pp. 247–254, Jan. 2017.

[55] Z. Wu, B. Willing, J. Bjerketorp, J. K. Jansson, and K. Hjort, "Soft inertial microfluidics for high throughput separation of bacteria from human blood cells," *Lab Chip*, vol. 9, no. 9, pp. 1193–9, May. 2009.

[56] A. J. Mach and D. di Carlo, "Continuous scalable blood filtration device using inertial microfluidics," *Biotechnol. Bioeng.*, vol. 107, no. 2, pp. 302–311, Oct. 2010.

[57] X. Wang, C. Liedert, R. Liedert, and I. Papautsky, "A disposable, roll-to-roll hot-embossed inertial microfluidic device for size-based sorting of microbeads and cells," *Lab Chip*, vol. 16, pp. 1821–1830, May. 2016.

[58] M. G. Lee, J. H. Shin, C. Y. Bae, S. Choi, and J. K. Park, "Label-free cancer cell separation from human whole blood using inertial microfluidics at low shear stress," *Anal. Chem.*, vol. 85, no. 13, pp. 6213–6218, Jun. 2013.

[59] N. Nivedita and I. Papautsky, "Continuous separation of blood cells in spiral microfluidic devices," *Biomicrofluidics*, vol. 7, no. 5, Sep. 2013.

[60] M. E. Warkiani *et al.*, "Slanted spiral microfluidics for the ultra-fast, label-free isolation of circulating tumor cells," *Lab Chip*, vol. 14, no. 1, pp. 128–37, Jan. 2014.

[61] T. H. Kim, H. J. Yoon, P. Stella, and S. Nagrath, "Cascaded spiral microfluidic device for deterministic and high purity continuous separation of circulating tumor cells," *Biomicrofluidics*, vol. 8, no. 6, p. 64117, Dec. 2014.

[62] A. A. S. Bhagat, H. W. Hou, L. D. Li, C. T. Lim, and J. Han, "Pinched flow coupled shear-modulated inertial microfluidics for high-throughput rare blood cell separation," *Lab Chip*, vol. 11, no. 11, pp. 1870–1878, Apr. 2011.

[63] S. Shen *et al.*, "High-throughput rare cell separation from blood samples using steric hindrance and inertial microfluidics," *Lab Chip*, vol. 14, no. 14, pp. 2525–38, Jul. 2014.

[64] D. Di Carlo, J. F. Edd, D. Irimia, R. G. Tompkins, and M. Toner, "Equilibrium separation and filtration of particles using differential inertial focusing," *Anal. Chem.*, vol. 80, no. 6, pp. 2204–2211, Feb. 2008.

[65] J. Boivin, L. Bunting, J. A. Collins, and K. G. Nygren, "International estimates of

infertility prevalence and treatment-seeking: Potential need and demand for infertility medical care," *Hum. Reprod.*, vol. 22, no. 6, pp. 1506–1512, Jun. 2007.

[66] T. G. Cooper *et al.*, "World Health Organization reference values for human semen characteristics," *Hum. Reprod. Update*, vol. 16, no. 3, pp. 231–245, May-Jun. 2009.

[67] R. Samuel *et al.*, "Microfluidics: The future of microdissection TESE?," *Syst. Biol. Reprod. Med.*, vol. 62, no. 3, pp. 161–70, Jun. 2016.

[68] K. Baker and E. Sabanegh, "Obstructive azoospermia: Reconstructive techniques and results," *Clinics*, vol. 68, no. S1, pp. 61–73, Feb. 2013.

[69] I. Craft *et al.*, "Percutaneous epididymal sperm aspiration and intracytoplasmic sperm injection in the management of infertility due to obstructive azoospermia," *Fertil. Steril.*, vol. 63, no. 5, pp. 1038–42, May. 1995.

[70] P. N. Schlegel, "Testicular sperm extraction: Microdissection improves sperm yield with minimal tissue excision," *Hum. Reprod.*, vol. 14, no. 1, pp. 131–135, Jan. 1999.

[71] P. N. Schlegel and L. M. Su, "Physiological consequences of testicular sperm extraction," *Hum. Reprod.*, vol. 12, no. 8, pp. 1688–1692, Aug. 1997.

[72] R. Kumar, "Medical management of non-obstructive azoospermia," *Clinics.* vol. 2013, pp. 75–79, Feb. 2013.

[73] P. Donoso, H. Tournaye, and P. Devroey, "Which is the best sperm retrieval technique for non-obstructive azoospermia? A systematic review," *Hum. Reprod. Update*, vol. 13, no. 6, pp. 539–549, Nov-Dec. 2007.

[74] C. Krausz, "Male infertility: Pathogenesis and clinical diagnosis," *Best Pract. Res. Clin. Endocrinol. Metab.*, vol. 25, no. 2, pp. 271–85, Apr. 2011.

[75] A. Bettegowda and M. F. Wilkinson, "Transcription and post-transcriptional regulation of spermatogenesis," *Philos. Trans. R. Soc. Lond. B. Biol. Sci.*, vol. 365, no. 1546, pp. 1637–1651, May. 2010.

[76] M. Ostad, D. Liotta, Z. Ye, P. N. Schlegel, "Teticular sperm extraction for nonobstructive azoospermia: Results of a multibiopsy approach with optimized tissue dispersion," *Urology*, vol. 4295, no. 98, pp. 692–696, Oct. 1998.

[77] L. Gambera, F. Serafini, G. Morgante, R. Focarelli, V. De Leo, and P. Piomboni, "Sperm quality and pregnancy rate after COX-2 inhibitor therapy of infertile males with abacterial leukocytospermia," *Hum. Reprod.*, vol. 22, no. 4, pp. 1047–1051, Apr. 2007.

[78] C. M. Peterson, A. O. Hammoud, E. Lindley, D. T. Carrell, and K. Wilson, "Assisted Reproductive Technology Practice Management", *Reproductive Endocrinology and Infertility*, D. T. Carrell, C. M. Peterson, Ed. New York: Springer, 2010, pp. 7-37.

[79] M. J. Chen and A. Bongso, "Comparative evaluation of two density gradient preparations for sperm separation for medically assisted conception," *Hum. Reprod.*, vol. 14, no. 3, pp. 759–764, Mar. 1999.

[80] L. J. Kricka *et al.*, "Micromachined analytical devices: Microchips for semen testing," *J. Pharm. Biomed. Anal.*, vol. 15, no. 9–10, pp. 1443–7, Jun. 1997.

[81] S. Tasoglu *et al.*, "Exhaustion of racing sperm in nature-mimicking microfluidic channels during sorting," *Small*, vol. 9, no. 20, pp. 3374–3384, Oct. 2013.

[82] B. S. Cho, T. G. Schuster, X. Zhu, D. Chang, G. D. Smith, and S. Takayama, "Passively driven integrated microfluidic system for separation of motile sperm," *Anal. Chem.*, vol. 75, no. 7, pp. 1671–1675, Feb. 2003.

[83] T. G. Schuster, B. Cho, L. M. Keller, S. Takayama, and G. D. Smith, "Isolation of motile spermatozoa from semen samples using microfluidics," *Reprod. Biomed. Online*, vol. 7, no. 1, pp. 75–81, Jan. 2003.

[84] H. Huang, "Motile human sperm sorting by an integrated microfluidic system," *J. Nanomed. Nanotechnol.*, vol. 5, no. 3, pp. 193-199, May. 2014.

[85] H.-Y. Huang *et al.*, "Isolation of motile spermatozoa with a microfluidic chip having a surface-modified microchannel," *J. Lab. Autom.*, vol. 19, no. 1, pp. 91–9, Feb. 2013.

[86] K. Matsuura, M. Takenami, Y. Kuroda, T. Hyakutake, S. Yanase, and K. Naruse, "Screening of sperm velocity by fluid mechanical characteristics of a cyclo-olefin polymer microfluidic sperm-sorting device," *Reprod. Biomed. Online*, vol. 24, no. 1, pp. 109–15, Jan. 2012.

[87] H. Sano, K. Matsuura, K. Naruse, and H. Funahashi, "Application of a microfluidic sperm sorter to the in-vitro fertilization of porcine oocytes reduced the incidence of polyspermic penetration," *Theriogenology*, vol. 74, no. 5, pp. 863–70, Sep. 2010.

[88] J. M. Wu, Y. Chung, K. J. Belford, G. D. Smith, S. Takayama, and J. Lahann, "A surface-modified sperm sorting device with long-term stability," *Biomed. Microdevices*, vol. 8, no. 2, pp. 99–107, Jun. 2006.

[89] S. Koyama, D. Amarie, H. Soini, M. Novotny, and S. Jacobson, "Chemotaxis assays of mouse sperm on microfluidic devices," *Anal. chem.*, vol. 78, no. 10, pp.

3354–3359, Apr. 2006.

[90] L. Xie *et al.*, “Integration of sperm motility and chemotaxis screening with a microchannel-based device,” *Clin. Chem.*, vol. 56, no. 8, pp. 1270–8, Aug. 2010.

[91] Y.-J. Ko, J.-H. Maeng, B.-C. Lee, S. Lee, S. Y. Hwang, and Y. Ahn, “Separation of progressive motile sperm from mouse semen using on-chip chemotaxis,” *Anal. Sci.*, vol. 28, no. 1, pp. 27–32, Jan. 2012.

[92] S. S. Suarez and M. Wu, “Microfluidic devices for the study of sperm migration,” *Mol. Hum. Reprod.*, pp. 1–8, Apr. 2017.

[93] C.-Y. Chen *et al.*, “Sperm quality assessment via separation and sedimentation in a microfluidic device,” *Analyst*, vol. 138, no. 17, pp. 4967–74, Sep. 2013.

[94] S. M. Knowlton, M. Sadasivam, and S. Tasoglu, “Microfluidics for sperm research,” *Trends Biotechnol.*, vol. 33, no. 4, pp. 221–229, Apr. 2015.

[95] R. Ma *et al.*, “In vitro fertilization on a single-oocyte positioning system integrated with motile sperm selection and early embryo development,” *Anal. Chem.*, vol. 83, no. 8, pp. 2964–2970, Mar. 2011.

[96] Y. Lin, P. Chen, R. Wu, L. Pan, and F. Tseng, “Micro diffuser-type movement inversion sorter for high-efficient sperm sorting,” *Int. Conf Nano/Micro Eng. Mol. Syst.*, pp. 7–10, Apr. 2013.

[97] M. D. C. Lopez-Garcia, R. L. Monson, K. Haubert, M. B. Wheeler, and D. J. Beebe, “Sperm motion in a microfluidic fertilization device,” *Biomed. Microdevices*, vol. 10, no. 5, pp. 709–718, Oct. 2008.

[98] M. Wheeler and M. Rubessa, “Integration of Microfluidics and Mammalian IVF,” *Mol. Hum Regrod,* vol. 23, iss. 4, pp. 248–256, Apr. 2017.

[99] R. S. Suh, X. Zhu, N. Phadke, D. A. Ohl, S. Takayama, and G. D. Smith, “IVF within microfluidic channels requires lower total numbers and lower concentrations of sperm,” *Hum. Reprod.*, vol. 21, no. 2, pp. 477–483, Feb. 2006.

[100] J. Son, K. Murphy, R. Samuel, B. Gale, D. Carrell, and J. Hotaling, “Non-motile sperm cell separation using a spiral channel,” *Anal. Methods*, iss. 7, pp. 8041-8047, May. 2015.

[101] S. S. Kuntaegowdanahalli, A. A. S. Bhagat, G. Kumar, and I. Papautsky, “Inertial microfluidics for continuous particle separation in spiral microchannels,” *Lab Chip*, vol. 9, no. 20, pp. 2973–80, Oct. 2009.

[102] P. R. Wheater, H. G. Burkitt, and V. G. Daniels, *Functional Histology. A Text and*

Colour Atlas. Edinburgh: Churchill, 1979.

[103] M. Diez-Silva, M. Dao, J. Han, C.-T. Lim, and S. Suresh, "Shape and biomechanical characteristics of human red blood cells in health and disease," *MRS Bull.*, vol. 35, no. 5, pp. 382–388, May. 2010.

[104] J. A. Mossman, J. T. Pearson, H. D. Moore, and A. A. Pacey, "Variation in mean human sperm length is linked with semen characteristics," *Hum. Reprod.*, vol. 28, no. 1, pp. 22–32, Jan. 2013.

[105] L. Maree, S. S. Du Plessis, R. Menkveld, and G. Van Der Horst, "Morphometric dimensions of the human sperm head depend on the staining method used," *Hum. Reprod.*, vol. 25, no. 6, pp. 1369–1382, Jun. 2010.

[106] J. E. Lackner, I. Märk, K. Sator, J. Huber, and M. Sator, "Effect of leukocytospermia on fertilization and pregnancy rates of artificial reproductive technologies," *Fertil. Steril.*, vol. 90, no. 3, pp. 869–871, Sep. 2008.

[107] N. Nivedita and I. Papautsky, "Continuous separation of blood cells in spiral microfluidic devices," *Biomicrofluidics*, vol. 7, no. 5, pp. 1–14, Sep. 2013.

[108] J.-P. Frimat *et al.*, "Make it spin: Individual trapping of sperm for analysis and recovery using micro-contact printing," *Lab Chip*, vol. 14, no. 15, pp. 2635–41, Aug. 2014.

[109] C. Ainsworth, B. Nixon, R. P. S. Jansen, and R. J. Aitken, "First recorded pregnancy and normal birth after ICSI using electrophoretically isolated spermatozoa," *Hum. Reprod.*, vol. 22, no. 1, pp. 197–200, Sep. 2007.

[110] R. Zeggari, B. Wacogne, C. Pieralli, C. Roux, and T. Gharbi, "A full micro-fluidic system for single oocyte manipulation including an optical sensor for cell maturity estimation and fertilisation indication," *Sensors Actuators, B Chem.*, vol. 125, no. 2, pp. 664–671, Aug. 2007.

[111] A. A. El-Ghobashy and C. R. West, "The human sperm head: A key for successful fertilization," *J. Androl.*, vol. 24, no. 2, pp. 232–8, Mar-Apr. 2003.

[112] WHO, *Examination and processing of human semen*, 5th ed, WHO, Geneva: Swiss. 2010.

[113] M. Ionescu *et al.*, "Enhanced biocompatibility of PDMS (polydimethylsiloxane) polymer films by ion irradiation," *Nucl. Inst. Methods Phys. Res. B*, vol. 273, pp. 161–163, Feb. 2012.

[114] C. Garrett, D. Y. Liu, R. I. McLachlan, and H. W. G. Baker, "Time course of changes in sperm morphometry and semen variables during testosterone-induced

suppression of human spermatogenesis," *Hum. Reprod.*, vol. 20, no. 11, pp. 3091–3100, Nov. 2005.

[115] N. Guz, M. Dokukin, V. Kalaparthi, and I. Sokolov, "If cell mechanics can be described by elastic modulus: Study of different models and probes used in indentation experiments," *Biophys. J.*, vol. 107, no. 3, pp. 564–575, Aug. 2014.

[116] X. Zhang *et al.*, "Lensless imaging for simultaneous microfluidic sperm monitoring and sorting," *Lab Chip*, vol. 11, no. 15, pp. 2535–2540, Aug. 2011.

[117] L. I. Segerink, A. J. Sprenkels, P. M. ter Braak, I. Vermes, and A. van den Berg, "On-chip determination of spermatozoa concentration using electrical impedance measurements," *Lab Chip*, vol. 10, no. 8, pp. 1018–24, Apr. 2010.

CHAPTER 6

CONCLUSION

6.1 Summary

In conclusion, this thesis successfully demonstrated the use of inertial microfluidic technology to purify sperm by focusing sperm in a spiral channel flow. Unlike conventional sperm separation techniques, the technique presented here was not dependent upon sperm motility, nor does it require any labels. Initial modelling of the sperm, RBCs, and WBCs as 5μm, 9μm, and 12μm diameter spheres respectively, allowed a set of spiral channel dimensions to be selected that adequately separated these cells, though further modelling may suggest better channel geometries for these asymmetric particles.

This study also successfully tested the biological effects and sample recovery capabilities of an inertial microfluidic device with significant numbers of healthy sperm samples. To show the biocompatibility influence of the proposed method, a series viability, time interval toxicity, and the recovery tests were performed. Results from the viability study showed clear evidence of statistically insignificant changes in the number of live sperm between control and collected samples during regular operation time (~5 minutes). The live sperm count data suggest that there are minimal negative effects on number of live sperm from the proposed approach. The viability study also showed statistically insignificant changes in morphology between control and processed samples. The normal morphology sperm count data also suggest minimal damage has occurred.

Lastly, this study proposed alternative modeling of sperm by utilizing head width (~3μm) as particle diameter for force equations (F_L and F_D). This new modeling technique is founded on a series of 2D COMSOL® simulations and the experimental study of single sperm-like-particle (SLP) behavior in curved channels. The study showed that the SLP would not continuously rotate while it was traveling through the curved channel, instead

the particle would mostly align with the primary flow direction in either the tail-lead position or head-lead position. This behavior was also confirmed by experimental study. The alignment behavior of the SLP gives a new understanding to adapt the new particle diameter within the lateral migration force equations (lift and Dean drag forces) for representing a new force effect surface. Two forces will mostly influence the long slim surface of the nonrotating sperm head which has a smaller surface than if one assumes a rotating sperm head particle based model (rotating ellipsoid: ~5μm rotating diameter). Based on the new understanding of the sperm-like particle behavior, the new particle modeling approach utilizes the width of the sperm head (~3μm) as the relevant diameter in force equations. The experimental results based on designs optimized by the new approach show significantly improved flow focusing of sperm compare to the initial approach (Chapters 2, 3). Overall, the presented new understanding of SLP behavior in the spiral channels improved modeling of SLP when using inertial microfluidics principles. This new approach can provide higher precision sperm separation from highly contaminated sperm samples such as mTESE samples, which can significantly reduce sperm searching efforts when compared to the conventional method.

6.2 Conclusions

The following statements are what can be learned from this study:

- Inertial microfluidics can be used to enhance sperm purity without sperm motility.
- For the case of RBCs and WBCs, the measured diameter can be used in the inertial effect equations.
- Rotation diameter of RBCs and WBCs are 9μm and 12μm, respectively, for modeling.

- Rotation diameter method cannot be used for sperm modeling due to the alignment behavior of the sperm.
- According to simulation and experimental studies, sperm typically align with the flow and experience minimal rotation (~<20% of total time)
- Lateral migration inducing forces (F_L and F_D) are the primary influence on the nonrotating, long, slim surface of the sperm head since a sperm-like-particle won't rotate like ellipsoids or spheres.
- The estimated width of a sperm head can be used as the model diameter in force equations.
- Inertial separation improvement occurs by sample concentration controls (length fraction changes).
- Range of equilibrium channel length estimation is also useful for cell experiments.
- Damage to sperm cells from centrifugal forces in spiral channels and the device materials was acceptable for clinical use.

6.3 Contributions

- MATLAB based spiral channel design tool utilizing inertial effects principles.
- 2D COMSOL modeling for traveling behavior of sperm-like-particle under laminar flow within a curved channel.
- Utilizing the alignment behavior of a sperm-like-particle in inertial microfluidic principles.
- Sample concentration dilution protocol for effective flow focusing of sperm and blood cells.

- The spiral channel device operation protocol for the sperm enhancement and separation.
- PDMS spiral device fabrication for pressure endurance purposes.

6.4 Future Work

Although this study successfully demonstrated enhancing highly contaminated sperm samples using a spiral channel, there are still many aspects of the proposed method that can be improved, from the channel design to the application protocol.

One obvious design improvement of the spiral channel can be generated from the new sperm modeling in Chapter 4. Since the use of the 3μm diameter in the force equations showed successful improvement to the flow focusing of sperm, a new design of the spiral channel can be developed and fabricated for generating sharp flow focusing of sperm with relatively lower injection flow rate than 1.7ml/min. The design change can be started by altering the radius, width, and height of the channel, which can lead to fewer channel turns and reduce the footprint of the device. This dimensional modification can lead to lower injection flow rates, which should help to prevent high pressure in the spiral channel system.

Another design change possibility is adopting a multistage spiral in the system, which can make separate collection steps for each cell type. This also can help to recapture possible lost sperm from the disposal outlet.

Another interesting topic is a more in-depth, specialized study about inertial effects on the particle. Using the particle equilibrium position shift towards the wall due to higher *Re* could be a good solution to achieving better separation between sperm and blood cells.

Since increasing *Re* can be achieved by increasing flow velocity or altering the viscosity of the media or altering the dimensions of the channel, a series of experimental studies can be performed under the high speed camera equipped microscope to observe behavior change of focused flow on different cells. While samples are prepared to be injected at the minimum flow rate to achieve flow focusing of each cell type ($R_f > 0.08$), the flow rate can be increased to observe equilibrium position shifting toward the wall. If there is an optimal *Re* to achieve better splitting of the focused flow of each cell type, a similar effect can be achieved to adjusting viscosity or channel dimension. The ratio between particle and channel dimension ($\lambda = a_p/D_h$) can also be utilized to control the equilibrium position of cells. By adjusting channel dimensions, finding a proper λ may be another solution to achieve better flow focusing of sperm and better splitting of the focused flow of each cell type.

Understanding particle behavior in the microfluidic channel can be a big branch of future study due to asymmetrical nature of cells and the natural flexibility of cell walls. A specialized study about the physical characteristics of sperm cell could lead to understanding of its behavior within a Poiseuille flow. Since this study presented 2D COMSOL® simulations about sperm-like behavior within curved channels, the 3D version of this simulation can provide additional understanding of Dean drag force effect on a sperm-like-particle. This additional simulation study should show a better understanding of the behavior of sperm-like-particles in a curved channel.

For clinical purposes, additional biocompatibility studies need to be done with better protocols and highly trained personnel who can read various sperm test samples more precisely. The reason behind this studies is a lack of complete data for current viability and

toxicity study which still don't have sufficient numbers to give assurance to the clinical community. Therefore, hundreds of sperm sample tests are needed; larger quantities of data may improve the trend of current statistics on the sperm tests. In order to improve the biocompatibility data, completing all sample reading procedures by highly trained personnel may also improve the test results and further improve the current data trend. Recovery tests for extremely low number sperm samples would also be an important addition. This recovery test should be conducted with an actual mTESE sample, so the clinical community can be convinced of the rapid sperm collecting capability of the spiral channel approach.